The Democratic and Popular Republic of Algeria
Higher Studies and Scientific Research Ministry

National Polytechnic School

Parameter Estimation of Multi-component Polynomial Phase Signals: Exploitation of the Spatial Information Provided by an Antenna Array.

Doctorate Thesis
Submitted to the Department of Electronics

by

Mounir Adjrad

In Fulfillment of the Requirements
for the Degree of Sate Doctorate

Jury members:

Chair:	Mohamed TADJINE (Professor, ENP)
Supervisor:	Adel BELOUCHRANI (Professor, ENP)
Examiners:	François GUILLET (Professor, Université de Saint-Etienne, France)
	M'hamed HAMADOUCHE (Directeur de recherche, DRD/CFDAT)
	Abdelaziz OULDALI (Maître de conférence, EMP)

2007

E.N.P. 10, Avenue HASSEN BADI –EL-HARRACH– ALGER

ملخص

في هذه الرسالة نركز على تطبيق طريقة وسيطة لمعالجة مشكلة تقدير إشارة متعددة التركيب و ذات طور متعدد الدرجات. كذلك نبين كيف أن التمثيل الحالي الفضائي و تطبيق مرشح Kalman يوفران عدة ايجابيات خاصة عند مزج هاذين الأخيرين مع استعمال هوائي متعدد المستقبلات؛ الشيء الذي يمكن من استعمال المعلومة الفضائية. أغلبية الطرق تقتصر على معالجة إشارات ضيقة المجال بالاستعانة بتمثيل ضيق المجال. عامة الطرق المقترحة لمعالجة الحالة واسعة المجال تستوجب تحويل الإشارات المستقبلة من الميدان الزماني إلى الميدان الترددي باستعمال محول Fourier. الأقلية من الباحثين عالجوا الحالة واسعة المجال في الميدان الزماني. في هذه الرسالة نذكر بالتعارف الخاصة بالحالات ضيقة المجال و واسعة المجال و تأثيرها على مشكلة التمثيل أين نأخذ بعين الاعتبار تمثيلا حقيقيا عكس التمثيل المركب الغالب الاستعمال. المحفزات وراء هذا الاختيار: معالجة الإشارات ضيقة المجال و واسعة المجال في الميدان الزماني باستعمال نفس الطريقة مع التخفيض من العبء الحسابي عكس التمثيل المركب. يمكن تطبيق الخوارزمية المقترحة في الحالات الوحيدة و المتعددة التركيب مع أداء حسن في حالة توفر عدد من المصادر أكبر من عدد المستقبلات. بالإضافة إلى تقدير وسيطات الطور الخوارزمية المحصل عليها تمكن تقدير زوايا وصول المصادر و تقدير درجة الطور (لما تكون هذه الأخيرة مجهولة). نقارن الخوارزمية المقترحة بطرق مسابقة أين نبرهن أن أداء طريقتنا مماثل أو أحسن من أداء الطرق الأخرى مع تخفيض عدد العمليات الحسابية.

مفتاح الكلمات

تقدير التأخر؛ اتجاه الوصول؛ مرشح Kalman ممدد؛ مصدر ضيق المجال؛ تقدير الوسائط؛ إشارة ذات طور متعدد الدرجات؛ تمثيل حالي فضائي؛ مصدر واسع المجال.

ABSTRACT

This thesis focuses on the application of a parametric approach to the problem of multicomponent polynomial phase signal parameters estimation. We show how the state-space modellisation and the application of the Kalman filter offer many advantages when combined with the use of multisensor array, exploiting the additional spatial information. Most conventional approaches are limited to processing narrowband data using narrowband assumption to model the problem. For tackling the wideband situation, the majority of the proposed methods require transforming the received signals from the time domain to the frequency domain using the Fourier transform as pre-processing step. Very few authors have dealt with the wideband situation in the time domain. In this thesis, we recall the definitions of narrowband and wideband signals and their effect on the problem modellisation where we consider a real-valued modellisation, as opposite to the most often used complex-valued modellisation. The drivers behind this choice are: Dealing with narrowband and wideband signals in the time domain using the same algorithm, and the reduction of the computational cost, as opposite to the complex-valued modellisation, optimising by this the memory use. The proposed algorithm can be applied in the monocomponent and multicomponent cases with good performance in the case where there are more sources than array sensors. In addition to the estimation of the signal phase parameters, the resulting algorithm allows the estimation of the sources directions of arrivals and the estimation of the order of the polynomial phase (when unknown). The proposed algorithm is compared to competitive methods and proven to perform as good or better than these latter with reduced computational cost.

KEYWORDS

Delay Estimation, Directions of Arrival, Extended Kalman Filter, Narrowband Source, Parameters Estimation, Polynomial-Phase Signal, State-Space Modellisation, , Wideband Source.

RÉSUMÉ

Dans cette thèse nous nous intéressons à l'application d'une approche paramétrique au problème d'estimation des paramètres des SPPs multi composantes où nous montrons que la modélisation utilisant l'espace d'état et l'application du filtre de Kalman offrent plusieurs avantages lorsque ces derniers sont combinés avec l'utilisation d'un réseau de plusieurs capteurs, exploitant par cette association l'information spatiale. La majorité des approches conventionnelles sont limitées au traitement des données en supposant le cas bande étroite dans la modélisation du problème. Généralement, les méthodes traitants le cas large bande requièrent la transformation des signaux reçus du domaine temporel vers le domaine fréquentiel en utilisant la transformée de Fourier comme étape de prétraitement. Peu d'auteurs ont traité le problème large bande dans le domaine temporel. Dans notre travail, nous rappelons les définitions des signaux à bande étroite et à large bande et leurs effets sur le problème de modélisation où nous considérons une modélisation à valeurs réelles. Les motivations derrière ce choix sont: Le traitement des cas large bande et à bande étroite dans le domaine temporel en utilisant le même algorithme et la réduction du coût de calcul, relativement au cas de modélisation à valeur complexe. L'algorithme proposé peut être appliqué aux cas mono composante et multi composantes avec de bonnes performances lorsque le nombre de sources surpasse celui des éléments de l'antenne. Aussi, l'algorithme résultant permet, en plus de l'estimation des paramètres des signaux, l'estimation des directions d'arrivées des sources (localisation) et l'estimation de l'ordre du polynôme de la phase (lorsque ce dernier est inconnu). L'algorithme est comparé à des méthodes compétitives et est prouvé avoir des performances aussi bonnes ou meilleures avec un coût de calcul réduit.

MOTS CLÉS

Estimation des Retards, Directions d'Arrivées, Filtre de Kalman Étendu, Source à bande Étroite, Estimation des Paramètres, Signal à Phase Polynomiale, Modélisation en Espace d'État, Source à Large bande.

1. RÉSUMÉ ÉTENDU

1.1 Introduction

La communauté scientifique du traitement du signal a consacré une attention particulière à l'étude des signaux phase polynomiale (SPPs). Ces signaux existent dans la nature ainsi que dans plusieurs applications. Par exemple, certaines chauves souris produisent des SPPs à phase hyperbolique et quadratique pour se localiser. Certains systèmes radar utilisent des SPPs quadratiques. Les tremblements de terre et les tests nucléaires sous terrains peuvent générer des SPPs non linéaires. L'altitude et la vélocité d'un avion peuvent être estimées à partir de la fréquence intermédiaire (FI) non linéaire du bruit produit par le moteur et atteignant le sol. Les SPPs sont aussi utilisés en communications, astronomie, télémétrie, et autres disciplines. De plus, selon le théorème de Stone-Weierstrass, toute fonction continue sur un intervalle fermé peut être uniformément approximée par une fonction polynomiale. La grande majorité des applications traitant le problème d'estimation des paramètres des SPPs considèrent le signal bruité modélisé par :

$$\begin{cases} y(t) = aexp[j\phi(t)] + v(t) \\ \phi(t) = \sum_{l=0}^{L} b_l t^l \end{cases} \tag{1.1}$$

L'amplitude du signal, a, est supposée constante et le polynôme de la phase $\phi(t)$ est de degré L (pour $L = 2$, le SPP est appelé chirp). L'amplitude et la phase instantanée sont à valeur réelle (VR). Le signal $v(t)$ est un bruit additif, blanc et Gaussien, indépendant du SPP.

Dans notre travail, nous nous intéressons à l'application d'une approche paramétrique au problème d'estimation des paramètres des SPPs multi composantes où nous montrons que la modélisation utilisant l'espace d'état et l'application du filtre de Kalman

offrent plusieurs avantages lorsque ces derniers sont combinés avec l'utilisation d'un réseau de plusieurs capteurs, exploitant par cette association l'information spatiale. La majorité des approches conventionnelles sont limitées au traitement des données en supposant, dans la modélisation du problème, le cas bande étroite. Généralement, les méthodes traitant le cas large bande requièrent la transformation des signaux reus du domaine temporel vers le domaine fréquentiel en utilisant la transformée de Fourier comme étape de prétraitement. Peu d'auteurs ont traité le problème large bande dans le domaine temporel. Dans ces méthodes, il est supposé que les fréquences instantanées des signaux ne changent pas durant le temps nécessaire à une onde pour traverser l'aperture de l'antenne. Cette supposition signifie que les signaux restent à bande étroite à chaque instant, et donc leurs largeurs de bandes instantanées restent petites comparées à l'inverse du temps de propagation de l'onde à travers l'antenne. Dans notre effort, nous rappelons les définitions des signaux à bande étroite et à large bande et leurs effets sur le problème de modélisation où nous considérons une modélisation VR. Les motivations derrière ce choix sont: Le traitement des cas large bande et bande étroite dans le domaine temporel en utilisant le m ême algorithme et la réduction du co ût de calcul, relativement au cas de modélisation à valeur complexe (VC). L'algorithme proposé peut être appliqué aux cas mono-composante et multi-composantes avec l'obtention de bonnes performances lorsque le nombre de sources surpasse celui des éléments de l'antenne. L'algorithme résultant permet, en plus de l'estimation des paramètres des SPPs, l'estimation des directions d'arrivée des sources (localisation) et l'estimation de l'ordre du polynôme de la phase (lorsque ce dernier est inconnu).

1.2 État de l'art

Les SPPs appartiennent à la classe des signaux non stationnaires, rendant les méthodes de traitement de ces derniers applicables aux premiers. Les objectifs des méthodes statistiques pour le traitement du signal sont l'extraction des paramètres à

partir d'observations bruitées. Les techniques d'estimation peuvent être classifiées en deux catégories principales : Non paramétriques (aussi appelées méthodes spectrales) et paramétriques. Dans les premières, des fonctions spectres sont formées, où par exemple dans le cas d'estimation des angles d'arrivée, les positions des plus hauts piques de la fonction en question sont considérées comme les estimées des angles d'arrivée. Les techniques paramétriques par contre nécessitent une recherche simultanée de tous les paramètres. Ces dernières généralement produisent un meilleur résultat, relativement aux approches non paramétriques, mais souvent au dépend d'une complexité de calcul élevée. Dans notre travail, nous résumons les différentes méthodes adaptées, à partir des problèmes généraux du traitement d'antenne, au problème d'estimation des paramètres des SPPs. Comme exemple de méthodes non paramétriques largement utilisées, on cite la méthode de Capon qui a été adaptée à l'estimation des paramètres de la phase des SPPs et présentée dans [10]. Elle permet la représentation de l'évolution temporelle de la phase dans un plan temps-fréquence. Similairement, on cite l'estimateur MUSIC présentée dans [11] avec l'hypothèse que le sous-espace bruit est Gaussien. Elle permet l'estimation des paramètres de la phase sans l'ajout d'une matrice diagonale de régularisation à la matrice d'auto corrélation, contrairement à la méthode de Capon. Bien que ces méthodes spectrales soient numériquement attractives, souvent elles n'offrent pas une exactitude suffisante; en particulier, pour des scénarios impliquant des signaux hautement corrélés (ou cohérents). Une alternative est d'exploiter le modèle des données de faon complète en utilisant les méthodes paramétriques. Pour ces dernières, la cohérence des signaux n'impose aucune difficulté conceptuelle. Le prix à payer pour cette efficacité et robustesse accrues est la nécessité d'une recherche multidimensionnelle pour l'estimation des paramètres. Probablement l'approche paramétrique la plus connue et fréquemment utilisée est l'algorithme maximum de vraisemblance (MV). L'application de l'algorithme MV standard reste assez limitée pour le traitement des SPPs car aucun avantage n'est pris concernant la structure spécifique des SPPs. Une variante de l'algorithme MV a été développée dans [16] prenant en compte cette structure particulière et util-

isant un réseau de capteurs pour l'estimation de SPPs multi-composantes. Une autre approche paramétrique pour l'analyse des SPPs, utilisant les fonctions d'ambiguté d'ordre supérieur, a été proposée dans [4]. Une version plus élaborée, utilisant le produit des fonctions d'ambiguïté d'ordre supérieur, a été développée dans [19] en considérant le produit de plusieurs fonctions d'ambiguté d'ordre supérieur de m ême ordre mais avec différents retards. Cette version vient améliorer le résultat d'estimation, particulièrement dans le cas où le rapport signal à bruit est faible. L'estimation des paramètres basée sur l'utilisation du filtre de Kalman (FK) a été largement étudiée pour le cas des SPPs noyés dans un bruit Gaussien. L'utilisation du FK est motivée par l'avantage qu'offre cette méthode au niveau pratique permettant la poursuite en temps réel de la variation des fréquences des signaux [24], [25]. Un premier travail effectué utilisant cette technique a été consacré à l'identification des signaux chirp. Un modèle d'état linéaire a été obtenu basé sur l'approximation de Tretter [26] permettant la transformation du bruit additif en un bruit sur la phase. Le modèle obtenu, étant linéaire et Gaussien, permet l'application du FK. Bien que ce filtre soit optimal dans le sens du minimum de variance, la méthode de Tretter reste approximative et seulement applicable au cas de signaux mono-composante. Dans [28] et [29], les auteurs ont étudié le problème d'identification des signaux chirp en utilisant le filtre de Kalman étendu (FKE) en proposant et comparant deux modèles des SPPs non linéaires et exacts: Le premier modèle est non linéaire par rapport à l'état alors que le second est non linéaire par rapport aux observations.

Récemment, nous avons proposé dans [30] une méthode d'estimation des signaux chirp en utilisant deux FKE en cascade. Dans [32] les auteurs ont proposé un FKE pour la démodulation des SPPs en utilisant une représentation d'état où la phase est exprimée en fonction des polynômes de Legendre.

1.3 Méthodologie proposée

Dans ce travail, nous présentons un nouvel algorithme basé sur le (FK). Notre approche, présentée dans [31] et [33], offre la possibilité d'étende l'estimation des paramètres des SPPs mono-composante au cas des SPPs multi composantes (MC-SPPs) et où l'algorithme développé dans [30] est généralisé au cas MCSPPs d'ordres arbitraires reus par une antenne à plusieurs éléments. Cette méthode présente un nombre de propriétés attractives. Elle est applicable pour les applications nécessitant le traitement des signaux en temps réel du fait de la nature récursive de l'algorithme résultant et l'utilisation modeste de mémoire (du fait de la nature du FK). En considérant la modélisation VR, nous proposons l'exploitation de l'information spatiale fournie par une antenne à plusieurs capteurs linéaires et uniformes. Dans ce cas, les observations obéissent au modèle suivant:

$$y_1(t) = \sum_{n=1}^{N} a_n \sin\left[\phi_n(t)\right] + v_1(t), \tag{1.2}$$

$$y_m(t) = \sum_{n=1}^{N} a_n \sin\left[\phi_n\left(t - \frac{\tau_{nm}}{\Delta}\right)\right] + v_m(t), \quad m = 2, \ldots, M, \tag{1.3}$$

où $\{v_m, m = 1, \ldots, M\}$ sont des bruit indépendants, a valeurs réelles, blancs et Gaussiens ayant des moyennes nulles et des variances $\{\sigma_m^2, m = 1, \ldots, M\}$. $\{\tau_{nm}, n = 1, \ldots, N, m = 2, \ldots, M\}$ sont des paramètres VR représentants les retards temporels de propagation de la n-ème source arrivant au niveau du m-ème capteur relativement au signal reu sur le premier capteur. La modélisation en espace d'état consiste à établir les équations d'état et de mesure d'après le choix du vecteur d'état. En pratique, selon (1.2), deux cas se présentent: des situations où les retards sont connus et des applications où ces derniers sont inconnus. Nous donnons alors la représentation d'état pour ces deux cas.

La modélisation en espace d'état consiste à définir les équations d'état et de mesures suivant le choix du vecteur d'état. En pratique, suivant l'équation (1.3), deux cas peuvent se manifester : Situations où les retards sont connus et applications

où ces paramètres sont inconnus. Dans le premier cas, le modèle d'état choisit possède le vecteur d'état suivant

$$\mathbf{x}(t) = \left[a_1 \;\; \phi_1(t) \;\; \phi_1^{(1)}(t) \ldots \phi_1^{(L_1)}(t) \ldots\ldots a_N \;\; \phi_N(t) \;\; \phi_N^{(1)}(t) \ldots \phi_N^{(L_N)}(t)\right]^T, \tag{1.4}$$

où $(.)^T$ et $(.)^{(l)}$ représentent, respectivement, les opérateurs transposée d'une matrice et la dérivée l-ème par rapport à t.

Le vecteur des paramètres est définit par

$$\theta = [a_1 \; b_{01} \; b_{11} \; \ldots \; b_{L_1 1} \; \ldots\ldots \; a_N \; b_{0N} \; b_{1N} \; \ldots \; b_{L_N N}]^T, \tag{1.5}$$

$$\hat{\theta}(t) = \beta \hat{\mathbf{x}}(t), \tag{1.6}$$

Où $\hat{\theta}$ et $\hat{\mathbf{x}}$ sont les estimées de θ et $\mathbf{x}$, respectivement, et β est un coefficient scalaire dépendant du choix des vecteurs d'état et du vecteur des paramètres. Dans le cas où ces retards sont inconnus, ils sont inclus en augmentant le vecteur d'état donné par (1.4)

$$\mathbf{x}(t) = \left[a_1 \;\; \tau_{12} \;\; \phi_1(t) \;\; \phi_1^{(1)}(t) \ldots \phi_1^{(L_1)}(t) \ldots\ldots a_N \;\; \tau_{N2} \;\; \phi_N(t) \;\; \phi_N^{(1)}(t) \ldots \phi_N^{(L_N)}(t)\right]^T. \tag{1.7}$$

Nous notons que seulement l'ensemble $\{\tau_{n2},\ n = 1, \ldots, N\}$ est pris en considération. Ceci est justifié par le fait que, pour un réseaux de capteurs linéaire et uniforme, les retards restants peuvent sont obtenus en utilisant la relation $\tau_{nm+1} = m\tau_{n2}$, $m = 2, \ldots, M$.

Dans ce cas, le vecteur des paramètres est définit par

$$\theta = [a_1 \; \tau_{12} \; b_{01} \; b_{11} \; \ldots \; b_{L_1 1} \; \ldots\ldots \; a_N \; \tau_{N2} \; b_{0N} \; b_{1N} \; \ldots \; b_{L_N N}]^T. \tag{1.8}$$

Les motivations principales derrières le choix de la structure du vecteur d'état sont: L'obtention d'un nombre minimal d'équations non linéaires et l'estimation directe des fréquences instantanées des signaux, FI, un paramètre très important comme souligné dans [23]. En effet, à partir de (1.4) et (1.7), il est possible d'estimer directement la FI de chaque composante, et donc minimiser l'erreur que pourrait résulter à partir d'une estimation indirecte. L'algorithme proposé est basé sur l'application du FKE M fois: Le premier FKE est appliqué sur le signal non retardé en calculant les valeurs prédises du vecteur d'état et de la matrice de covariance de l'erreur de prédiction. Ceci est suivi par le calcul du gain du FK, les estimées du vecteur d'état et la matrice d'erreur de covariance d'estimation, après l'introduction de l'observation du premier capteur. Le résultat est ensuite utilisé comme prédiction dans le second FKE appliqué sur le signal retardé par τ_{n2}. Le gain de Kalman est alors calculé avec l'estimée du vecteur d'état et la matrice erreur de covariance d'estimation après l'inclusion de la mesure du second capteur. Cette procédure est répétée jusqu'à l'application du M-ème FKE. Les estimées finales de ce dernier filtre constitue la sortie de l'estimateur et sont aussi utilisées par le premier FKE dans les équations de prédiction pour fermer la boucle de l'algorithme.

En utilisant notre approche, l'estimation des angles d'arrivée est pratiquement directe du fait que ces derniers sont liés aux paramètres retard temporels comme nous allons voir ci-dessous.

Considérons N SPPs arrivants sur un réseau d'antenne uniforme et linéaire constitué de M capteurs. Les sorties des capteurs obéissent le modèle présenté dans (1.2) et (1.3).

En considérant les N sources localisées par les directions α_1, α_2,$\cdots$,α_M, les retards temporels τ_{nm} y sont liés par la relation

$$\tau_{nm} = \frac{(m-1)d}{c}\cos(\alpha_n), \quad n = 1, \ldots, N, \quad m = 1, \ldots, M \tag{1.9}$$

Où c est la célérité de propagation des ondes, et d est la distance séparant deux capteurs adjacents. D'où le problème d'estimation des angles d'arrivée est résolu par

le remplacement, dans (1.7) et dans les équation du filtre de Kalman étendu, des paramètres retards temporels $\tau_{n2}, \quad n = 1, \ldots, N$ par les angles d'arrivée correspondants $\alpha_n, \quad n = 1, \ldots, N$, résultant en la relation suivante

$$\mathbf{x}(t) \;=\; \left[a_1 \;\; \alpha_1 \;\; \phi_1(t) \;\; \phi_1^{(1)}(t) \ldots \phi_1^{(L_1)}(t) \ldots\ldots a_N \;\; \alpha_N \;\; \phi_N(t) \;\; \phi_N^{(1)}(t) \ldots \phi_N^{(L_N)}(t)\right]^T,$$

1.4 Résultats de simulation

Un nombre de simulation est effectué pour évaluer les performances de l'algorithme. Ces performances sont mesurées en comparant les erreurs quadratiques moyennes avec les bornes inférieures de Cramèr-Rao, après dérivation de ces dernières en considérant la modélisation du problème, leurs correspondant. Les exemples suivants sont considérés:

1. Cas de *Trois sources* linéairement modulées en fréquence arrivants par des angles différents sur un réseau à *quatres capteurs*. Les ordres des phases des signaux sont supposés connus, puis inconnu (surestimés).

2. Scénario 1. avec la présence de deux sources ayant le m ême angle d'arrivée.

3. Scénario 1. et où les degrés des phases des signaux sont connus et égalant à 5.

4. Signal Chirp à large bande et comparaison avec la méthode de [34].

5. Scénario 1. et comparaison avec la méthode de [19].

6. SPPs à large bande et comparaison avec la méthode de [16].

7. Cas de *trois sources* à large bande arrivants par des angles différents sur un réseau d'antenne à *deux capteurs* (nombre de sources supérieur à celui des capteurs d'antenne)

Les résultats des simulations (illustrés dans Chapitre 5) montrent que la méthode proposée offre des résultats satisfaisants, comparatifs/supérieurs a ceux des méthodes récentes avec un coup de calcul réduit.

1.5 Conclusion

Dans notre étude, nous avons effectué un travail de synthèse des méthodes existantes dans la littérature et traitant le problème d'estimation des paramètres des signaux à phase polynomiale. Nous avons identifié les problèmes et restrictions rencontrées par ces dernières: La majorité des approches proposées sont seulement applicables aux cas des signaux mono- composante. Pour les méthodes extensibles aux cas de signaux à composantes multiples, un rapport signal à bruit élevé est nécessaire pour garantir un bon résultat d'estimation des paramètres. Aussi, la majorité des méthodes existantes n'adressent pas directement le problème de localisation de la source lors de l'identification des signaux, et requièrent l'utilisation de techniques dédiées, rendant le problème de la résolution conjointe de l'identification et la localisation très complexe. De plus, lors du traitement des sources à large bande, la majorité des techniques utilisent une étape de prétraitement et une transformation vers le domaine fréquentiel, augmentant pas cela le co ût de calcul.

Ce travail présente une nouvelle méthodologie combinant la représentation en espace d'état et l'utilisation de la technique du filtrage de Kalman avec l'exploitation de l'information spatiale disponible par le biais d'un réseau d'antenne. Nous avons démontré comment cette association présente de nouvelles perspectives et offre des avantages pour la résolution de problème dans ce domaine:

- L'approche améliore le résultat d'estimation comparée au cas où aucune information spatiale n'est exploitée (utilisation d'un seul capteur)

- L'algorithme est applicable dans les cas de signaux mono-composante ou multi-composantes et permet l'estimation conjointe des paramètres de la phase des signaux et leurs angles d'arrivée.

- Le choix particulier du vecteur d'état permet une estimation directe de la fréquence instantanée des signaux, un paramètre très important dans plusieurs applications, et donc permettant la réduction de son erreur d'estimation.

- la performance de l'algorithme reste assez bonne dans le cas où le nombre des sources est supérieur au nombre des éléments d'antenne, et dans des situations où le degré du polynôme de la phase est inconnu.

- L'approche proposée est applicable pour des situations nécessitants le traitement des signaux en temps réel, ceci gr âce à la nature m ême du filtre de Kalman.

- Finalement, et en particulier, notre approche permet le traitement des signaux à large bande dans le domaine temporel et sans aucun co ût de traitement additionnel (en comparaison avec le cas des signaux à bande étroite).

L'implémentation de l'algorithme sur des DSP ou FPGAs et sa validation en utilisant des signaux réels restent des domaines à explorer. Durant notre travail de recherche, nous avons utilisé uniquement des signaux simulés pour le développement de l'algorithme et l'ensemble de nos résultats est basé sur ces données simulées. Alors que la performance de l'algorithme est consistante avec le test théorique résidant dans la bande inférieure de Cramér-Rao, les données réelles doivent être collectées et utilisées pour vérifier les performances pratique de notre méthode. De plus, les éléments du réseau d'antenne ont été considérés comme identiques et parfaitement calibrés. La robustesse de l'algorithme à ces hypothèses doit être alors étudiée.

PARAMETER ESTIMATION OF MULTI-COMPONENT POLYNOMIAL PHASE SIGNALS: EXPLOITATION OF THE SPATIAL INFORMATION PROVIDED BY AN ANTENNA ARRAY.

A Thesis

Submitted to the Department

of

Electronics and Electrical Engineering

by

Mounir Adjrad

In Fulfillment of the

Requirements for the Degree

of

State Doctorate

Year 2007

National Polytechnic School

El Harrach, Algiers

ABSTRACT

This thesis focuses on the application of a parametric approach to the problem of multicomponent polynomial phase signal parameter estimation. We show how the state-space modellisation and the application of the Kalman filter offer many advantages when combined with the use of multisensor array, exploiting the additional spatial information. Most conventional approaches are limited to processing narrowband data using narrowband assumption to model the problem. For tackling the wideband situation, the majority of the proposed methods require transforming the received signals from the time domain to the frequency domain using the Fourier transform as pre-processing step. Very few authors have dealt with the wideband situation in the time domain.

In this thesis, we recall the definitions of narrowband and wideband signals and their effect on the problem modellisation where we consider a real-valued modellisation, as opposite to the most often used complex-valued modellisation. The drivers behind this choice are: Dealing with narrowband and wideband signals in the time domain using the same algorithm, and the reduction of the computational cost, as opposite to the complex-valued modellisation, optimising by this the memory use. The proposed algorithm can be applied in the monocomponent and multicomponent cases with good performance in the case where there are more sources than array sensors. In addition to the estimation of the signal phase parameters, the resulting algorithm allows the estimation of the source directions of arrivals and the estimation of the order of the polynomial phase (when unknown).

The proposed algorithm is compared to competitive methods and proven to perform as good or better than these latter with reduced computational cost.

ACKNOWLEDGMENTS

The years I spent working on this thesis have been both very challenging and very enjoyable; I had the opportunity to work on a very interesting topic.

I wish to thank Pr. Adel Belouchrani for supervising and supporting my work. His enthusiasm, approachability and patience were essential to the completion of this thesis.

I also would like to thank my parents, brothers, and sisters, who are a great source of support and inspiration, for their encouragement which played an instrumental role in completing this project.

Finally, to all you involved in this chapter of my life - THANK YOU!

TABLE OF CONTENTS

Page

LIST OF TABLES

LIST OF FIGURES

SYMBOLS

x	Scalar
$\mathbf{x}$	Vector
$\mathbf{Y}$	Matrix
$\mathbf{Y}^T$	Matrix transpose
$\mathbf{Y}^H$	Hermitian transpose
$\|\mathbf{Y}\|$	Determinant
$tr(\mathbf{Y})$	Trace of matrix
N	Number of sources
P	Number of snapshots
L	Degree of the phase polynomial
ϕ	Phase of the source signal
M	Number of sensors
d	Antenna inter-elements spacing
c	Velocity of propagation
Δ	Sampling time
α	Direction-of-arrival

ABBREVIATIONS

AML	Asymptotic Maximum Likelihood
AOA	Angle-Of-Arrival
AWGN	Additive White Gaussian Noise
CAF	Complex Ambiguity Function
CC	Computational Cost
CDMA	Code Division Multiple Access
CRLB	Cramér-Rao Lower Bound
CSM	Coherent Signal-subspace Method
CV	Complex Valued
DOA	Direction-Of-Arrival
DSP	Digital SignalProcessors
EKF	Extended Kalman Filter
FIM	Fisher Information Matrix
FM	Frequency Modulation
FPGA	Field-Programmable Gate Array
FT	Fourier Transform
GSM	Global System for Mobile Communication
HAF	High-order Ambiguity Function
HT	Hilbert Transform
IF	Instantaneous Frequency
KF	Kalman Filter
LL	Log-Likelihood
MC	Multicomponent
MCPPS	Multicomponent Polynomial Phase Signal

ML	Maximum Likelihood
M-MUSIC	Modified MUSIC
MSE	Mean Square Error
MUSIC	MUltiple SIgnal Classification
PHAF	Product High-order Ambiguity Function
PPS	Polynomial Phase Signal
PPT	Polynomial Phase Transform
RV	Real Valued
SNR	Signal-to-Noise Ratio
TCT	Two-sided Correlation Transformation
TDMA	Time Division Multiple Access
ULA	Uniform Linear Array

1. INTRODUCTION

Statistical methods for signal processing have a wide range of different applications, such as, for example, radar, sonar, wireless communications, telephony, and geophysics. However, the objectives are often the same, namely, the extraction of parameters of interest from noisy observations.

Array signal processing focuses on signals conveyed by propagating waves. An array of sensors located at distinct spatial locations is deployed to measure a propagating electromagnetic, acoustic, or seismic wavefield. The goals of array signal processing are to combine sensor' outputs cleverly so as: To characterize the field by detecting the number of sources and locating these sources; to track the instantaneous positions of the sources as they move in space; and to enhance the quality of the target sources by spatial filtering the interfering sources and noises.

Depending on the application, the processing might be batch mode or off-line, where the data are collected before processing, or sequential or online, when the algorithm proceeds as the observations are collected. There are many classical methods of either type, addressing each of the objectives.

Particular and commonly used signals used in the different applications are the constant amplitude, time varying phase signals [1], because they are relatively easy to generate and have a good power efficiency. Continuous phase is used in some cases (eg., analog FM), while in other cases the phase is discontinuous (e.g., phase-shift keying or direct spread spectrum). Constant amplitude, polynomial phase signals will be considered in this thesis.

1.1 *Array Processing*

Sensor arrays have been in use for several decades in many practical signal processing applications. An array is used to filter signals in a space-time field by exploiting their spatial and temporal characteristics. This filtering may be expressed in terms of a dependence upon angle or wavenumber.

An array consists of a set of sensors that are located at different points in space with respect to a common reference point. These sensors listen to the incoming signals and provide a means of sampling these signals in space. Depending on the sensor characteristics and the propagation path, the source waveforms undergo deterministic and/or random modifications. The sensor outputs are composed of these signal components and additive contaminations such as measurement noise and thermal noise. The outputs are combined such that target signals from a set of angles are enhanced by a constructive combination and unwanted signals from other angles are rejected by destructive combination. Sensor array systems can be divided into two classes: active and passive. In active sensing situations, a known waveform of finite duration is generated, which in turn propagates through a medium and is reflected by some target back to the point of origin. The transmitted signal is usually modified both in amplitude and phase by the target characteristics, which by themselves might be changing with time and its position in space. These disturbances give rise to a random return signal. In the passive context the signal received at the array is generated by the target, such as propeller or engine noise from submarines.

Applications for sensor arrays [2], [3] include the following areas:

Radar - Radar is the area in which antenna arrays were first used. Most radar systems are active, and the antenna array is used for both transmission and reception of signals. Radar technologies are used in military applications, including ballistic missile detection and numerous airborne systems. On the other hand, non-military applications include air traffic control, depth-sounding, impulse radar, etc.

Radio Astronomy - Unlike radar systems, radio astronomy systems are passive and are used to detect celestial objects and estimate their characteristics. These systems usually employ arrays with very long baselines, extending from hundreds of meters to nearly the diameter of the earth.

Sonar - Sonar systems can be active or passive. The theory of active sonar systems has much in common with radar, but sonar systems deal with acoustic energy into the water while the radar systems deal with electromagnetic energy in the atmosphere. The main application in sonar systems is the detection and tracking of submarines, and in the fishing industry for detecting schools of fish.

Seismology - There are two main areas of seismology in which array processing plays an important role. The first area is the detection and location of underground nuclear explosions. The other area is exploration seismology that is to construct an image of the subsurface in which the structure and physical properties are described.

Tomography - Tomography is the cross-sectional imaging of objects from transmitted or reflected data. The object is illuminated from a number of different directions and data are collected at a receiving array. The cross-sectional image can then be reconstructed from the data. Medical diagnosis and treatment are examples of successful applications of tomography.

Communications - Antenna arrays are used in many communication systems. Several satellite systems utilize phased arrays in either the earth terminal or space segment for applications like tracking and data relay. Wireless cellular systems also utilize various types of multiple access techniques such as Time Division Multiple Access (TDMA), Code Division Multiple Access (CDMA), and Global System for Mobile

Communications (GSM).

Array processing deals with methods for processing the sensors' output data in the above applications in order to obtain insight into the structure of the waves traversing the array. The practical problems of interest in array signal processing are extracting the desired parameters such as the directions-of-arrival (DOA), power levels, impinging signal parameters, and cross-correlations of the signals present in the scene from the available information including the measured data. Often one may also be specifically interested in the actual waveform corresponding to one of these sources, and in that case it is necessary to estimate the actual waveform associated with the desired signal while at the same time suppress the other signals. At times, the desired signal structure might be only known partially, and the objective in that case is to detect its presence in the available noisy data. This situation is often encountered in sonar to detect the presence of the signature of a specific class of submarine. Though the signal structure is known, it may still contain unknown parameters such as angle-of-arrival (AOA) or random phase. All these problems fall into one of two categories: detection or estimation of signals. In cases where the AOA of the signals are time-varying, instantaneous estimation or tracking will be deployed.

1.2 *Polynomial Phase Signals*

Since many years and till now the signal processing scientific community paid a particular attention to the study of polynomial phase signals (PPS). The phase of these signals can be modelled by a polynomial that we note $\phi(t)$. In the case the degree of $\phi(t)$ is greater or equal to 2, the PPS are non stationary. PPS occur both in nature and in man-made applications [4]. For example, the sonar systems of some bats use hyperbolic and quadratic PPS for echo location. Some radar systems use quadratic PPS pulse compression signals. Earthquake and underground nuclear tests may generate nonlinear PPS seismic signals in some long-propagation modes. The

altitude and speed of an aircraft may be estimated from the nonlinear instantaneous frequency (IF) of the engine noise reaching the ground. PPS signals also appear in communications, astronomy, telemetry, and other disciplines. Moreover, due to the Stone-Weierstrass theorem [5], any continuous function over a closed interval can be approximated uniformly by a polynomial function. This approximation theorem assures that polynomial approximation can get arbitrarily close to any continuous function as the polynomial order is increased. Let $f(x)$ be continuous on a real interval I. Then for any $\varepsilon > 0$, there exists an nth-order polynomial $P_n(f, x)$, where n depends on ε, such that $|P_n(f, x) - f(x)| < \varepsilon$ for all $x \in I$. Thus, any continuous function can be well approximated arbitrarily by means of a polynomial.

The majority of applications treat the PPS parameter estimation considering the noisy signal $y(t)$ given by

$$\begin{cases} y(t) = aexp[j\phi(t)] + v(t) \\ \phi(t) = \sum_{l=0}^{L} b_l t^l \end{cases} \tag{1.1}$$

The signal amplitude a is assumed constant and the polynomial phase $\phi(t)$ is of degree L (for $L = 2$, the PPS is called chirp). The amplitude and instantaneous phase are real valued. The signal $v(t)$ is an additive white Gaussian noise (AWGN) independent from the PPS.

1.3 *Scope of the Thesis*

This thesis focuses on the application of a parametric approach to the problem of multicomponent polynomial phase signal parameter estimation. We show how the state-space modellisation and the application of the Kalman filter offer many advantages when combined with the use of multisensor array, exploiting the additional spatial information.

Most conventional approaches are limited to processing narrowband data using narrowband assumption to model the problem. The majority of the proposed methods for tackling the wideband situation require transforming the received signals from the

time domain to the frequency domain using Fourier transform as pre-processing step. Very few authors have dealt with the wideband situation in the time domain. In these methods, it is assumed that the instantaneous signal frequencies do not change during the time necessary for a wave to travel across the array aperture. This assumption means that the signals remain narrowband in each snapshot, i.e., their instantaneous bandwidths are small compared with the inverse of the wavefront propagation time across the array. Still the authors consider the signals to be wideband at the full observation interval because the propagation time across the aperture is usually much smaller than the sampling interval.

In this thesis, we highlight the definition of wideband signals and its effect on the problem modellisation where we consider a real-valued (RV) modellisation, opposite to the most often used complex-valued (CV) modellisation. The drivers behind this choice are: Dealing with narrowband and wideband signals in time domain using the same algorithm, and the reduction of the computational cost, as opposite to the complex-valued modellisation, optimising by this the memory use.

The proposed algorithm can be applied in the monocomponent and multicomponent cases with good performance in the case where there are more sources than array sensors. In addition to the estimation of the PPS signal phase parameters, the resulting algorithm allows the estimation of the direction of arrival of the sources and the estimation of the order of the polynomial phase (when unknown).

1.4 *Thesis Organization*

The thesis is divided into five main chapters and a concluding chapter:

- Chapter 2 presents the different array processing methods adapted to the PPSs parameter estimation problem and highlights the definition of narrowband and wideband source cases.

- Chapter 3 presents the details of the proposed algorithm where a state-space modellisation is proposed and the Kalman filter technique is used to estimate the source parameters.
- Chapter 4 presents the DOAs estimation problem and the application of our method to the estimation of these parameters.
- Chapter 5 presents the performance evaluation of the algorithm applied for the case of a chirp signal, and multicomponent PPSs as well as the derivation of the Cramér-Rao Lower Bound (CRLB).
- Finally, the conclusion of the thesis is presented as Chapter 6.

2. ARRAY PROCESSING TECHNIQUES AS PPS ANALYSIS TOOLS

PPSs belong to the class of non-stationary signals, rending the methods for processing these latter applicable to the formers. Example of previous work analysing PPSs can be found in [6] - [9]. As mentioned at the beginning of Chapter 1, the objectives of statistical methods for signal processing are the extraction of parameters of interest from noisy observations. We classify the parameter estimation techniques into two main categories, namely spectral-based (non-parametric) and parametric approaches. In the former, one forms some spectrum-like function of the parameter(s) of interest, e.g., the AOA. The locations of the highest (separated) peaks of the function in question are recorded as the AOA estimates. Parametric techniques, on the other hand, require a simultaneous search for all parameters of interest. The latter approach often results in more accurate estimates, but at the expense of an increased computational complexity. In the following section, we list these different techniques in the context of PPS processing approaches.

2.1 *Non-parametric Approaches*

2.1.1 Capon's method for PPSs estimation

In [10], the author proposes a modified version of Capon's estimator for the analysis of PPSs. By considering a multicomponent PPS:

$$s(t) = \sum_{n=1}^{N} a_n e^{j\phi_n(t)}, \quad t = 0, \ldots, P-1, \tag{2.1}$$

where the amplitudes a_n are constant and every phase ϕ_n is a polynomial of degree L_n. By passing the signal $s(t)$ through a variable filter of order p such that only one

component with polynomial phase is selected at a time. The filter output for the phase $exp[j\phi_n(t)]$ is given by:

$$H(t,\mathbf{b}) = \sum_{u=t-p}^{t} h(t,u)e^{-j[\phi(t)-\phi(u)]} = \mathbf{h}^T\mathbf{b}_p(t,\mathbf{b}). \tag{2.2}$$

Where $\mathbf{h}(t)$ is the impulsive response of the filter given by

$$\mathbf{h}(t) = [h(t,t), h(t,t-1), \ldots, h(t,t-p)]^T, \tag{2.3}$$

and the vector $\mathbf{b}_p(t,\mathbf{b})$ is given by

$$\mathbf{b}_p(t,\mathbf{b}) = \left[1, e^{-j[\phi(t)-\phi(t-1)]}, \ldots, e^{-j[\phi(t)-\phi(t-p)]}\right]^T. \tag{2.4}$$

The vector $\mathbf{b} = [b_1, b_2, \ldots, b_L]$ includes the coefficients of the phase functions

$$\phi(t) = \sum_{i=1}^{L} b_i t^i. \tag{2.5}$$

In order to select a component with polynomial phase of the signal of (2.1), we need to resolve the minimisation problem

$$min_{\mathbf{h}(t)}\mathbf{h}^T(t)\mathbf{R}_{s,p}(t)\mathbf{h}^*(t), \tag{2.6}$$

under the constraint

$$\mathbf{h}^T(t)\mathbf{b}_p(t,\mathbf{b}) = 1. \tag{2.7}$$

The solution of (2.6) is obtained through quadratic minimisation and is given by

$$\mathbf{h}^*_{opt}(t) = \frac{\mathbf{R}^{-1}_{s,p}\mathbf{b}_p(t,\mathbf{b})}{\mathbf{b}_p(t,\mathbf{b})\mathbf{R}^{-1}_{s,p}(t)\mathbf{b}_p(t,\mathbf{b})}. \tag{2.8}$$

We obtain a time-coefficient representation

$$P_{M-Capon}(t,\mathbf{b}) = \frac{1}{\mathbf{b}^H_p(t,\mathbf{b})\mathbf{R}^{-1}_{s,p}(t)\mathbf{b}_p(t,\mathbf{b})}, \tag{2.9}$$

where $\mathbf{R}_{s,p}(t)$ is the autocorrelation matrix of vector $\mathbf{s}(t)$ defined by

$$\mathbf{s}(t) = [s(t), s(t-1), \ldots, s(t-p)]^T . \tag{2.10}$$

The idea of modified Capon's estimator (M-Capon) for the PPS coefficients estimation consists of performing a sweep using a family of polynomial phase rather than a sweep on the frequency axis as is the case for the classical capon's estimator of pure frequencies.

We notice that $\mathbf{R}_{s,p}$ is a singular matrix since it is estimated through a single realisation vector. To calculate the inverse of $\mathbf{R}_{s,p}$ in (2.9), we need to add a diagonal load

$$\mathbf{R}_{s,p}(t) = E\left\{\mathbf{s}(t)\mathbf{s}^H(t)\right\} + \rho\mathbf{I}, \quad \rho > 0. \tag{2.11}$$

The expression of $\mathbf{R}_{s,p}^{-1}$ is obtained using the lemma of matrix inversion

$$\mathbf{R}_{s,p}^{-1}(t) = \frac{1}{\rho}\left(\mathbf{I} - \frac{\mathbf{s}(t)\mathbf{s}^H(t)}{\rho + \mathbf{s}(t)\mathbf{s}^H(t)}\right). \tag{2.12}$$

Capon's modified estimator can be re-written under the following form parameterized by ρ

$$P_{M-Capon}(t, \mathbf{b}, \rho) = \frac{\rho}{(\rho+1)\left[|\mathbf{b}_p(t, \mathbf{b})\mathbf{s}(t)|^2/(\rho + \|\mathbf{s}(t)\|^2)\right]}. \tag{2.13}$$

We conclude that Capon's method relies on the addition of a diagonal matrix $\rho\mathbf{I}$ that will allow the inversion of the signal autocorrelation matrix. The choice of ρ in equation (2.13) influence the performance of the estimator.

2.1.2 MUSIC algorithm for PPS parameters estimation

We suppose that PPSs are affected by a Gaussian noise. The modified Multiple Signal Classification (MUSIC) estimator (M-MUSIC) is defined by [11]

$$P_{M-MUSIC}(t, \mathbf{b}) = \frac{1}{\mathbf{b}_p^H(t, \mathbf{b})\mathbf{E}_{s,p}\mathbf{E}_{s,p}^H\mathbf{b}_p(t, \mathbf{b})}. \tag{2.14}$$

Where the matrix $\mathbf{E}_{s,p} = [e_{Q+1}, e_{Q+2}, \ldots, e_p]$ is obtained through eigenvalues decomposition of $\mathbf{R}_{s,p}$ and by retaining the eigenvectors associated with the $p - Q$ smallest eigenvalues of $\mathbf{R}_{s,p}$. The inverse of $\mathbf{R}_{s,p}$ can be written as follows [12]

$$\mathbf{R}_{s,p}^{-1}(t) = \frac{1}{\sigma_\omega^2}\left[\mathbf{I} - \sum_{i=1}^{p} \mathbf{v}_i (1 + \frac{\sigma_\omega^2}{\lambda_i})^{-1} \mathbf{v}_i^H\right], \tag{2.15}$$

where $\mathbf{v}_i$ and λ_i are the eigenvectors and eigenvalues of $\mathbf{R}_{s,p}$, respectively. For the multicomponents signal given by (2.1), the eigenvectors are proportional to the signal components. This results into a linear combination of the spectrograms of each component normalised by its amplitude [12]

$$P_{M-MUSIC}(t, \mathbf{b}) = \frac{1}{(p+1) - \sum_{n=1}^{Q} SPEC_{s_n}(t, \mathbf{b})/b_n^2}, \tag{2.16}$$

where $SPEC_{s_n}$ are the spectrograms of the eigenvectors. The theoretical study shows that Capon's and MUSIC estimators adapted to PPSs parameter estimation are written in function of the spectrogram and possess the same resolution capability for two coefficients belonging to two different components. However, MUSIC estimator presents two major advantages compared to Capon's estimator. The first advantage permits to avoid the diagonal loading of the signal autocorrelation matrix and hence the choice of the parameter ρ. The second advantage is that the signal and noise sub-spaces can be obtained without passing through the decomposition of the autocorrelation matrix by using techniques such as the propagator [13] - [15] that allows reducing the computation complexity.

2.2 *Parametric Methods*

While the spectral-based methods presented in the previous section are computationally attractive, they do not always yield sufficient accuracy. In particular, for scenarios involving highly correlated (or even coherent) signals, the performance of spectral-based methods may be insufficient. An alternative is to more fully exploit the underlying data model, leading to the so-called parametric array processing methods.

For such methods, coherent signals impose no conceptual difficulties. The price to pay for this increased efficiency and robustness is that the algorithms typically require a multidimensional search to find the estimates.

2.2.1 Maximum Likelihood Approach

Perhaps the most well known and frequently used model-based approach in signal processing is the maximum likelihood (ML) technique. This methodology requires a statistical framework for the data generation process. Let us consider a monocomponent PPS defined by (1.1) where the noise is assumed complex-valued, white, and Gaussian of variance σ^2. The analytic version of the noise-corrupted observed signal has $x(t)$ as real part and $z(t)$ as imaginary part. The noise-free signal real and imaginary parts are $s(t,\theta)$ and $r(t,\theta)$, respectively. The parameter vector is given by $\theta = [a, b_0, b_1, \ldots, b_L]^T$. The probability density function of $y(t)$ is

$$p(y,\theta) = \frac{1}{\sigma^2 2\pi} exp\left[\frac{-1}{2\sigma^2}\sum_{t=0}^{P-1}\left(x(t)-s(t,\theta)\right)^2 + \left(z(t)-r(t,\theta)\right)^2\right]. \tag{2.17}$$

The ML estimate of θ needs that p, (or $log(p)$) be maximized over θ. The maximum value of p happens at the maximum of

$$\Lambda_0 = -\frac{1}{P}\sum_{t=0}^{P-1}\left[\left(x(t)-s(t,\theta)\right)^2 + \left(z(t)-r(t,\theta)\right)^2\right]. \tag{2.18}$$

Given $\sum x^2(t)$ and $\sum z^2(t)$ (corresponding to the observed signal energy) are independent of θ, the maximization of Λ_0 over the parameter vector is equivalent to the maximization of

$$\Lambda = \frac{2}{P}\sum_{t=0}^{P-1}\left[x(t)s(t,\theta) + z(t)r(t,\theta)\right] - \frac{1}{P}\sum_{t=0}^{P-1}\left[s^2(t,\theta) + r^2(t,\theta)\right]. \tag{2.19}$$

By replacing $s(t,\theta)$ and $r(t,\theta)$ by their respective expressions given by $s(t,\theta) = a\cos\left[j\sum_{l=0}^{L} b_l t^l\right]$ and $r(t,\theta) = a\sin\left[j\sum_{l=0}^{L} b_l t^l\right]$; we then get

$$\Lambda = 2a\Re\left[exp(-jb_0)f(b_1, b_2, \ldots, b_L)\right] - a^2. \tag{2.20}$$

Where the function f, of L variables, is given by

$$f(b_1, b_2, \ldots, b_L) = \frac{1}{P}\sum_{t=0}^{P-1}\left[y(t)exp\left(-j\sum_{i=1}^{L}(b_i t^i)\right)\right]. \tag{2.21}$$

The maximization of Λ over the initial phase b_0 is analytically determined by the following expression $\hat{b}_0 = arg[f(b_1, b_2, \ldots, b_L)]$. By replacing that expression in (2.20), we obtain $\Lambda = 2a_0|f(b_1, b_2, \ldots, b_L)| - a^2$. Similarly, we can determine the analytical expression of the amplitude a that maximizes the function Λ: $\hat{a} = |f(b_1, b_2, \ldots, b_L)|$. Hence, the function to maximize is written as

$$\Lambda = |f(b_1, b_2, \ldots, b_L)|^2. \tag{2.22}$$

The ML solution requires the maximization of Λ (2.22) over the L unknowns $b_1, b_2, \ldots, b_L$.

Hence, the search space dimension has been reduced from $(L+2)$ to L. Nevertheless, the function to maximize is non-linear rending its maximization non resolvable analytically where there is need to use numerical optimization methods (The convergence of these numerical methods is not guaranteed except at the neighbourhood of the optimal value). A bad initialisation of the algorithm might conduct the optimization procedure to finding a local optimum. The presented ML technique has limited application to the PPS case because they do not take any advantage of the specific PPS structure. A novel ML algorithm has been developed in [16]overcoming this problem. Assuming N constant amplitude PPSs impinging on a linear array of M omnidirectional sensors. Then, the vector array outputs obey the following model:

$$\mathbf{y}(t) = \mathbf{W}(t)\mathbf{s}(t) + \mathbf{v}(t), \quad t = 0, 1, \ldots, P-1. \tag{2.23}$$

Where

$\mathbf{W}(t)$: MxN time-varying direction matrix

$\mathbf{s}(t)$: $Nx1$ vector of non-stationary source waveforms

$\mathbf{v}(t)$: $Mx1$ vector of complex circularly Gaussian zero-mean temporally and spatially white sensor noise

P: Number of snapshots

The n-th polynomial phase source waveform can be modelled as

$$\begin{aligned} s_n(t) &= a_n e^{j\left(b_{n,0}t+b_{n,1}t^2/2+\ldots+b_{n,L-1}t^L/L\right)} \\ &= a_n g(\mathbf{b}_n, t). \end{aligned} \tag{2.24}$$

Where

$$g(\mathbf{b}_n, t) \triangleq exp\left(j\sum_{l=0}^{L-1} b_{n,l}\frac{t^{l+1}}{1+l}\right), \tag{2.25}$$

and a_n is the initial amplitude, $b_{n,l}$ $(n = 1, 2, \ldots, N; l = 0, 1, \ldots, L-1)$ are the unknown discrete-time frequency parameters, and

$$\tilde{b}_n(t) = \sum_{l=0}^{L-1} b_{n,l}t^l, \tag{2.26}$$

is the discrete-time instantaneous frequency of the n-th waveform.

The $L \times 1$ vector $\mathbf{b}_n \triangleq [b_{n,0}, b_{n,1}, \ldots, b_{n,L-1}]^T$ contains the unknown discrete-time frequency parameters of the n-th signal, and L is the order of the polynomial phase model, assumed known. The direction matrix

$$\begin{aligned} \mathbf{W}(\alpha, \tilde{\mathbf{b}}) &\triangleq \left[\mathbf{w}(\alpha_1, \tilde{b}_1(t)), \ldots, \mathbf{w}(\alpha_L, \tilde{b}_L(t))\right] \\ &= [\mathbf{w}(\alpha_1, \mathbf{b}_1, t), \ldots, \mathbf{w}(\alpha_L, \mathbf{b}_L, t)] \\ &= \mathbf{W}(\alpha, \mathbf{B}, t), \end{aligned} \tag{2.27}$$

consists of the time-varying steering vector

$$\mathbf{W}(\alpha_n, \mathbf{b}_n, t) = \left[1, exp\left(j\frac{\tilde{\mathbf{b}}_n(t)}{c\Delta t}d_1 \sin\alpha_l\right), \ldots, exp\left(j\frac{\tilde{\mathbf{b}}_n(t)}{c\Delta t}d_{M-1}\sin\alpha_l\right)\right]^T, \quad (2.28)$$

where

$$\begin{aligned} \alpha &\triangleq [\alpha_1, \alpha_2, \ldots, \alpha_N]^T \\ \mathbf{B} &\triangleq \left[\mathbf{b}_1^T, \mathbf{b}_2^T, \ldots, \mathbf{b}_N^T\right]^T \\ \tilde{\mathbf{b}}(t) &\triangleq \left[\tilde{b}_1(t), \tilde{b}_2(t), \ldots, \tilde{b}_N(t)\right]^T, \end{aligned} \quad (2.29)$$

where α_l is the DOA of the n-th source, and d_i is the spacing between the first and the $(i+1)$-th array sensor. As follows from (2.27), the direction matrix can be written as a function either of the frequency parameters or of instantaneous frequencies (2.29). Note that in (2.28), it is assumed that the instantaneous signal frequencies $\tilde{b}_n(t)(t = 0, \ldots, P-1)$ do not change during the time necessary for a wave to travel across the array aperture.

Using (2.24)-(2.29), model (2.23) can be rewritten as

$$\begin{aligned} \mathbf{y}(t) &= \mathbf{W}(\alpha, \mathbf{B}, t)\mathbf{G}(\mathbf{B}, t)\mathbf{a} + \mathbf{v}(t) \\ &= \tilde{\mathbf{W}}(\alpha, \mathbf{B}, t)\mathbf{a} + \mathbf{v}(t). \end{aligned} \quad (2.30)$$

Where

$$\begin{aligned} \mathbf{a} &\triangleq [a_1, a_2, \ldots, a_N]^T \\ \mathbf{G}(\mathbf{B}, t) &\triangleq diag\left\{g(\mathbf{b}_1, t), \ldots, g(\mathbf{b}_n, t)\right\} \\ \tilde{W}(\alpha, \mathbf{B}, t) &\triangleq \mathbf{W}(\alpha, \mathbf{B}, t)\mathbf{G}(\mathbf{B}, t). \end{aligned} \quad (2.31)$$

Note that all nuisance parameters (the initial source amplitudes) are now included in the vector $\mathbf{a}$.

The ML estimator of the source DOAs and frequency parameters is derived [16] based on the assumption that the initial signal amplitudes are constant (deterministic) values. The negative log-likelihood (LL) function is given by

$$\begin{aligned} L_p(\theta) &= \sum_{t=0}^{P-1} \|\mathbf{y}(t) - \mathbf{W}(\alpha, \mathbf{B}, t)\mathbf{G}(\mathbf{B}, t)\mathbf{a}\|^2 \\ &= \sum_{t=0}^{P-1} \|\mathbf{y}(t) - \tilde{\mathbf{W}}(\alpha, \mathbf{B}, t)\mathbf{a}\|^2, \end{aligned} \tag{2.32}$$

where the vector of unknown model parameters is defined as

$$\theta \triangleq \left[\alpha^T, \mathbf{B}^T, \mathbf{a}^T\right]^T. \tag{2.33}$$

Rewrite (2.32) as

$$\begin{aligned} L_p(\theta) &= \mathbf{a}^H \left\{\sum_{t=0}^{P-1} \tilde{\mathbf{W}}^H(\alpha, \mathbf{B}, t)\tilde{\mathbf{W}}(\alpha, \mathbf{B}, t)\right\}\mathbf{a} - \left\{\sum_{t=0}^{P-1} \mathbf{y}^H(t)\tilde{\mathbf{W}}(\alpha, \mathbf{B}, t)\right\}\mathbf{a} \\ &\quad -\mathbf{a}^H \left\{\sum_{t=0}^{P-1} \tilde{\mathbf{W}}^H(\alpha, \mathbf{B}, t)\mathbf{y}(t)\right\} + \sum_{t=0}^{P-1} \mathbf{y}^H(t)\mathbf{y}(t). \end{aligned} \tag{2.34}$$

The minimization of L_p over $\mathbf{a}$ leads to

$$\hat{\mathbf{a}} = \left\{\sum_{t=0}^{P-1} \tilde{\mathbf{W}}^H(\alpha, \mathbf{B}, t)\tilde{\mathbf{W}}(\alpha, \mathbf{B}, t)\right\}^{-1} \left\{\sum_{t=0}^{P-1} \tilde{\mathbf{W}}^H(\alpha, \mathbf{B}, t)\mathbf{y}(t)\right\}. \tag{2.35}$$

Substituting (2.35) into (2.34), we obtain the concentrated negative LL function

$$\begin{aligned} L_p(\alpha, \mathbf{B}) &= \sum_{t=0}^{P-1} \mathbf{y}^H(t)\mathbf{y}(t) - \left\{\sum_{t=0}^{P-1} \mathbf{y}^H\tilde{\mathbf{W}}(\alpha, \mathbf{B}, t)\right\} \times \\ &\quad \left\{\sum_{t=0}^{P-1} \tilde{\mathbf{W}}^H(\alpha, \mathbf{B}, t)\tilde{\mathbf{W}}(\alpha, \mathbf{B}, t)\right\}^{-1} \times \left\{\sum_{t=0}^{P-1} \tilde{\mathbf{W}}^H(\alpha, \mathbf{B}, t)\mathbf{y}(t)\right\} \end{aligned} \tag{2.36}$$

Ignoring the constant terms, the positive concentrated LL function is given by

$$L_p(\alpha, \mathbf{B}) = \left\{ \sum_{t=0}^{P-1} \mathbf{y}^H \tilde{\mathbf{W}}(\alpha, \mathbf{B}, t) \right\} \times \left\{ \sum_{t=0}^{P-1} \tilde{\mathbf{W}}^H(\alpha, \mathbf{B}, t) \tilde{\mathbf{W}}(\alpha, \mathbf{B}, t) \right\}^{-1} \times \left\{ \sum_{t=0}^{P-1} \tilde{\mathbf{W}}^H(\alpha, \mathbf{B}, t) \mathbf{y}(t) \right\}. \quad (2.37)$$

The ML estimator is then

$$\left[\hat{\alpha}, \hat{\mathbf{B}} \right] = argmax_{\alpha, \mathbf{B}} L_p(\alpha, \mathbf{B}). \quad (2.38)$$

The above estimator jointly estimates the source directions and their frequency parameters α and $\mathbf{B}$, respectively, and generally requires a highly nonlinear optimization of (2.37) over these variables. However, if properly initialized, the optimization of the LL function may be implemented by means of simple local optimization algorithms.

2.2.2 High Ambiguity Function

PPS detection algorithms such as the HAF have been used and evaluated in previous works [17]. They can be studied from the perspective of complex ambiguity function (CAF) [18]. This method realizes the PPS detection by exploiting the origin passing property of an auto-term in a CAF plane. Let's first define the CAF. By considering the noise-free signal model (chirp signal case):

$$s(t) = \sum_{n=1}^{N} s_n(t) = \sum_{n=1}^{N} a_n e^{j\left(\phi_n + 2\pi f_n t + 0.5\gamma_n t^2\right)}. \quad (2.39)$$

With $s(t)$ having limited time and frequency supports $|s(t)| = 0$ for $|t| > \frac{T}{2}$ and for $|S(f)| = 0$ for $|f| > \frac{F}{2}$ (S being the Fourier transform of s). The CAF of $s(t)$ is defined as:

$$A(\upsilon, \tau) = \int R(t, \tau) e^{-j2\pi\upsilon t} dt = \sum_{n,i}^{N} A_{s_{ni}}(\upsilon, \tau). \quad (2.40)$$

Where υ and τ represent the frequency shift and time delay variables, respectively. $R(t,\tau)$ is the temporal correlation function of s.

The terms with $n = i$ are called auto-terms and are given by:

$$A_{s_{nn}}(\epsilon,\tau) = \begin{cases} \int_{-\frac{1}{2}(T-|\tau|)}^{\frac{1}{2}(T-|\tau|)} s_n\left(t+\frac{\tau}{2}\right) s_n^*\left(t-\frac{\tau}{2}\right) e^{-2j\pi\upsilon t} dt = a_n^2\left(T-|\tau|\right) e^{j2\pi f_n \tau} \times \\ sinc\left[\left(\upsilon - \frac{\tau\gamma_n}{2\pi}\right)\left(T-|\tau|\right)\right], \quad |\tau| \leq T \\ 0, \quad Otherwise \end{cases} \tag{2.41}$$

A peak point along the υ axis can be found at $\left(\frac{\tau\gamma_n}{2\pi}\right)$.

Polynomial phase transform (PPT) and its spectral form, high-order ambiguity function (HAF) are developed below to process monocomponent PPS's. An L-th order PPS signal is given as

$$s(t) = ae^{j\phi(t)}. \tag{2.42}$$

with $\phi(t) = \sum_{l=0}^{L} b_l t^l$.

For $\tau \neq 0$, a second order PPT operation can be defined as $PPT_2[s,\tau] = s(t+\tau)s(t-\tau)$.

A higher order operators is then defined iteratively

$$PPT_L[s,\tau] = PPT_2\left[PPT_{L-1}[s,\tau]\right]. \tag{2.43}$$

Since a second order operator applies a difference operation on the L-th order phase function $\phi(t)$, its result is a phase function with $(L-1)$-th order. The iterative use of PPT_2 operator, which equivalent to a higher order operator, reduces $s(t)$ to a single tone sinusoid with a constant amplitude. For $s(t)$ defined by (2.39)

$$PPT_L[s,\tau] = b^{2^{L-1}} e^{j\hat{\omega}t+\hat{\phi}}. \tag{2.44}$$

With

$$\begin{aligned}\hat{\omega} &= L!\tau^{L-1}b_L \\ \hat{\phi} &= (L-1)!\tau^{L-1}b_{L-1} - 0.5L!(L-1)\tau^L b_L. \end{aligned} \tag{2.45}$$

By using spectral analysis methods, we can determine $\hat{\omega}$ from $PPT_L[s,\tau]$ and thus obtain the L-th order coefficient b_L. The lower order coefficients can then be calculated by an $L-1$ order operation PPT_{L-1} on a demodulated signal. By repeating this procedure, all the coefficients b_l can then be determined.

By taking a Fourier transform on an L-th order PPT, we obtain an L-th order HAF which can be expressed as an operator by

$$HAF_L[s,\tau,\upsilon] = \int_{-\infty}^{\infty} PPT_L[s,\tau]e^{-j2\pi\tau\upsilon}. \tag{2.46}$$

Since HAF_L is simply L consecutive HAF_2 operations, we only consider HAF_2 in the remaining explanation.

From its definition, we see that HAF_2 is related to the (CAF). For each τ, an application of HAF_2 forms a CAF line that is parallel to the υ-axis of the CAF plane, and this line intercepts the τ-axis of the CAF plane at 2τ. From this, we can see that the detection of $\hat{\omega}$ is simply a pulse searching along the points of this υ-axis. HAF can fail when an auto-term line demonstrates modulus variation, this happens when an auto-term is generated from a chirp group. It can fail when a cross-term appears as a ridge, which can create a pulse appearance on any line parallel to the υ-axis.

An enhanced version of HAF, called Product High-order Ambiguity Function (PHAF) was developed by taking the product of several HAF's of the same order but with different lags as the chirp detector function (reference [19] provides detailed explanation of the algorithm implementation). Seeking simplicity, we consider the use of $PHAF_2$.

A simple illustration of $PHAF_2$ is given in Figure 2.1 that shows a CAF plane of a signal containing two chirps of a same rate.

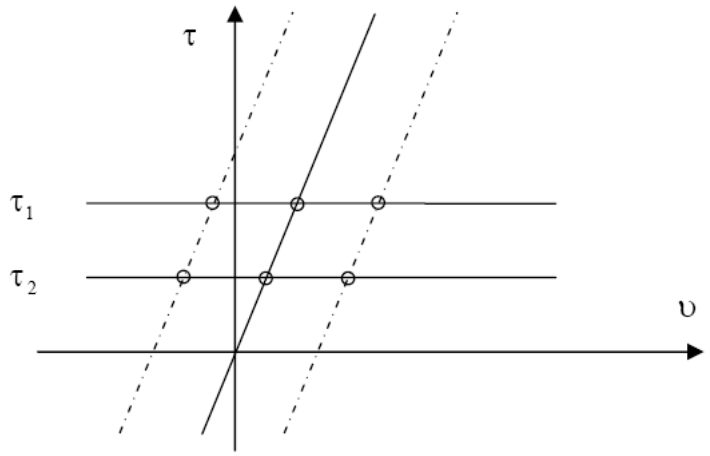

Fig. 2.1. $PHAF_2$ Auto-term Identification

In the figure, two cross terms, shown as dashed lines also appear as ridge lines on the CAF plane. By using only one lag $\tau = \tau_1$, HAF has no way to tell which one of the three non-zero value points, indicated by the interchanging points along the line $\tau = \tau_1$, originates from the auto-term.

Compared to this, $PHAF_2$ introduces an extra CAF line with a different lag τ_2, and by doing so three more non-zero points can be identified on the line $\tau = \tau_2$.

Taking one non-zero point from each of the two υ-axis parallel lines to form a pair, we have nine point pairs altogether. Among these pairs, only one can form an origin-passing line on the CAF plane. This line indicates not only the existence but also the chirp rate of the auto-term.

The chirp detector function of the PHAF algorithm can be written as

$$\eta(\gamma_c) = \prod_{i=1}^{I} \left| A\left(\frac{\gamma_c \tau_i}{2\pi}, \tau_i\right) \right|. \tag{2.47}$$

Where $\{\tau_i, i = 1, 2, \ldots, I\}$ are the lags used for the HAF operators, and γ_c is a candidate chirp rate under testing.

The HAF alone can do nothing against spurious harmonics, not even in the asymptotic case. To eliminate these undesired components, it is necessary to use the PHAF

operator, consisting of the multiplication of scaled HAF's, computed using different sets of lags. The scaling operation (See [19]) moves the position of the spurious peaks, whereas the position of the useful components remains unchanged. Therefore, successive multiplications enhance the useful peaks with respect to the spurious ones. Furthermore, the PHAF provides also a consistent advantage with respect to the cross terms. In fact, two effects follow from the computation of the PHAF. First of all, the scaling operation moves the position of the cross terms, in the frequency domain, so that, even if some cross terms peak somewhere, it is unlikely that they will peak in the same position as some other cross terms, after scaling. Second, even in the worst possible situations in which two peaks of amplitude proportional to $T^{(L-1)/L}$ lie in the same position after scaling, their product will go like $T^{2(L-1)/L}$ whereas the peak corresponding to the useful component will be proportional to T^2. Iterating this kind of reasoning, it is clear that, at each iteration, the ratio between the useful peaks and undesired peaks increases, testifying the enhancement of the useful terms with respect to spurious harmonics and cross terms of any order obtained using the PHAF.

2.2.3 Kalman Filter Approach

The Kalman filter (KF) addresses the general problem of estimating the state of a discrete-time controlled process that is governed by a linear stochastic difference equation [20]. It estimates the process by using a form of feedback control: the filter estimates the process state at some time and then obtains feedback in the form of noisy measurements. As such, the equations for the KF fall into two groups: time update equations and measurement update equations. The time update equations are responsible for projecting forward (in time) the current state and error covariance estimates to obtain the a priori estimates for the next time step. The measurement update equations are responsible for the feedback, i.e., for incorporating a new measurement into the a priori estimate to obtain an improved a posteriori estimate. The

time update equation can also be thought of as predictor equations, while the measurement update equations can be thought of as corrector equations. Indeed the final estimation algorithm resembles that of a predictor-corrector algorithm for solving numerical problems. Some of the most successful applications of Kalman filtering have been in situations with nonlinear dynamics and/or nonlinear measurement relationships which are the case of PPS's parameter estimations problem. Two basic ways of linearizing the problem exist: one is to linearize about some nominal trajectory in state-space that does not depend on the measurement data. The resulting filter is usually referred to as a linearized KF. The other method is to linearize about a trajectory that is continually updated with the state estimates resulting from the measurements. When this is done, the filter is called an extended KF (EKF). The former assumes that an approximate trajectory may be determined by some means. This assumption is less likely to be true in the majority of radar, sonar and communications applications. This last point explains the use of the EKF version of the KF for the KF approach used in this work. Details of this technique are given in Chapter 3.

2.3 *Narrowband and Wideband Situations*

When an advancing plane wave passes through a non-dispersive medium [21], the signal output at any sensor element immersed in that medium can be represented as a time-advanced/delayed version of the signal relative to a reference element. Figure 2.2 depicts an example of a uniform linear array of sensors, this latter is the array geometry considered in our work, where the time delay between two successive sensors when a signal is traversing along the array is $\tau = \frac{d}{C}\sin(\alpha)$ with d denoting the interspacing distance between two successive sensors, and C representing the velocity of propagation. With the absence of noise, let $y_0(t) = s(t)$ denote the signal at the reference element (sensor_0), where $s(t)$ is a plane wave impinging onto the array, and

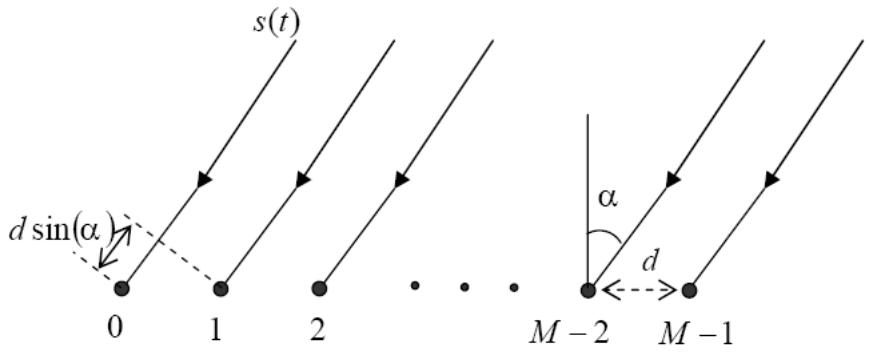

Fig. 2.2. Definition of Symbols for Linear Antenna Array Scenario

$y_1(t)$ be the output at the second sensor from the reference point in absolute units. Therefore, $y_1(t)$ can be related to $y_0(t)$ as follows

$$y_1(t) = y_0(t - \tau) = s(t - \tau). \tag{2.48}$$

For all M sensors, the output vector, $\mathbf{y}(t)$, also known as the observation, can be written as

$$\begin{aligned} \mathbf{y}(t) &= [y_0(t), y_1(t), \ldots, y_{M-1}(t)]^T \\ &= [s(t), s(t - \tau), \ldots, s(t - (M - 1)\tau)]^T . \end{aligned} \tag{2.49}$$

In the case where there are K sources, the m-th sensor output in response to K signals from distinct angles of arrival, $\alpha_k, k = 1, \ldots, K$, can be expressed as

$$y_m(t) = \sum_{k=0}^{K-1} s_k(t - m\tau_k), \tag{2.50}$$

where $s_k(t)$ is the k-th source, and τ_k is the corresponding time delay between adjacent sensors, defined as $\tau_k = \frac{d}{C} \sin(\alpha_k)$

2.3.1 Narrowband Situation

If the signals under consideration are narrowband, that is, the carrier frequency is fairly large compared to the bandwidth of the signal, then the signal can be treated as quasi-static during time intervals of order τ, and $y_m(t)$ can be rewritten as [21], [22], and [23].

$$\begin{aligned} y_m(t) &= \sum_{k=0}^{K-1} s_k(t) exp\left(-j\frac{m\omega_0 d\sin(\alpha_k)}{C}\right) \\ &= \sum_{k=0}^{K-1} s_k(t) exp\left(-j\frac{m2\pi d\sin(\alpha_k)}{\lambda}\right), \end{aligned} \tag{2.51}$$

where ω_0 is the operating frequency and λ is the associated carrier wavelength. As a result, the sensor output vector, $\mathbf{y}(t)$, can be then expressed as $\mathbf{y} = \mathbf{W}(\alpha)\mathbf{s}(t)$ where $\alpha \in \Re^K$ and $\mathbf{W}(\alpha) \in C^{MxK}$ is known as the steering matrix, the k-th column of which is defined as

$$\mathbf{w}(\alpha_k) = \left[1, exp\left(-j\frac{2\pi d\sin(\alpha_k)}{\lambda}\right), \ldots, exp\left(-j\frac{2\pi(M-1)d\sin(\alpha_k)}{\lambda}\right)\right]^T. \tag{2.52}$$

For narrowband signals, the time delay can be approximated by a pure phase delay of the reference signal, and this phase delay depends only on the spacing between the sensors in question, the angle of arrival of the plane wave, and the frequency of the propagating wave.

The structure of the steering matrix varies with the geometry of the array. In particular, when the array elements are arranged in a straight line and are uniformly spaced, we assume $d \leq \frac{\lambda}{2}$, where λ is the wavelength. However, this structure is subject to an ambiguity problem, for it can resolve only one angular component (For example, in the case of a vertically erected linear array, azimuth angle cannot be resolved, and an ambiguity exists as to whether the wave is incident from the front or back of the array), leading to a cone of uncertainty and right/left ambiguities. To resolve this problem, a circular array can be used. Nevertheless, because of its

simplicity, the uniform linear array is commonly used in the literature, and for this reason this thesis adopts this simple structure. With the consideration of observation noise, the snapshot vector at the sampling time t can then be expressed as

$$\mathbf{y}(t) = \mathbf{W}(\alpha)\mathbf{s}(t) + \mathbf{v}(t). \tag{2.53}$$

Where $\mathbf{v}$ is the observation noise. We assume that the noise is a Gaussian random variable. Various methods have been developed according to this narrowband model to resolve the detection and estimation problems.

2.3.2 Wideband Situation

While the time delays of narrowband signals can be approximated by their respective phase delays, wideband sources require more signal processing prior to applying existing approaches to solve for detection and estimation problems. Using the time shifting property of the Fourier transform (FT), the m-th sensor output can be rewritten as

$$\begin{aligned} Y_m(\omega) &= FT\left[\sum_{k=0}^{K-1} s_k(t - m\tau_k)\right] \\ &= \sum_{k=0}^{K-1} S_k(\omega) exp(-jm\omega\tau_k), \end{aligned} \tag{2.54}$$

where $S_k(\omega)$ represents the FT of $s_k(t)$. Thus the snapshot vector in frequency domain can be written as

$$\mathbf{Y}(\omega) = \mathbf{W}(\tau, \omega)S(\omega). \tag{2.55}$$

Where $\mathbf{W}(\tau, \omega) \in C^{MxK}$ is known as the location matrix, the k-th column of which is defined as $\mathbf{w}(\tau_k, \omega) = [1, exp(-j\omega\tau_k), \ldots, exp(-j(M-1)\omega\tau_k)]^T$.

Structurally, (2.53) and (2.55) are identical, but $\mathbf{w}(\tau_k, \omega)$ for $k = 0, \ldots, K-1$ is dependent on every ω. The steering matrix and the location matrix are structurally

similar, and hence those approaches that were developed for narrowband signals can be applied to the wideband signals in the frequency domain. That is, the received data in the presence of noise is defined as follows

$$\mathbf{Y}(\omega) = \mathbf{W}(\tau, \omega)S(\omega) + \mathbf{v}(\omega). \tag{2.56}$$

Where $\mathbf{v}(\omega)$ is the Fourier Transform of the observation noise. As in the narrowband scenario, we assume the observation noise is a Gaussian random variable and uncorrelated with the signal sources.

Let us define a bandpass signal whose maximum complex envelope bandwidth equals B_s. In the majority of the literature treating the problem of PPS's localization and parameter estimation, the sources are considered narrowband if the following inequality is verified: $B_s \Delta T_{max} \ll 1$, where ΔT_{max} is the maximum travel time between any two elements in the array. For a linear array, it would be the travel time between the two elements at the ends of the array for a signal arriving along the array axis (endfire). This means that propagation over the length of the array is a function of only the phase of the incident wave. In this case, the amplitude of the incident wave is stationary over the length of time required for a point on the wave to completely traverse the array. Under the wideband assumption, signals occupy a significant frequency band, and hence the propagation delays cannot be represented by phase shifts as with narrowband signals. Here, the waveform changes during the time it interacts with the array. We see the previous definitions as consequences of the signal being narrowband or wideband, or as a definition relative to the used sensor array. Most algorithms developed to solve problems for wideband signals usually transform the received signals from the time domain to the frequency domain using FT as a pre-processing step. The motivation of this transformation is that the transformed model in the frequency domain is structurally similar to that for narrowband signals in the time domain. In addition, if the sources are uncorrelated in frequency as well as uncorrelated with each other, their frequency spectra in a large set of discretized frequency bins can be considered independent and narrowband. As

a result, the algorithms for the narrowband case can be reused in the transformed model for the wideband case. Given that the time delay parameters are seldom scalar multiples of the sampling rate, resolving signals from different delays is very difficult, unless the sampling rate is increased significantly, so that the error between the inter-sensor delay and the closest sampling instant is reduced sufficiently. In other words, if one develops an algorithm in an attempt to resolve wideband signals in the time domain, oversampling may be required and more sophisticated hardware is also required. These burdens are further reasons why most algorithms for wideband signal processing operate in the frequency domain.

The instantaneous frequency (IF) of PPSs is an important parameter to estimate [23]. Let us consider a real polynomial phase signal of the form $a(t)\cos[\phi(t)]$ arriving at the antenna port of a receiver. Most receivers generate an in-phase and quadrature-phase versions of the received signal to form the quadrature equivalent signal of the form $a(t)e^{j\phi(t)}$.

For the sake of getting the best result for the IF estimation, it is desirable that the Hilbert Transformed signal approximates the quadrature signal [23]. This latter occurs if following equation is verified:

$$a(t)\cos[\phi(t)] + jHT(a(t)\cos[\phi(t)]) = a(t)e^{j\phi(t)}. \tag{2.57}$$

The solution is found using Bedrosian's product theorem [24]. It leads to the following result: Equation (2.57) is valid if the spectrum $A(f) = F\{a(t)\}$ lies entirely in the region $|f| < f_0$ and the spectrum $F\{\cos[\phi(t)]\}$ exists outside this region.

In other words, the more closely a signal approaches a narrow-band condition, the more likely equation 2.57 becomes verified.

Major works in the literature treating the PPS parameter estimation problem use the quadratic signal modellisation, in both narrowband and wideband situations, compromising the good estimation of the IF in the latter case. For our work we have chosen the RV modellisation:

$$y(t) = a\sin(\phi[t]) + v(t). \tag{2.58}$$

In addition to the above mentioned reasons behind this choice, taking a real valued modellisation allows considering half of the number of the data needed in the complex valued case, which optimizes the needed memory for handling the data in practical applications.

2.4 *Conclusion*

In this chapter, we presented different methods adapted, from the general problems of array processing, to the problem of PPS parameters estimation. As examples of widely used non-parametric methods, we presented Capon's method adapted to the estimation of the PPSs phase parameters. It allows representing the temporal evolution of the phase in a time-frequency plan. Similarly, we presented the MUSIC estimator with the Gaussian assumption on the noise sub-space. It allows the phase parameters estimation without the addition of a diagonal load to the autocorrelation matrix as was the case for Capon's estimator. As parametric methods previously applied for the problem at hand, we reviewed the ML estimator and its adaptation to the PPS parameters estimation along with the polynomial phase transform that has been the subject of multiple publications. We also presented a summary of the Kalman filter technique that is the method chosen in our work to deal with the problem at hand and that will be developed in the next chapter. Most of these techniques have been used to solve for detection and estimation problems for narrowband signals. However, for wideband signals it becomes cumbersome as a huge amount of data is required and more computational efforts are demanded to solve the same problems, even though in both cases the models are similar, where the only difference is in the domain where each model is defined. We summarized the cases of narrowband and wideband PPSs as presented in the literature and highlighted the issue with the adopted definition that is a consequence instead of a definition. We presented our point of view on this subject justifying the real-valued modellisation choice.

3. STATE SPACE REPRESENTATION-BASED APPROACH

The Kalman filter-based parameter estimation has been largely studied for the case of PPS corrupted by Gaussian noise. The use of the Kalman filter is motivated by the advantages that it offers on the practical level allowing the tracking of the signal frequency [25] - [27]. The primary work in this field has been dedicated to chirp signals identification. A linear state model has been obtained based on Tretter's approximation [28] that transforms the additive noise into a phase noise. This model is linear and Gaussian, and allows the application of the Kalman filter. Although The Kalman estimator is optimal in the minimum variance sense, Tretter's method remain approximate and only applicable for the monocomponent case. In [29] and [30], the authors have studied the identification problem of chirp signals using the extended Kalman filter by proposing and comparing two exact nonlinear models of the signal: The first model is nonlinear with respect to the state and the second with respect to the observables. More recently, in [31] the authors have proposed a method to estimate chirp signals using two cascaded extended Kalman filters. In [32] the authors have proposed an extended Kalman filter for PPS demodulation using a PPS state representation where the phase is expressed in function of the polynomials of Legendre. This chapter presents a new technique based on the Kalman filter (KF) algorithm. It offers the possibility of extending the monocomponent PPS parameter estimation to the Multi-Components (MC) case [33] where the approach proposed in [34] is generalized to the MCPPSs case of any order impinging on a multisensor array. The method presents a number of other attractive features. It is very adequate for real-time applications because of the recursive nature of the resulting algorithm and the modest use of memory (due to the nature of the KF itself). Moreover, in contrast to the majority of the literature, it allows the consideration of a real-valued

(RV) modellisation hence the applicability of the algorithm to situations where the source signals are wideband without need to transform the received signals from the time domain to the frequency domain.

3.1 *Modellisation*

We recall that the general modellisation of MCPPSs considered in the majority of literature is $s(t) = \sum_{n=1}^{N} a_n \exp[\phi_n(t)]$ with $\phi_n(t) = \sum_{l=0}^{L_n} b_{ln}(t\Delta)^l$ for $t = 0, \ldots, P-1$, where P, N, and L_n represent the sample size, the number of components, and the component phase degree, respectively. The amplitude a_n is a real-valued (RV) constant, the instantaneous phase $\phi_n(t)$ of each component is a polynomial, and Δ represents the sampling interval.

In many practical applications, the original sources are RV, while most of the previously mentioned methods assume the data consisting of a double number of complex-valued (CV) PPSs. To do so, knowing that generally the transmitted signal parameters are unknown, we apply the Hilbert transform (HT) on the RV data. Modelling the signals by an exponential assumes that the HT exactly generates the quadrature component of the RV PPS. This assumption is always verified for narrowband signals, where the PPS's amplitude and phase spectrums are separated (See Chapter 2). This is the absolute definition of a narrowband PPS. In the majority of the literature, the narrowband situation is defined relatively to the sensor array where a signal is considered narrowband if its complex envelope satisfies the condition $B_s\tau_{max} \ll 1$ with B_s representing the maximum bandwidth of the signal complex envelope and τ_{max} equalling the maximum travel time between any two elements in the array. This latter is considered as a consequence of the narrowband assumption on the source signals rather than a definition. The conclusion for this analysis is as follows: the more closely a signal approaches a narrowband condition, the better the Hilbert-transformed signal approximates the quadrature signal, and the more likely the Hilbert-based analytic signal is to provide an accurate model of a real system

with a particular Instantaneous Frequency (IF); also the better in general will be the estimate of the instantaneous frequency. This justifies the following modellisation choice: $s(t) = \sum_{n=1}^{N} a_n \sin[\phi_n(t)]$.

We propose to exploit the spatial information provided by a Uniform linear array (ULA) of sensors. Hence, the vector array outputs $\{y_m, m = 1, \ldots, M\}$ obey the following model:

$$y_1(t) = \sum_{n=1}^{N} a_n \sin[\phi_n(t)] + v_1(t), \tag{3.1}$$

$$y_m(t) = \sum_{n=1}^{N} a_n \sin\left[\phi_n\left(t - \frac{\tau_{nm}}{\Delta}\right)\right] + v_m(t), \quad m = 2, \ldots, M, \tag{3.2}$$

where $\{v_m, m = 1, \ldots, M\}$ are independent, real valued, additive white Gaussian noises (AWGNs) with zero means and variances $\{\sigma_m^2, m = 1, \ldots, M\}$. $\{\tau_{nm}, n = 1, \ldots, N, m = 2, \ldots, M\}$ are RV parameters representing the propagation time delays of the n-th source waveform impinging at the m-th array sensor with respect to the signal received at the first sensor (These delays are not necessarily multiples of the sampling period). The state-space modellisation consists of putting the state and measurement equations according to the state-vector choice. In practice, from (3.2), two cases can arise: situations where the delays are known and applications where these parameters are unknown. We then provide the state-space representation for both cases.

Known Delays:

The chosen state-model has the following state-vector:

$$\mathbf{x}(t) = \left[a_1 \;\; \phi_1(t) \;\; \phi_1^{(1)}(t) \ldots \phi_1^{(L_1)}(t) \ldots\ldots a_N \;\; \phi_N(t) \;\; \phi_N^{(1)}(t) \ldots \phi_N^{(L_N)}(t)\right]^T, \tag{3.3}$$

where $(.)^T$ and $(.)^{(l)}$ stand for the matrix transpose operator and the l-th derivative operator with respect to t, respectively (the component phase degrees L_n are assumed known, but we will see later in this chapter that this assumption can be relaxed). The dimension of $\mathbf{x}(t)$ is given by $d_N = \sum_{n=1}^{N} (L_n + 2)$ (Since the n-th signal component is represented in the state-vector by $(L_n + 2)$ elements).

The following state-model is in order:

$$\begin{cases} \mathbf{x}(t+1) = \mathbf{F}\mathbf{x}(t) \\ y_m(t) = g_m\left[\mathbf{x}(t)\right] + v_m(t),\ m = 1, \ldots, M \end{cases}. \tag{3.4}$$

Where $\mathbf{F}$ and g are given by

$$\mathbf{F} = \begin{bmatrix} \mathbf{F}_1 & 0 & \cdots & 0 \\ 0 & \mathbf{F}_2 & \ddots & \vdots \\ \vdots & \ddots & \ddots & 0 \\ 0 & \cdots & 0 & \mathbf{F}_N \end{bmatrix}, \tag{3.5}$$

with

$$\mathbf{F}_n = \begin{bmatrix} 1 & 0 & 0 & \cdots & 0 \\ 0 & 1 & \frac{\Delta}{1!} & \cdots & \frac{\Delta^{L_n}}{L_n!} \\ \vdots & \ddots & \ddots & \ddots & \vdots \\ \vdots & \ddots & \ddots & 1 & \frac{\Delta}{1!} \\ 0 & \cdots & \cdots & 0 & 1 \end{bmatrix}, \quad n = 1, \ldots, N, \tag{3.6}$$

and

$$\begin{aligned} g_1\left[\mathbf{x}(t)\right] = {} & x_1(t)\sin\left[x_2(t)\right] + x_{1+d_1}(t)\sin\left[x_{2+d_1}(t)\right] + \cdots \\ & + x_{1+d_{N-1}}(t)\sin\left[x_{2+d_{N-1}}(t)\right], \end{aligned}$$

$$g_m\left[\mathbf{x}(t)\right] = x_1(t)\sin\left[\sum_{l=0}^{L_1} \frac{(-\tau_{1m})^l}{l!} x_{l+2}(t)\right]$$

$$+ x_{1+d_1}(t) \sin \left[\sum_{l=0}^{L_2} \frac{(-\tau_{2m})^l}{l!} x_{l+2+d_1}(t) \right] + \cdots$$
$$+ x_{1+d_{N-1}}(t) \sin \left[\sum_{l=0}^{L_N} \frac{(-\tau_{Nm})^l}{l!} x_{l+2+d_{N-1}}(t) \right],$$
$$m = 2, \ldots, M, \tag{3.7}$$

where $\{x_k(t), k = 1, \ldots, d_N\}$ are the entries of $\mathbf{x}(t)$.

By defining the parameter vector as

$$\theta = [a_1 \ b_{01} \ b_{11} \ \ldots \ b_{L_1 1} \ \ldots\ldots \ a_N \ b_{0N} \ b_{1N} \ \ldots \ b_{L_N N}]^T, \tag{3.8}$$

one obtains

$$\hat{\theta}(t) = \mathbf{A}\mathbf{F}^{-t}\hat{\mathbf{x}}(t), \tag{3.9}$$

where $\hat{\theta}$, $\hat{\mathbf{x}}$ are the estimates of θ and $\mathbf{x}$, respectively, $\mathbf{F}$ is as defined in (3.6) and $\mathbf{A}$ is given by

$$\mathbf{A} = \begin{bmatrix} \mathbf{A}_1 & 0 & \cdots & 0 \\ 0 & \mathbf{A}_2 & \ddots & \vdots \\ \vdots & \ddots & \ddots & 0 \\ 0 & \cdots & 0 & \mathbf{A}_N \end{bmatrix}, \tag{3.10}$$

where

$$\mathbf{A}_n = \begin{bmatrix} 1 & 0 & \cdots & \cdots & 0 \\ 0 & 1 & \ddots & \ddots & \vdots \\ \vdots & \ddots & \frac{1}{1!} & \ddots & \vdots \\ \vdots & \ddots & \ddots & \ddots & 0 \\ 0 & \cdots & \cdots & 0 & \frac{1}{L_n!} \end{bmatrix}, \quad n = 1, \ldots, N. \tag{3.11}$$

Unknown Delays:

In this situation, the delays need to be included by augmenting the state-vector given by (3.3) where the n-th signal component will be represented in the state-vector by (L_n+3) elements and the dimension of $\mathbf{x}(t)$ becomes equal to $d_N = \sum_{n=1}^{N}(L_n+3)$. The state-vector expression is given by

$$\mathbf{x}(t)=\Big[a_1 \;\; \tau_{12} \;\; \phi_1(t) \;\; \phi_1^{(1)}(t)\ldots\phi_1^{(L_1)}(t)\ldots\ldots a_N \;\; \tau_{N2} \;\; \phi_N(t) \;\; \phi_N^{(1)}(t)\ldots\phi_N^{(L_N)}(t)\Big]^T. \tag{3.12}$$

We note that only the set $\{\tau_{n2},\, n=1,\ldots,N\}$ has been included. The reason is because for an ULA, the remaining delays are found using the relation $\tau_{nm+1} = m\tau_{n2}$, $m = 2,\ldots,M$.

The same state-model and state transition matrix given by (3.4) and (3.5), respectively, are considered with new expressions for $\mathbf{F}_n$ and g

$$\mathbf{F}_n = \begin{bmatrix} 1 & 0 & 0 & \cdots & \cdots & 0 \\ 0 & 1 & 0 & \cdots & \cdots & 0 \\ 0 & 0 & 1 & \frac{\Delta}{1!} & \cdots & \frac{\Delta^{L_n}}{L_n!} \\ \vdots & \vdots & \ddots & \ddots & \ddots & \vdots \\ \vdots & \vdots & \ddots & \ddots & 1 & \frac{\Delta}{1!} \\ 0 & \cdots & \cdots & \cdots & 0 & 1 \end{bmatrix}, \quad n=1,\ldots,N, \tag{3.13}$$

$$g_1\left[\mathbf{x}(t)\right] = x_1(t)\sin\left[x_3(t)\right] + x_{1+d_1}(t)\sin\left[x_{3+d_1}(t)\right] + \cdots + x_{1+d_{N-1}}(t)\sin\left[x_{3+d_{N-1}}(t)\right],$$

$$g_m\left[\mathbf{x}(t)\right] = x_1(t)\sin\left[\sum_{l=0}^{L_1}\frac{(-(m-1)x_2)^l}{l!}x_{l+3}(t)\right] + x_{1+d_1}(t)\sin\left[\sum_{l=0}^{L_2}\frac{\left(-(m-1)x_{2+d_1}\right)^l}{l!}x_{l+3+d_1}(t)\right] + \cdots + x_{1+d_{N-1}}(t)\sin\left[\sum_{l=0}^{L_N}\frac{\left(-(m-1)x_{2+d_{N-1}}\right)^l}{l!}x_{l+3+d_{N-1}}(t)\right],$$

$$m = 2, \ldots, M. \tag{3.14}$$

The parameter vector given by (3.8) is augmented by the inclusion of the nuisance parameters as follows:

$$\theta = [a_1 \ \tau_{12} \ b_{01} \ b_{11} \ \ldots \ b_{L_1 1} \ \ldots\ldots \ a_N \ \tau_{N2} \ b_{0N} \ b_{1N} \ \ldots \ b_{L_N N}]^T . \tag{3.15}$$

The same relation as (3.9) relates the parameter vector to the estimated state-vector with $\mathbf{F}$ and $\mathbf{A}$ defined in (3.5) and (3.10), respectively ($\mathbf{F}_n$ is given by (3.13)). $\mathbf{A}_n$ expression is as follows:

$$\mathbf{A}_n = \begin{bmatrix} 1 & 0 & \cdots & \cdots & \cdots & 0 \\ 0 & 1 & \ddots & \ddots & \ddots & \vdots \\ 0 & 0 & 1 & \ddots & \ddots & \vdots \\ \vdots & \ddots & \ddots & \frac{1}{1!} & \ddots & \vdots \\ \vdots & \ddots & \ddots & \ddots & \ddots & 0 \\ 0 & \cdots & \cdots & \cdots & 0 & \frac{1}{L_n!} \end{bmatrix}, \quad n = 1, \ldots, N. \tag{3.16}$$

The main motivations behind the chosen structure of the state vector are: obtaining a minimum number of nonlinear equations and direct estimation of the instantaneous frequency (IF), a very important parameter as stressed in [23] and [35]. Indeed, from (3.4), we obtain a state-space modellisation with a linear state equation and nonlinear observation equations. Furthermore, from (3.3) and (3.12), it is possible to directly estimate the IF $\{\phi_n^{(1)}(t), \ \ n = 1, \ldots, N\}$ of each component, and hence minimizing the estimation error that would have resulted from indirect estimation. In the next subsection, we present the EKF-based algorithm.

3.2 *Kalman Filter-Based Technique*

The EKF technique consists of linearizing, to the first order, models (3.1) and (3.2) and applying an optimal state estimation filter. The filter equations are given for both cases of known and unknown delay parameters.

Known Delays:

The update equations are given as follows:

$$\begin{cases} \hat{\mathbf{x}}^{-}(t) = \mathbf{F}\hat{\mathbf{x}}_M(t) \\ \mathbf{P}^{-}(t) = \mathbf{F}\mathbf{P}_M(t)\mathbf{F}^T \end{cases}, \tag{3.17}$$

where $\hat{\mathbf{x}}^{-}(t)$ and $\mathbf{P}^{-}(t)$ are the predicted state-vector and covariance error matrix at the time instant t, respectively.

The estimation equations are given below

$$\begin{cases} \mathbf{k}_1(t) = \mathbf{P}^{-}(t)\mathbf{g}_1^T(t)\left[\mathbf{g}_1(t)\mathbf{P}^{-}(t)\mathbf{g}_1^T(t) + \sigma_1^2\right]^{-1} \\ \hat{y}_1(t) \ = \hat{x}_1^{-}(t)\sin\left[\hat{x}_2^{-}(t)\right] + \hat{x}_{1+d_1}^{-}(t)\sin\left[\hat{x}_{2+d_1}^{-}(t)\right] \\ \qquad\quad + \cdots + \hat{x}_{1+d_{N-1}}^{-}(t)\sin\left[\hat{x}_{2+d_{N-1}}^{-}(t)\right] \\ \hat{\mathbf{x}}_1(t) = \hat{\mathbf{x}}^{-}(t) + \mathbf{k}_1(t)\left[y_1(t) - \hat{y}_1(t)\right] \\ \mathbf{P}_1(t) \ = \left[\mathbf{I} - \mathbf{k}_1(t)\mathbf{g}_1(t)\right]\mathbf{P}^{-}(t) \end{cases}, \tag{3.18}$$

$$
\begin{cases}
\mathbf{k}_2(t) = \mathbf{P}_1(t)\mathbf{g}_2^T(t)\left[\mathbf{g}_2(t)\mathbf{P}_1(t)\mathbf{g}_2^T(t) + \sigma_2^2\right]^{-1} \\
\hat{y}_2(t) \;= \hat{x}_1^{\mathbf{1}}(t)\sin\left[\hat{x}_2^{\mathbf{1}}(t)\right] + \hat{x}_{1+d_1}^{\mathbf{1}}(t)\sin\left[\hat{x}_{2+d_1}^{\mathbf{1}}(t)\right] \\
\qquad\quad + \cdots + \hat{x}_{1+d_{N-1}}^{\mathbf{1}}(t)\sin\left[\hat{x}_{2+d_{N-1}}^{\mathbf{1}}(t)\right] \\
\hat{\mathbf{x}}_2(t) = \hat{\mathbf{x}}_1(t) + \mathbf{k}_2(t)\left[y_2(t) - \hat{y}_2(t)\right] \\
\mathbf{P}_2(t) \;= \left[\mathbf{I} - \mathbf{k}_2(t)\mathbf{g}_2(t)\right]\mathbf{P}_1(t) \\
\vdots \\
\mathbf{k}_M(t) = \mathbf{P}_{M-1}(t)\mathbf{g}_M^T(t)\left[\mathbf{g}_M(t)\mathbf{P}_{M-1}(t)\mathbf{g}_M^T(t) + \sigma_M^2\right]^{-1} \\
\hat{y}_M(t) \;= \hat{x}_1^{\mathbf{M-1}}(t)\sin\left[\hat{x}_2^{\mathbf{M-1}}(t)\right] + \hat{x}_{1+d_1}^{\mathbf{M-1}}(t)\sin\left[\hat{x}_{2+d_1}^{\mathbf{M-1}}(t)\right] \\
\qquad\quad + \cdots + \hat{x}_{1+d_{N-1}}^{\mathbf{M-1}}(t)\sin\left[\hat{x}_{2+d_{N-1}}^{\mathbf{M-1}}(t)\right] \\
\hat{\mathbf{x}}_M(t) = \hat{\mathbf{x}}_{M-1}(t) + \mathbf{k}_M(t)\left[y_M(t) - \hat{y}_M(t)\right] \\
\mathbf{P}_M(t) \;= \left[\mathbf{I} - \mathbf{k}_M(t)\mathbf{g}_M(t)\right]\mathbf{P}_{M-1}(t)
\end{cases}, \tag{3.19}
$$

where $\{\hat{\mathbf{x}}_m(t), m = 1, \ldots, M, t = 0, \ldots, P-1\}$ are the estimated state-vectors, $\{\hat{x}_k^-, k = 1, \ldots, 2 + d_{N-1}\}$ and $\{\hat{x}_k^{\mathbf{m}}, k = 1, \ldots, 2 + d_{N-1}, \mathbf{m} = 1, \ldots, M-1\}$ are the entries of $\hat{\mathbf{x}}^-$ and $\{\hat{\mathbf{x}}_m, m = 1, \ldots, M-1\}$, respectively. $\{\mathbf{P}_m(t), m = 1, \ldots, M\}$ are the covariance error matrices, $\{\mathbf{k}_m, m = 1, \ldots, M\}$ are the Kalman filter gain vectors and $\mathbf{I}$ is the $(d_N \times d_N)$ identity matrix.

The filter is initialized by $\hat{\mathbf{x}}_0^-$ and $\mathbf{P}_0^-$. The final estimate $\hat{\mathbf{x}}$ of $\mathbf{x}$ equals $\hat{\mathbf{x}}_M(P-1)$. The vectors $\{\mathbf{g}_m, m = 1, \ldots, M\}$ are found by linearizing, at the first order, the first and second expressions of (3.7) around the predicted state-vector and the estimated state-vector, respectively. Hence, the following relations

$$
\mathbf{g}_1(t) = \left(\frac{\partial g_1[\mathbf{x}(t)]}{\partial \mathbf{x}(t)}\right)_{\mathbf{x}(t)=\hat{\mathbf{x}}^-(t)},
$$

$$
\mathbf{g}_m(t) = \left(\frac{\partial g_m[\mathbf{x}(t)]}{\partial \mathbf{x}(t)}\right)_{\mathbf{x}(t)=\hat{\mathbf{x}}_{m-1}(t)}, \quad m = 2, \ldots, M, \tag{3.20}
$$

where ∂ stands for the partial derivation operator. We then find

$$\mathbf{g}_1(t) = [\mathbf{g}_{1,1}(t) \quad \dots \quad \mathbf{g}_{1,N}(t)],$$

$$\mathbf{g}_m(t) = [\mathbf{g}_{m,1,\tau_{1m}}(t) \quad \dots \quad \mathbf{g}_{m,N,\tau_{Nm}}(t)], \quad m = 2, \dots, M, \tag{3.21}$$

where

$$\mathbf{g}_{1,1}(t) = \left[\sin\left[\hat{x}_2^-(t)\right] \quad \hat{x}_1^-(t)\cos\left[\hat{x}_2^-(t)\right] \quad 0 \dots 0\right],$$

$$\mathbf{g}_{1,n}(t) = [\sin\left[\hat{x}_{2+d_{n-1}}^-(t)\right] \quad \hat{x}_{1+d_{n-1}}^-(t)\cos\left[\hat{x}_{2+d_{n-1}}^-(t)\right] \quad 0 \dots 0], \quad n = 2, \dots, N,$$

$\mathbf{g}_{m,1,\tau_{1m}}^T(t) =$

$$\begin{bmatrix} \sin\left[\alpha_{1\tau_{1m}}\left(\hat{\mathbf{x}}_{m-1}(t)\right)\right] \\ \hat{x}_1^{\mathbf{m-1}}(t)\cos\left[\alpha_{1\tau_{1m}}\left(\hat{\mathbf{x}}_{m-1}(t)\right)\right] \\ \frac{-\tau_{1m}}{1!}\hat{x}_1^{\mathbf{m-1}}(t)\cos\left[\alpha_{1\tau_{1m}}\left(\hat{\mathbf{x}}_{m-1}(t)\right)\right] \\ \vdots \\ \frac{(-\tau_{1m})^{L_1}}{L_1!}\hat{x}_1^{\mathbf{m-1}}(t)\cos\left[\alpha_{1\tau_{1m}}\left(\hat{\mathbf{x}}_{m-1}(t)\right)\right] \end{bmatrix}$$

$$m = 2, \dots, M,$$

$\mathbf{g}_{m,n,\tau_{nm}}^T(t) =$

$$\begin{bmatrix} \sin\left[\alpha_{n\tau_{nm}}\left(\hat{\mathbf{x}}_{m-1}(t)\right)\right] \\ \hat{x}^{\mathbf{m-1}}_{1+d_{n-1}}(t)\cos\left[\alpha_{n\tau_{nm}}\left(\hat{\mathbf{x}}_{m-1}(t)\right)\right] \\ \frac{-\tau_{nm}}{1!}\hat{x}^{\mathbf{m-1}}_{1+d_{n-1}}(t)\cos\left[\alpha_{n\tau_{nm}}\left(\hat{\mathbf{x}}_{m-1}(t)\right)\right] \\ \vdots \\ \frac{(-\tau_{nm})^{L_n}}{L_n!}\hat{x}^{\mathbf{m-1}}_{1+d_{n-1}}(t)\cos\left[\alpha_{n\tau_{nm}}\left(\hat{\mathbf{x}}_{m-1}(t)\right)\right] \end{bmatrix}$$

$$n = 2, \ldots, N, \quad m = 2, \ldots, M, \tag{3.22}$$

where $\{\alpha_{n\tau_{nm}}, n = 1, \ldots, N, m = 2, \ldots, M\}$ are given by

$$\alpha_{1\tau_{1m}}\left(\hat{\mathbf{x}}_{m-1}(t)\right) = \sum_{l=0}^{L_1} \frac{\left(-\tau_{1m}\right)^l}{l!}\hat{x}^{\mathbf{m-1}}_{l+2}(t),$$

$$\alpha_{n\tau_{nm}}\left(\hat{\mathbf{x}}_{m-1}(t)\right) = \sum_{l=0}^{L_n} \frac{\left(-\tau_{nm}\right)^l}{l!}\hat{x}^{\mathbf{m-1}}_{l+2+d_{n-1}}(t),$$
$$n = 2, \ldots, N. \tag{3.23}$$

Unknown Delays:

As performed in the previous section, the state-vector will be augmented. The update equation follows (3.17) where the same definitions hold as in the previous subsection. The remaining equations are given hereafter

$$\begin{cases} \mathbf{k}_1(t) = \mathbf{P}^-(t)\mathbf{g}_1^T(t)\left[\mathbf{g}_1(t)\mathbf{P}^-(t)\mathbf{g}_1^T(t)+\sigma_1^2\right]^{-1} \\ \hat{y}_1(t) \ = \hat{x}_1^-(t)\sin\left[\hat{x}_3^-(t)\right] + \hat{x}_{1+d_1}^-(t)\sin\left[\hat{x}_{3+d_1}^-(t)\right] \\ \qquad\quad + \cdots + \hat{x}_{1+d_{N-1}}^-(t)\sin\left[\hat{x}_{3+d_{N-1}}^-(t)\right] \\ \hat{\mathbf{x}}_1(t) = \hat{\mathbf{x}}^-(t) + \mathbf{k}_1(t)\left[y_1(t)-\hat{y}_1(t)\right] \\ \mathbf{P}_1(t) \ = \left[\mathbf{I}-\mathbf{k}_1(t)\mathbf{g}_1(t)\right]\mathbf{P}^-(t) \end{cases}, \tag{3.24}$$

$$\begin{cases} \mathbf{k}_2(t) = \mathbf{P}_1(t)\mathbf{g}_2^T(t)\left[\mathbf{g}_2(t)\mathbf{P}_1(t)\mathbf{g}_2^T(t)+\sigma_2^2\right]^{-1} \\ \hat{y}_2(t) \ = \hat{x}_1^{\mathbf{1}}(t)\sin\left[\hat{x}_3^{\mathbf{1}}(t)\right] + \hat{x}_{1+d_1}^{\mathbf{1}}(t)\sin\left[\hat{x}_{3+d_1}^{\mathbf{1}}(t)\right] \\ \qquad\quad + \cdots + \hat{x}_{1+d_{N-1}}^{\mathbf{1}}(t)\sin\left[\hat{x}_{3+d_{N-1}}^{\mathbf{1}}(t)\right] \\ \hat{\mathbf{x}}_2(t) = \hat{\mathbf{x}}_1(t) + \mathbf{k}_2(t)\left[y_2(t)-\hat{y}_2(t)\right] \\ \mathbf{P}_2(t) \ = \left[\mathbf{I}-\mathbf{k}_2(t)\mathbf{g}_2(t)\right]\mathbf{P}_1(t) \\ \vdots \\ \mathbf{k}_M(t) = \mathbf{P}_{M-1}(t)\mathbf{g}_M^T(t)\left[\mathbf{g}_M(t)\mathbf{P}_{M-1}(t)\mathbf{g}_M^T(t)+\sigma_M^2\right]^{-1} \\ \hat{y}_M(t) \ = \hat{x}_1^{\mathbf{M-1}}(t)\sin\left[\hat{x}_3^{\mathbf{M-1}}(t)\right] + \hat{x}_{1+d_1}^{\mathbf{M-1}}(t)\sin\left[\hat{x}_{3+d_1}^{\mathbf{M-1}}(t)\right] \\ \qquad\quad + \cdots + \hat{x}_{1+d_{N-1}}^{\mathbf{M-1}}(t)\sin\left[\hat{x}_{3+d_{N-1}}^{\mathbf{M-1}}(t)\right] \\ \hat{\mathbf{x}}_M(t) = \hat{\mathbf{x}}_{M-1}(t) + \mathbf{k}_M(t)\left[y_M(t)-\hat{y}_M(t)\right] \\ \mathbf{P}_M(t) \ = \left[\mathbf{I}-\mathbf{k}_M(t)\mathbf{g}_M(t)\right]\mathbf{P}_{M-1}(t) \end{cases}, \tag{3.25}$$

with g_1 given by (3.21) and

$$\mathbf{g}_m(t) = \left[\mathbf{g}_{m,1}(t) \quad \ldots \quad \mathbf{g}_{m,N}(t)\right], \quad m = 2,\ldots,M \tag{3.26}$$

where

$$\mathbf{g}_{1,1}(t) = \left[\sin\left[\hat{x}_3^-(t)\right] \ 0 \ \hat{x}_1^-(t)\cos\left[\hat{x}_3^-(t)\right] \quad 0\ldots 0\right],$$

$$\begin{aligned} \mathbf{g}_{1,n}(t) = [&\sin\left[\hat{x}_{3+d_{n-1}}^-(t)\right] \ 0 \ \hat{x}_{1+d_{n-1}}^-(t)\cos\left[\hat{x}_{3+d_{n-1}}^-(t)\right] \\ &0\ldots 0], \quad n = 2,\ldots,N, \end{aligned} \tag{3.27}$$

$$\mathbf{g}_{m,1}^{T}(t) =$$

$$\begin{bmatrix} \sin\left[\alpha_1\left(\hat{\mathbf{x}}_{m-1}(t)\right)\right] \\ \hat{x}_1^{\mathbf{m-1}}(t)\sum_{l=1}^{L_1}\frac{(-(m-1))^l\left(\hat{x}_2^{\mathbf{m-1}}\right)^{l-1}}{(l-1)!}\hat{x}_{l+3}^{\mathbf{m-1}}(t) \times \cos\left[\alpha_1\left(\hat{\mathbf{x}}_{m-1}(t)\right)\right] \\ \hat{x}_1^{\mathbf{m-1}}(t)\cos\left[\alpha_1\left(\hat{\mathbf{x}}_{m-1}(t)\right)\right] \\ \frac{-(m-1)\hat{x}_2^{\mathbf{m-1}}}{1!}\hat{x}_1^{\mathbf{m-1}}(t)\cos\left[\alpha_1\left(\hat{\mathbf{x}}_{m-1}(t)\right)\right] \\ \vdots \\ \frac{\left(-(m-1)\hat{x}_2^{\mathbf{m-1}}\right)^{L_1}}{L_1!}\hat{x}_1^{\mathbf{m-1}}(t)\cos\left[\alpha_1\left(\hat{\mathbf{x}}_{m-1}(t)\right)\right] \end{bmatrix}$$

$$m = 2, \ldots, M,$$

$$\mathbf{g}_{m,n}^{T}(t) =$$

$$\begin{bmatrix} \sin\left[\alpha_n\left(\hat{\mathbf{x}}_{m-1}(t)\right)\right] \\ \hat{x}^{\mathbf{m-1}}_{1+d_{n-1}}(t)\sum_{l=1}^{L_1}\frac{(-(m-1))^l\left(\hat{x}^{\mathbf{m-1}}_{l+2+d_{n-1}}\right)^{l-1}}{(l-1)!}\hat{x}^{\mathbf{m-1}}_{l+3+d_{n-1}}(t) \\ \qquad\qquad \times\cos\left[\alpha_n\left(\hat{\mathbf{x}}_{m-1}(t)\right)\right] \\ \hat{x}^{\mathbf{m-1}}_{1+d_{n-1}}(t)\cos\left[\alpha_n\left(\hat{\mathbf{x}}_{m-1}(t)\right)\right] \\ \frac{-(m-1)\hat{x}^{\mathbf{m-1}}_{2+d_{n-1}}}{1!}\hat{x}^{\mathbf{m-1}}_{1+d_{n-1}}(t)\cos\left[\alpha_n\left(\hat{\mathbf{x}}_{m-1}(t)\right)\right] \\ \vdots \\ \frac{\left(-(m-1)\hat{x}^{\mathbf{m-1}}_{2+d_{n-1}}\right)^{L_n}}{L_n!}\hat{x}^{\mathbf{m-1}}_{1+d_{n-1}}(t) \\ \qquad\qquad \times\cos\left[\alpha_{n\tau_{nm}}\left(\hat{\mathbf{x}}_{m-1}(t)\right)\right] \end{bmatrix}$$

$$n=2,\ldots,N,\quad m=2,\ldots,M, \tag{3.28}$$

where $\{\alpha_n, n=1,\ldots,N, m=2,\ldots,M\}$ are given by

$$\alpha_1\left(\hat{\mathbf{x}}_{m-1}(t)\right)=\sum_{l=0}^{L_1}\frac{\left(-(m-1)\hat{x}^{\mathbf{m-1}}_2\right)^l}{l!}\hat{x}^{\mathbf{m-1}}_{l+3}(t),$$

$$\alpha_n\left(\hat{\mathbf{x}}_{m-1}(t)\right)= \sum_{l=0}^{L_n}\frac{\left(-(m-1)\hat{x}^{\mathbf{m-1}}_{l+2+d_{n-1}}\right)^l}{l!}\hat{x}^{\mathbf{m-1}}_{l+3+d_{n-1}}(t),$$

$$n=2,\ldots,N. \tag{3.29}$$

We note the dependence of g upon the delay parameters, which shows the importance of correct estimation of these latter when unknown.

3.3 *Algorithm Description*

The proposed algorithm is illustrated in Figure 3.1. It is based on the application of the EKF M times: The first EKF is applied on the non-delayed signal by computing the predicted values of the state-vector and the covariance matrix of the prediction error. This is followed by the computation of the Kalman filter gain, the estimated values of the state-vector and of the estimation error covariance matrix after introduction of the first sensor observation. The result is used as prediction for the second EKF applied on the signal delayed by τ_{n2}. The Kalman gain is then computed as well as the state-vector estimate with the corresponding estimation error covariance matrix after introducing the second sensor measurement. This procedure is repeated until the application of the M^{th} EKF, where the estimation result of the $(m-1)^{th}$ EKF is used as prediction for the m^{th} EKF applied on the delayed signal by τ_{nm}. The final estimates of the M^{th} EKF constitute the estimator outputs and in the same time are used by the first EKF as prediction equations to project ahead and close the algorithm loop.

The algorithm can diverge if the reference about which the linearization takes place is poor. The most common situation of this type occurs at the initial starting point of the recursive process. Frequently, the *a priori* information about the true state of the system is poor. This causes a large error in $\hat{\mathbf{x}}_0^-$ and forces $\mathbf{P}_0^-$ to be large. Thus two problems can arise in getting the extended filter started [20]:

1. A very large $\mathbf{P}_0^-$ combined with low-noise measurements at the first step will cause the $\mathbf{P}$ matrix to "jump" from a very large value to a small value in one step. In practice this is permissible. However, this can lead to numerical problems due to roundoff. A non-positive definite $\mathbf{P}$ matrix at any point in the recursive process usually leads to divergence.

2. If the error in $\hat{\mathbf{x}}_0^-$ is large, the first-order approximation used in the linearization will be poor, and divergence may occur, even with perfect arithmetic.

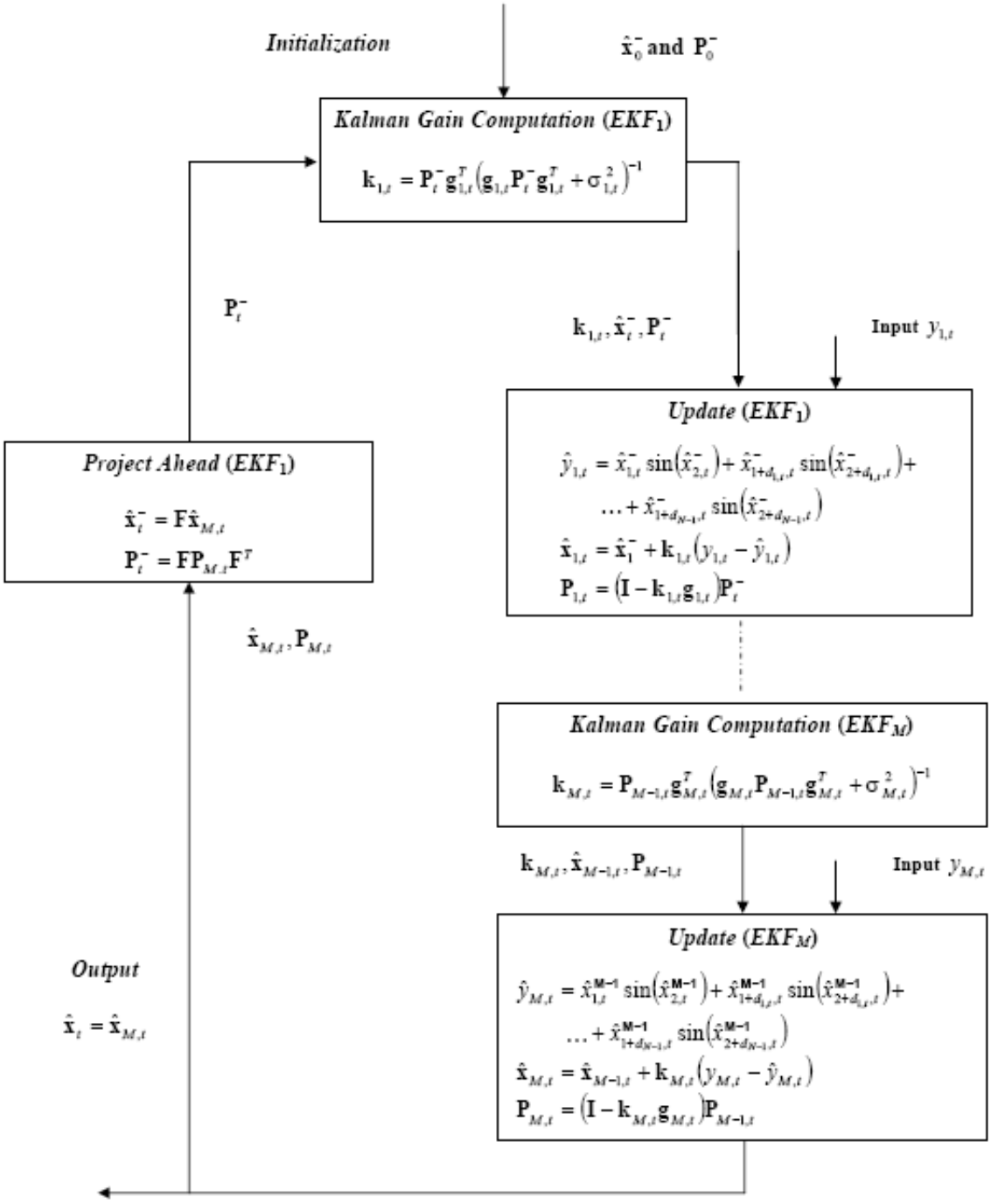

Fig. 3.1. Flow chart of the proposed extended Kalman filter-based algorithm.

With respect to problem 1, we should be especially careful to use all the usual numerical precautions to preserve the symmetry and positive definiteness of the $\mathbf{P}$ matrix on the first step. In some cases, simply using the symmetric form of the $\mathbf{P}$-update equation is sufficient to ward off the divergence. This form is as follows:

$\mathbf{P}_{M,t} = (\mathbf{I} - \mathbf{k}_{M,t}\mathbf{g}_{M,t})\mathbf{P}_{M-1,t}(\mathbf{I} - \mathbf{k}_{M,t}\mathbf{g}_{M,t})^T + \mathbf{k}_{M,t}\sigma^2_{M,t}\mathbf{k}^T_{M,t}$.

Another way of mitigating the numerical problem is to let $\mathbf{P}_0^-$ be considerably smaller than would normally be dictated by the true a priori uncertainty in $\hat{\mathbf{x}}_0^-$. This will cause suboptimal operation for the first few steps, but this is better than divergence! A similar result can be accomplished by letting $\sigma^2_{M,t}$ be abnormally large for the first few steps. There is no one single cure for all numerical problems. Each case must be considered on its own merits.

Problem 2 is more subtle than problem 1. Even with perfect arithmetic, poor linearization can cause a poor $\hat{\mathbf{x}}_0^-$ to be updated into an even poorer *a posteriori* estimate, which in turn gets projected on ahead, and so forth. One remedy to the poor-linearization problem, that works quite well when the information contained in the initial measurement is sufficient to determine the initial state-vector algebraically, is to use the initial measurement to solve for the state-vector, just as if there were no measurement error. It is hoped this will yield a better estimate of the state-vector than the original coarse $\hat{\mathbf{x}}_0^-$.

It must be noted that none of the solutions just mentioned play any role in the basic filtering process. Their sole purpose is simply to provide a good reference for linearization, so that the EKF can do its job of suboptimal estimation (In our simulations, we assumed the parameter initializations at 20 % of their actual values, following [29]).

In [34], one finds an approach using an EKF applied for a single-component chirp signal case. The analytical signal of the chirp was considered, leading to complex valued measurement equations. An EKF was applied twice for the parameter estimations. A first EKF was applied on the real part of the signal model. A second EKF was applied using the imaginary part of the signal model by taking the first filter

estimations as prediction results. Our algorithm originality consists of bypassing the prediction equations of the m^{th} EKF's, for $m = 2, \ldots, M$, and substituting them by the outputs of the $(m-1)^{th}$ EKF's, hence, leading to an anticipation in the process. The same approach is applied for the prediction equations of the first EKF where the output of the M^{th} EKF is used speeding up the convergence process.

In comparison with the method used in [34], where the linearization was made around the predicted state-vector, we note that our linearization point is the preceding EKF estimated state-vector, which represents a better linearization point, compared to the predicted state-vector, since it is closer to the solution (When the filter converges). Furthermore, [34] second observation equation does not carry any new information compared to the first observation equation (Since these equations represent the analytical signal components). In contrast, in our approach we can find a new information represented by the time delays. Finally, [34] assumes the chirp analytical signal representation, hence constraining the algorithm applicability to the narrowband case only, whereas our algorithm can be applied in the case of narrowband and wideband signals.

3.4 *Conclusion*

This chapter was dedicated to the proposed EKF-based approach deriving a new algorithm for MCPPSs parameter estimations impinging on a multisensor array. The combination of this scheme with the exploitation of spatial information given by a multisensor array is the key point of our approach. The drivers behind the chosen structure of the state vector were the minimisation of the number of nonlinear equations (where in our case we reduced the nonlinearity to the observation equations only) and the direct estimation of the instantaneous frequency (IF). The two situations of known and unknown delays were considered with the presentation of the EKF equations. In the next chapters, our algorithm will be compared to competitive algorithms to evaluate its performance. In addition, we will demonstrate through

simulations that the proposed method performs well in both cases of wideband and narrowband signals and in situations where the number of sources is superior to the number of sensors.

4. APPLICATION TO SOURCE LOCALISATION

The DOA estimation problem has been extensively studied in the signal processing literature. However, only a small number of proposed solutions are capable of handling both narrowband and wideband cases. In addition, many of these methods suffer in performance when the targets are moving relatively fast during the estimation batch (i.e., the snapshot period). In this section, we recall the different existing algorithm to solve the problem of DOA estimation, and present our approach with simulation examples.

4.1 *Narrowband Source Localisation*

Subspace methods With the knowledge of the number of sources, the signal subspace and noise subspace can be estimated with the corresponding eigenvectors. There are three classical methods that can estimate the directions of arrival by exploiting a fundamental property between the two sets of eigenvectors $\widehat{\mathbf{E}}_S$ and $\widehat{\mathbf{E}}_N$. These methods are the Pisarenko pseudo spectrum [36], the multiple signal classification (MUSIC) algorithm [37], and the Root-MUSIC [38], [39] method. Given the fact that $\widehat{\mathbf{E}}_S^H \widehat{\mathbf{E}}_N \approx 0$ such that

$$\widehat{e}_s^H \widehat{e}_n \approx 0, \quad \widehat{e}_s \in \widehat{\mathbf{E}}_S, \quad \widehat{e}_n \in \widehat{\mathbf{E}}_N, \tag{4.1}$$

if the signal vector is in the signal DOA's subspace, the magnitude of the projection onto $\widehat{\mathbf{E}}_N$ should be small. On the other hand, a projection onto $\widehat{\mathbf{E}}_S$ will result in a large magnitude. As a result, the search for signal vectors is equivalent to searching for vectors that are most closely orthogonal to the noise subspace as follows

$$\|\mathbf{s}(\phi)^H \widehat{\mathbf{E}}_N\| \longrightarrow 0 \quad when \quad \phi \in \Theta, \tag{4.2}$$

where $s(\phi)$ is a column of the steering matrix and Θ is the set of the actual DOA. Based on this orthogonality property, the Pisarenko pseudo spectrum (Pisarenko, 1973) projects a steering vector onto a single noise eigenvector when estimating the DOAs. The Pisarenko pseudo spectrum for a particular noise eigenvector is defined as

$$\widehat{P}_{Pis}(\phi) = \frac{1}{\mathbf{s}^H(\phi)\widehat{\mathbf{e}}_k\widehat{\mathbf{e}}_k^H\mathbf{s}(\phi)}, \quad k \in [k_0, M-1]. \tag{4.3}$$

It is well known that unless the number of sources is correct, it is not possible to tell which peak shown in the Pisarenko pseudo spectrum are attributed to the sources and which are spurious. Unlike the Pisarenko method, the MUSIC algorithm [37] involves a projection of a steering vector onto the whole noise subspace. The MUSIC pseudo spectrum is defined as

$$\widehat{P}_{MUSIC}(\phi) = \frac{1}{\mathbf{s}^H(\phi)\widehat{\mathbf{E}}_N\widehat{\mathbf{E}}_N^H\mathbf{s}(\phi)}. \tag{4.4}$$

Unlike the Pisarenko method, even if the number of sources is over estimated, the MUSIC method will perform well. The Root-MUSIC algorithm [38], [39], developed specifically for uniform linear arrays (ULAs), is motivated by the fact that

$$\mathbf{s}^H(\omega_k)e_j = 0, \quad j = k_0, \ldots, M-1, \tag{4.5}$$

where ω_k is a signal frequency, and $\omega_k = \frac{2\pi\Delta}{\lambda}sin(\phi_k)$. Define the polynomials using the eigenvectors corresponding to the noise subspace, i.e.,

$$e_j(z) = \frac{1}{\sqrt{M}}\sum_{m=0}^{M-1} e_{jm}z^{-m}, \quad j = k_0, \ldots, M-1, \tag{4.6}$$

such that the signal zeros, $z_k = e^{j\omega_k}, \quad k = 0, \ldots, k_0 - 1$, are roots of each of the above polynomials. Define another polynomial $\widehat{P}_{RMUSIC}(z)$ as follows

$$\widehat{P}_{RMUSIC}(z) = \sum_{j=k_0}^{M-1} e_j(z)e_j^*(1/z^*),$$

$$
\begin{aligned}
&= \prod_{m=0}^{M-1} (1 - z_m z^{-1})(1 - z_m^* z), \\
&= D(z) D^*(1/z^*),
\end{aligned} \tag{4.7}
$$

where $D(z) = \prod_{m=0}^{M-1}(1 - z_m z^{-1})$ can be obtained by a spectral factorization [40] of $\widehat{P}_{RMUSIC}(z)$ and has its roots inside or on the unit circle. The k_0 signal zeros are the roots of $D(z)$ that are closest to the unit circle, i.e. $|z| = 1$, thereby recovering the signal angles $\phi_k, k = 0, \ldots, k_0 - 1$.

Maximum Likelihood methods When *a priori* density of a parameter is known, techniques must be developed that make no presumption about the relative possibilities of parameter values. In the event of DOA estimation, the maximum likelihood (ML) estimator can be used that maximizes the likelihood function of the observation $\mathbf{y}(n)$, given other parameters. According to the observation model in (2.53) with the noise being a Gaussian random variable, we can define the likelihood function as follows

$$
l(\phi; \mathbf{y}(n)) \triangleq (\mathbf{y}(n)|\phi) \sim N(\mathbf{S}(\phi)\mathbf{a}(n), \sigma_\nu^2 \mathbf{I}_M), \tag{4.8}
$$

where $N(m, \Sigma)$ refers to a normal distribution with mean m and covariance matrix Σ. Note that this is a function of the parameter ϕ and not of $\mathbf{y}(n)$. The value of the parameter that maximizes this function is called the maximum-likelihood estimate, defined by

$$
\widehat{\phi}_{ML} = arg\ max_{\phi \in \Phi} p(\mathbf{y}|\phi). \tag{4.9}
$$

The ML estimator in (4.9) can be interpreted as a search for a set of ϕ such that the sum of the Euclidean distances between the observations $\mathbf{y}(n)$ and the estimates $\widehat{\mathbf{y}}(n|\phi)$ is minimized, i.e.,

$$
\widehat{\phi}_{ML} = arg\ min_{\phi \in \Phi} \sum_{n=1}^{N_t} \|\mathbf{y}(n) - \widehat{\mathbf{y}}(n|\phi)\|^2. \tag{4.10}
$$

The estimates $\widehat{\mathbf{y}}(n|\phi)$ are obtained by the least-squares estimate of the amplitude $\mathbf{a}(n)$ as follows

$$\widehat{\mathbf{y}}(n|\phi) = \mathbf{S}(\phi)\widehat{\mathbf{a}}(n) \tag{4.11}$$

where, according to (2.53), the least-squares estimate $\widehat{\mathbf{a}}(n)$ is given by

$$\widehat{\mathbf{a}}(n) = \left[\mathbf{S}^H(\phi)\mathbf{S}(\phi)\right]^{-1}\mathbf{S}^H(\phi)\mathbf{y}(n). \tag{4.12}$$

Defining a model dependent projector matrix by $\mathbf{P}_S(\phi)$ as

$$P_S(\phi) = \mathbf{S}(\phi) = \mathbf{S}(\phi)\left[\mathbf{S}^H(\phi)\mathbf{S}(\phi)\right]^{-1}\mathbf{S}^H(\phi), \tag{4.13}$$

and its orthogonal complement as

$$\mathbf{P}_S^{\perp}(\phi) = \mathbf{I} - \mathbf{P}_S(\phi), \tag{4.14}$$

We can rewrite the estimate $\widehat{y}(n|\phi)$ as

$$\widehat{\mathbf{y}}(n|\phi) = \mathbf{P}_S(\phi)\mathbf{y}(n), \tag{4.15}$$

such that the ML estimator in (4.9) becomes

$$\begin{aligned}
\widehat{\phi}_{ML} &= arg\ min_{\phi\in\Phi}\sum_{n=1}^{N_t}\|\mathbf{y}(n) - \widehat{\mathbf{y}}(n)\|^2, \\
&= arg\ min_{\phi\in\Phi}\sum_{n=1}^{N_t}\|(\mathbf{I} - \widehat{\mathbf{P}}_S(\phi))\mathbf{y}(n)\|^2, \\
&= arg\ min_{\phi\in\Phi}\sum_{n=1}^{N_t} tr(\mathbf{P}_S^{\perp}(\phi)\widehat{\mathbf{R}}_{yy}), \\
&= arg\ min_{\phi\in\Phi}\sum_{n=1}^{N_t} tr(\mathbf{P}_S(\phi)\widehat{\mathbf{R}}_{yy}),
\end{aligned} \tag{4.16}$$

where $tr(.)$ is the trace operator, and $\widehat{\mathbf{R}}_{yy}$ is the sample covariance matrix. The same result can also be obtained in a Bayesian context [41], [42], [43], [44]. Since the

ML estimator does not take any prior knowledge of the parameters into account, it is expected that the error characteristics of the resulting estimates could be worse than those that can use prior knowledge. Moreover, like many other optimization problems, the ML estimation problem is well known to be difficult, as the function to optimize shows many saddle points and local extrema. Any gradient based method would need a good initialization in order to succeed.

4.2 *Wideband Source Localisation*

Focusing technique the coherent Signal-Subspace Method (CSM) [45] is a focusing technique that transforms the signal subspaces spanned by the columns of $\mathbf{S}(\phi, \omega_j)$ in all frequency bins $j = 0, \ldots, J-1$ and overlaps them in a predefined subspace, known as the focusing subspace [45]. Given a predefined focusing frequency ω_F and hence the focusing location matrix $\mathbf{S}(\phi, \omega_F)$, the objective of the focusing technique is to find the solution $\mathbf{T}(\omega_j)$ of the equations given by

$$\mathbf{T}(\omega_j)\mathbf{S}(\phi, \omega_j) = \mathbf{S}(\phi, \omega_F), \quad j = 0, \ldots, J-1. \tag{4.17}$$

Using the focusing matrices $\mathbf{T}(\omega_j)$, the snapshots at different frequency bins can be transformed into the focusing subspace, i.e.,

$$\mathbf{y}^{(j)}(n) = \mathbf{T}(\omega_j)\mathbf{y}(n), \tag{4.18}$$

and then a set of sample covariance matrices at different frequency bins can be constructed as

$$\widehat{\mathbf{R}}_{yy}^{(j)} = \frac{J}{N_t} \sum_{n=1+j}^{jN_t/j} \mathbf{y}^{(j)}(n)\mathbf{y}^{(j)^H}(n), \quad j = 0, \ldots, J-1 \tag{4.19}$$

Eventually, a universal focused sample covariance matrix that can be used for detection and estimation can be obtained as follows

$$\begin{aligned}\widehat{\mathbf{R}}_{yy}^{(F)}=&\frac{1}{J}\sum_{j=0}^{J-1}\widehat{\mathbf{R}}_{yy}^{(j)},\\ =&\mathbf{S}(\phi,\omega_F)\widehat{\mathbf{R}}_{aa}^{(F)}\mathbf{S}^H(\phi,\omega_F)+\mathbf{R}_{\nu}^{(F)}\end{aligned} \tag{4.20}$$

where

$$\begin{aligned}\widehat{\mathbf{R}}_{aa}^{(F)}=&\frac{1}{J}\sum_{j=0}^{J-1}\widehat{\mathbf{R}}_{aa}(\omega_j),\\ \mathbf{R}_{\nu}^{(F)}=&\frac{1}{J}\sum_{j=0}^{J-1}\mathbf{T}(\omega_j)\Sigma_{\nu}(\omega_j)\mathbf{T}^H(\omega_j).\end{aligned} \tag{4.21}$$

Given that the sample covariance matrix in (4.20) approximately corresponds to that for narrowband signals, it is then possible to apply narrowband methods to the wideband problem. While the CSM algorithm improves the efficiency of the estimation by considering the energy in the sub-bands into the focusing signal subspace, it suffers from a few problems that degrade the overall performance. Firstly, the transformation involving the matrices $\mathbf{T}(\omega_j)$ will change the original noise structure as well as the SNR levels at the output of the processor. In particular, if the observation noise is Gaussian and white, the transformed noise is no longer white. Secondly, it was pointed out that the method suffers from an asymptotic bias of the peaks in the spatial spectrum. This bias increases with the bandwidth of the sources and the deviation of the focusing points from the true DOAs. Nevertheless, it was shown [46] that if the matrices $\mathbf{T}(\omega_j)$ are unitary transformations, the focusing is lossless. The Two-sided Correlation Transformation (TCT), which is another focusing technique and uses a similar focusing concept as in the CSM, performs the focusing transformation on the covariance matrix of the sources instead of the location matrix. The transformation matrix at each frequency bin is unitary and minimizes the distance between the focusing subspace and the transformed signal subspace. The TCT and the CSM differ in two areas. Firstly, the transformation of the subspace using the TCT is performed through a two-sided transformation applied to the source covariance matrix, which

can be shown to result in a smaller error. Secondly, given that many high resolution algorithms for DOA estimation are based on the eigen-decomposition of the covariance matrix, the TCT applies the transformation on the source covariance matrix instead of the location matrix. Similar to the CSM procedures, a predefined focusing covariance matrix is given, and the objective of the TCT is to find all solutions of the transformation matrices that minimize the distance between the focusing covariance matrix and source covariance matrices in all frequency bins, under the constraint that the transformation matrices are kept unitary. Let $\widehat{\mathbf{R}}_{aa}^{(F)}$ be the focusing covariance matrix, and $\mathbf{U}(\omega_j)$ for $j = 0, \ldots, J-1$ be the focusing matrices. Then the TCT focusing matrices can be found by the following optimization

$$\begin{aligned} min_{\mathbf{U}(\omega_j)} \|\widehat{\mathbf{U}}(\omega_j) - \mathbf{U}(\omega_j)\widehat{\mathbf{R}}_{aa}^{(F)}\mathbf{U}^H(\omega_j)\| \\ s.t. \quad \mathbf{U}^H(\omega_j)\mathbf{U}(\omega_j) = \mathbf{I} \end{aligned} \tag{4.22}$$

for $j = 0, \ldots, J-1$. Once the set of focusing matrices is obtained, the transformed covariance matrices at different frequency bins can be constructed as

$$\widehat{\mathbf{R}}_{yy}(\omega_j) = \frac{J}{N_t} \sum_{n=1+j}^{jN_t/J} \mathbf{y}^{(j)}(n)\mathbf{y}^{(j)^H}(n), \quad j = 0, \ldots, J-1, \tag{4.23}$$

where

$$\mathbf{y}^{(j)}(n) = \mathbf{U}(\omega_j)\mathbf{y}(n). \tag{4.24}$$

Finally, a universal focused sample covariance matrix can be constructed as follows

$$\widehat{\mathbf{R}}_{yy}^{(F)} = \frac{1}{J} \sum_{j=0}^{J-1} \widehat{\mathbf{R}}_{yy}(\omega_j). \tag{4.25}$$

The covariance matrix in (4.25) is approximatively equal to that for narrowband signals, and hence can be applied to narrowband methods previously developed for detection and estimation problems when the signals are narrowbamd. If the observation noise is Gaussian and white, then a preprocessing step can be taken to reduce

the noise components in the covariance matrices. This step requires a low-resolution beamformer to estimate the number of sources and the DOAs of the sources. With the knowledge of the estimated number of sources, performing an eigen-decomposition on the covariance matrices $\widehat{\mathbf{R}}_{yy}(\omega_j)$ at the jth frequency bin yields an estimate of the noise power as follows

$$\widehat{\sigma}_{\nu}^{2}(\omega_j) = \frac{1}{M-k_0} \sum_{m=k_0}^{M-1} \widehat{\lambda}_m \left(\widehat{\mathbf{R}}_{yy}(\omega_j) \right), \tag{4.26}$$

where $\widehat{\lambda}_m \left(\widehat{\mathbf{R}}_{yy}(\omega_j) \right)$ for $m = 0, \ldots, M-1$ are the estimated eigenvalues of the $\widehat{\mathbf{R}}_{yy}(\omega_j)$ that are arranged in descending order. Therefore, the source covariance matrices can be rewritten as

$$\widehat{\mathbf{R}}_{aa}(\omega_j) = \mathbf{B}(\omega_j) \left[\widehat{\mathbf{R}}_{yy}(\omega_j) - \widehat{\sigma}_{\nu}^{2}(\omega_j)\mathbf{I} \right] \mathbf{B}^{H}(\omega_j), \quad j = 0, \ldots, J-1 \tag{4.27}$$

where

$$\mathbf{B}(\omega_j) = \left[\mathbf{S}^{H}(\phi, \omega_j)\mathbf{S}(\phi, \omega_j) \right]^{-1} \mathbf{S}^{H}(\phi, \omega_j) \tag{4.28}$$

As a result, the noise-free focused sample covariance matrix can be simplified as

$$\widehat{\mathbf{R}}_{yy}^{(F)} = \mathbf{S}(\phi, \omega_F)\widehat{\mathbf{R}}_{aa}^{(F)}\mathbf{S}^{H}(\phi, \omega_F) \tag{4.29}$$

where

$$\widehat{\mathbf{R}}_{aa}^{(F)} = \frac{1}{J} \sum_{j=0}^{J-1} \widehat{\mathbf{R}}_{aa}(\omega_j), \tag{4.30}$$

$$\mathbf{S}(\phi, \omega_F) = \mathbf{U}(\omega_j)\mathbf{S}(\phi, \omega_j), \quad j = 0, \ldots, J-1 \tag{4.31}$$

Finally, the desired focused covariance matrix will be applied to appropriate algorithms for detection and estimation. The TCT method has a smaller subspace fitting error than the CSM, and has unbiased estimates of the DOAs, regardless of

the bandwidth of the signals. Both the CSM and the TCT techniques transform the wideband signals into a common subspace, where the transformed signals approximately become narrowband. Since these methods operate in the frequency domain, and the accuracy of the focusing relies on the size of the frequency bins, they require a relatively larger amount of data than other competing methods. Furthermore, it is assumed that an appropriately selected focusing matrix or focusing frequency ω_F will be given in each method, but such a selection could be arbitrary. When an inappropriate focusing matrix is selected, the overall detection and estimation performance is significantly degraded.

Asymptotic Maximum-Likelihood Methods The asymptotic maximum - likelihood (AML) method [47], [48], and [3] are extension of the ML estimators. In particular, when the signals in the estimation problem are wideband and J is sufficiently large and there is no frequency correlation in the sources, the set of frequency spectra $\mathbf{Y}(\omega_j)$ for all j can be considered independent so that the AML methods can perform DOA estimation jointly in J frequency bins. Denote the AML estimate of the DOAs by $\widehat{\phi}_{AML}$. We define $\widehat{\mathbf{P}}_j$ as the projection matrix for $\omega = \omega_j$ onto the range of $\mathbf{S}(\widehat{\phi}_{AML}, \omega_j)$, given by

$$\widehat{\mathbf{P}}_j = \mathbf{S}(\widehat{\phi}_{AML}, \omega_j) \left[\mathbf{S}(\widehat{\phi}_{AML}, \omega_j)\mathbf{S}^H(\widehat{\phi}_{AML}, \omega_j)\right]^{-1} \mathbf{S}^H(\widehat{\phi}_{AML}, \omega_j), \quad j = 0, \ldots, J-1, \tag{4.32}$$

and $\widehat{\mathbf{C}}_{yy}(\omega_j)$ as the sample covariance matrix for the observations at ω_j, given by

$$\widehat{\mathbf{C}}_{yy}(\omega_j) = \frac{1}{N_t} \sum_{n=1}^{N_t} \mathbf{Y}(\omega_j)\mathbf{Y}^H(\omega_j), \quad j = 0, \ldots, J-1. \tag{4.33}$$

Accordingly, the orthogonal complement of $\widehat{P}_j$ is given by

$$\widehat{\mathbf{P}}_j^{\perp} = \mathbf{I} - \widehat{\mathbf{P}}_j. \tag{4.34}$$

Depending on the knowledge of the observation noise variance σ_ν^2 at ω_j, there are three cases by which the total likelihood function $L_l(\widehat{\phi}_{AML}), l = 1, 2, 3$, can be

defined [3], provided the number of sources k_0 is available. In each case, the AML estimate $\widehat{\phi}_{AML}$ can be obtained by

$$\widehat{\phi}_{AML} = arg\ max_{\phi\in\Phi} \sum_{j=0}^{J-1} L_l(\widehat{\phi}_{AML}), \quad l = 1, 2, 3, \tag{4.35}$$

1. When $\eta_j \triangleq \sigma_\nu^2(\omega_j), \quad j = 0, \ldots, J-1$, is known, the total likelihood function $L_1(\widehat{\phi}_{ML})$ is defined by

$$L_1(\widehat{\phi}_{ML}) = \sum_{j=0}^{J-1} \frac{-1}{\eta_j} tr\left[\widehat{\mathbf{P}}_j^{\perp}\widehat{\mathbf{C}}_{yy}(\omega_j)\right] - log\ det\left[\widehat{\mathbf{P}}_j\widehat{\mathbf{C}}_{yy}(\omega_j)\widehat{\mathbf{P}}_j + \eta_j\widehat{\mathbf{P}}_j^{\perp}\right] \tag{4.36}$$

2. When $\eta_j \triangleq \sigma_\nu^2(\omega_j), \quad j = 0, \ldots, J-1$, is unknown, then an estimate of η_j is computed as follows

$$\eta_j = \frac{tr\left[\widehat{\mathbf{P}}_j^{\perp}\widehat{\mathbf{C}}_{yy}(\omega_j)\right]}{M - k_0}, \tag{4.37}$$

such that the total likelihood function $L_2(\widehat{\phi}_{AML})$ is given by

$$L_2(\widehat{\phi}_{AML}) = -\varphi(\widehat{\phi}_{AML}) - (M - k_0)\sum_{j=0}^{J-1} log\ tr\left[\widehat{\mathbf{P}}_j^{\perp}\widehat{\mathbf{C}}_{yy}(\omega_j)\right], \tag{4.38}$$

where

$$\varphi(\widehat{\phi}_{AML}) = \sum_{j=0}^{J-1} log\ det\left[\widehat{\mathbf{P}}_j\widehat{\mathbf{C}}_{yy}(\omega_j)\widehat{\mathbf{P}}_j + \widehat{\mathbf{P}}_j^{\perp}\right]. \tag{4.39}$$

3. When $\eta_j \triangleq \sigma_\nu^2(\omega_j) = \sigma_\nu^2, \quad j = 0, \ldots, J-1$, and σ_ν^2 is unknown, then an estimate of η_j is computed as follows

$$\widehat{\eta} = \frac{\sum_{j=0}^{J-1} tr\left[\widehat{\mathbf{P}}_j^{\perp}\widehat{\mathbf{C}}_{yy}(\omega_j)\right]}{J(M - k_0)} \tag{4.40}$$

such that the total likelihood function $L_3(\widehat{\phi}_{AML})$ is given by

$$L_3(\widehat{\phi}_{AML}) = -\varphi(\widehat{\phi}_{AML}) - J(M-k_0)log\sum_{j=0}^{J-1} tr\left[\widehat{\mathbf{P}}_j^{\perp}\widehat{\mathbf{C}}(\omega_j)\right]. \tag{4.41}$$

It is possible performing parameter estimation by maximum likelihood in the frequency domain, but the global search in the parameter space of interest is computationally complex and generally not used in practice. In particular, to sustain a high accuracy in the estimation, the number of frequency bins J and the number of snapshots N_t need to be large, adding more computational burden to the algorithm. Furthermore, the knowledge of the model and the the initial estimates play a critical role in the performance of the method. The estimates can be unreliable if the model is inaccurate or the initial estimates are not precise enough. More detailed discussion of the AML estimator for wideband signals can be found in [49], [50].

4.3 *Application of the Proposed Algorithm*

Using our approach, the estimation of the DOA is almost straightforward since these later are related to the time delay parameters as we will see below.

If we consider N PPS sources impinging on an ULA of sensors consisting of M sensors. The outputs of the array sensors obey the model presented by (3.1) and (3.2).

If the N sources are located at the directions α_1, α_2,$\cdots$,α_N, the time delay τ_{nm} is related to these DOA through the equation

$$\tau_{nm} = \frac{(m-1)d}{c}\cos(\alpha_n), \quad n = 1,\ldots,N, \quad m = 1,\ldots,M \tag{4.42}$$

where c is the wave propagation speed, and d is the inter-sensor separation distance. Hence, the DOA estimation problem is resolved by replacing in (3.12) the time delay parameters $\tau_{n2}, \quad n = 1,\ldots,N$ by their corresponding DOAs $\alpha_n, \quad n = 1,\ldots,N$ (and accordingly replacing the delays in the EKF equations) leading to the following expression

$$\mathbf{x}(t)=\left[a_1 \;\; \alpha_1 \;\; \phi_1(t) \;\; \phi_1^{(1)}(t)\ldots\phi_1^{(L_1)}(t)\ldots\ldots a_N \;\; \alpha_N \;\; \phi_N(t) \;\; \phi_N^{(1)}(t)\ldots\phi_N^{(L_N)}(t)\right]^T,$$

We have seen in Section 3 that our approach allows the simultaneous estimation of the time delay parameters and the PPS parameters (by incorporating the time delays within the state vector), implicating the simultaneous estimation of the PPS parameters and their DOAs. In addition, the same algorithm can be used for both narrowband and wideband cases without need of any transformation.

We provide below an example illustrating the performance of our algorithm in terms of time delay parameters estimation.

We consider the case of three linear frequency modulated sources impinging on a 4-sensor array arriving from directions $\alpha_1 = 10^o$, $\alpha_2 = 20^o$, and $\alpha_3 = 30^o$ with respect to the broadside [33]. Hence, we have $N = 3$, $L_1 = L_2 = L_3 = 2$ and $M = 4$ with:

$$\begin{aligned}
a_1 = 1.0,\ \ b_{01} = \tfrac{\pi}{2} \text{ rd},\ \ b_{11} = 0.5\ \tfrac{rd}{s},\ \ b_{21} = \ \ 0.0025\ \tfrac{rd}{s^2}.\\
a_2 = 0.8,\ \ b_{02} = \tfrac{\pi}{4} \text{ rd},\ \ b_{12} = 1.5\ \tfrac{rd}{s},\ \ b_{22} = -0.0020\ \tfrac{rd}{s^2}.\\
a_3 = 0.7,\ \ b_{03} = \tfrac{\pi}{6} \text{ rd},\ \ b_{13} = 0.1\ \tfrac{rd}{s},\ \ b_{23} = \ \ 0.0010\ \tfrac{rd}{s^2}.
\end{aligned}$$

We consider 512 samples and choose the initial diagonal covariance matrix with the following diagonal elements 10^{-2}, 10^{-2}, 10^{-3}, 10^{-8}, 10^{-2}, 10^{-2}, 10^{-2}, 10^{-8}, 10^{-2}, 10^{-2}, 10^{-4}, 10^{-8}.

Figure 4.1 illustrates the the MSEs/CRLBs comparison for the three estimated DOAs and where we conclude that the algorithm performs well since the estimator MSEs achieve their corresponding CRLBs for SNR lower than 7 dB.

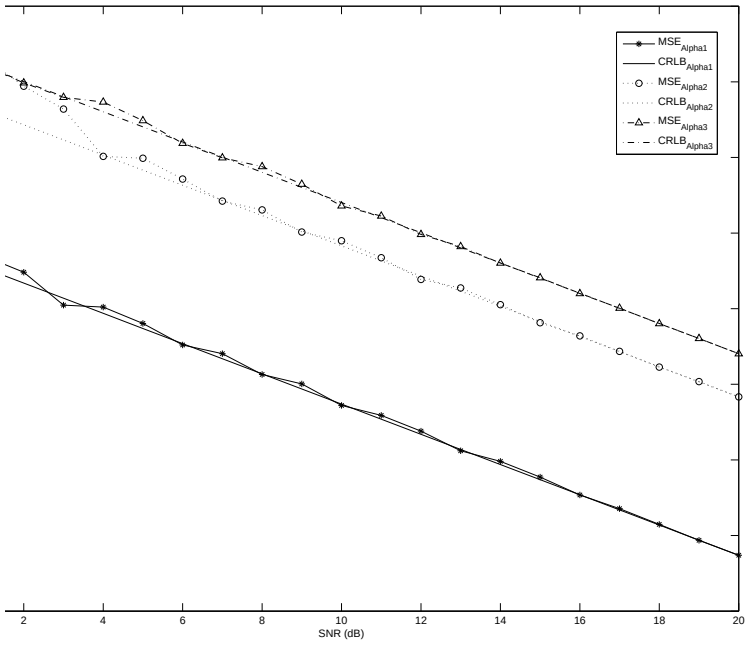

Fig. 4.1. Proposed algorithm DOAs estimation example: case of 3 PPS sources impinging, from different directions, on a 4 sensor array.

5. PERFORMANCE EVALUATION

In this chapter, we present the performance of the proposed approach. In all our simulation examples, we assume a ULA with omnidirectional sensors. The sonar case is considered with the sound propagation speed $v = 1500m/s$ and the inter-element spacing $d = 1.5m/s$. The sampling period and a sample size of 1 second and 512 samples are considered, respectively. The parameter initializations are at 20% of the actual values. The signal-to-noise ratio is defined by $SNR\ (dB) = 10\log_{10}\left[\sum_{n=1}^{N}\left(a_n^2\right)/(2\sigma^2)\right]$ and ranges from 0 dB to 20 dB, where the additive noises are zero-mean white Gaussian with variances $\{\sigma_i^2,\ i = 1,\ldots,N\}$. The performances are measured by comparing the mean square errors (MSE's), obtained through 100 Monte-Carlo trials, with their corresponding Cramér-Rao lower bounds (CRLB's). The delays are assumed unknown in all our simulation examples. Hence, the state-vector form given in (3.12) is considered. These nuisance parameters are initialized at 20% of their actual values.

5.1 *Cramèr-Rao Lower bound Derivation*

In this section, we derive for our model the Fisher information matrix (FIM). We assume M deterministic signals $\{s_m(t,\mathbf{\Psi}), m = 1,\ldots,M\}$ with unknown parameter vector $\mathbf{\Psi}$ observed in zero mean independent AWGNs $\{v_m(t), m = 1,\ldots,M\}$ of variances $\{\sigma_m^2, m = 1,\ldots,M\}$, respectively. For $t = 0,\ldots,P-1$, we have

$$\begin{cases} y_1(t,\mathbf{\Psi}) &= s_1(t,\mathbf{\Psi}) + v_1(t) \\ \vdots & \\ y_M(t,\mathbf{\Psi}) = s_M(t,\mathbf{\Psi}) + v_M(t) \end{cases}. \tag{5.1}$$

The $\mathbb{FIM}$ elements $\{FIM(\mathbf{\Psi})_{i,j}\}$, as defined in [51], are given by

$$FIM(\mathbf{\Psi})_{i,j} = -E\left(\frac{\partial^2 ln\ p\{y_1(t,\mathbf{\Psi}),\ldots,y_M(t,\mathbf{\Psi})\}}{\partial\psi_i\partial\psi_j}\right), \tag{5.2}$$

where ψ_i, ψ_j are the entries of the vector $\mathbf{\Psi}$ and p stands for the probability density. Having $\{y_m, m=1,\ldots,M\}$ mutually independent, we get

$$\begin{aligned} &p\{y_1(t,\mathbf{\Psi}),\ldots,y_M(t,\mathbf{\Psi})\} = \\ &\quad p\{y_1(t,\mathbf{\Psi})\}\times p\{y_2(t,\mathbf{\Psi})\}\times\cdots\times p\{y_M(t,\mathbf{\Psi})\}, \end{aligned} \tag{5.3}$$

and

$$\begin{aligned} &\frac{\partial^2 ln\ p\{y_1(t,\mathbf{\Psi}),\ldots,y_M(t,\mathbf{\Psi})\}}{\partial\psi_i\partial\psi_j} = \\ &\frac{1}{\sigma_1^2}\sum_{t=0}^{P-1}\left[(y_1(t,\mathbf{\Psi})-s_1(t,\mathbf{\Psi}))\frac{\partial^2 s_1(t,\mathbf{\Psi})}{\partial\psi_i\partial\psi_j}\right] \\ &-\frac{1}{\sigma_1^2}\sum_{t=0}^{P-1}\frac{\partial s_1(t,\mathbf{\Psi})}{\partial\psi_i}\frac{\partial s_1(t,\mathbf{\Psi})}{\partial\psi_j}+\cdots \\ &+\frac{1}{\sigma_M^2}\sum_{t=0}^{P-1}\left[(y_M(t,\mathbf{\Psi})-s_M(t,\mathbf{\Psi}))\frac{\partial^2 s_M(t,\mathbf{\Psi})}{\partial\psi_i\partial\psi_j}\right] \\ &-\frac{1}{\sigma_M^2}\sum_{t=0}^{P-1}\frac{\partial s_M(t,\mathbf{\Psi})}{\partial\psi_i}\frac{\partial s_M(t,\mathbf{\Psi})}{\partial\psi_j}. \end{aligned} \tag{5.4}$$

We then obtain

$$\begin{aligned} FIM(\mathbf{\Psi})_{i,j} &= \frac{1}{\sigma_1^2}\sum_{t=0}^{P-1}\left(\frac{\partial s_1(t,\mathbf{\Psi})}{\partial\psi_i}\frac{\partial s_1(t,\mathbf{\Psi})}{\partial\psi_j}\right) \\ &+\cdots+\frac{1}{\sigma_M^2}\sum_{t=0}^{P-1}\left(\frac{\partial s_M(t,\mathbf{\Psi})}{\partial\psi_i}\frac{\partial s_M(t,\mathbf{\Psi})}{\partial\psi_j}\right). \end{aligned} \tag{5.5}$$

The CRLB expression is then deduced from the following equation

$$\mathbb{CRLB}\left(\mathbf{\Psi}\right) = \mathbb{FIM}\left(\mathbf{\Psi}\right)^{-1}. \tag{5.6}$$

In application to our model defined by the equations 3.1 and 3.2, we get

$$\begin{cases} s_1\left(t, \mathbf{\Psi}\right) = \sum_{n=1}^{N} a_n \sin\left[\phi_n(t)\right] \\ s_2\left(t, \mathbf{\Psi}\right) = \sum_{n=1}^{N} a_n \sin\left[\phi_n\left(t - \frac{\tau_{n2}}{\Delta}\right)\right] \\ \vdots \\ s_M\left(t, \mathbf{\Psi}\right) = \sum_{n=1}^{N} a_n \sin\left[\phi_n\left(t - \frac{\tau_{nM}}{\Delta}\right)\right] \\ \mathbf{\Psi} = [a_1 \ \tau_{12} \ b_{01} \ b_{11} \ \ldots \ b_{L_1 1} \ \ldots\ldots \ a_N \ \tau_{N2} \ b_{0N} \ b_{1N} \\ \qquad \ldots \ b_{L_N N}]^T = [\psi_1 \ \psi_2 \ \ldots \ \psi_{d_N}]^T \end{cases}. \tag{5.7}$$

We give below the FIM entry expressions for the monocomponent chirp signal impinging on two-sensor array by using (5.5) and (5.7) (the FIM element expressions for the general case of MCPPS's impinging on a multi-sensor array are too heavy to present on this document)

$$\begin{aligned} FIM\left(\mathbf{\Psi}\right)_{11} =& \frac{1}{\sigma_1^2}\sum_{t=0}^{P-1}\sin^2\left[\phi_1(t)\right] + \frac{1}{\sigma_2^2}\sum_{t=0}^{P-1}\sin^2\left[\phi_2(t)\right] \\ FIM\left(\mathbf{\Psi}\right)_{12} =& \frac{1}{\sigma_2^2}\sum_{t=0}^{P-1}\{a_1\left(2b_2\left(\tau - t\Delta\right) - b_1\right) \\ & \times \sin\left[\phi_2(t)\right]\cos\left[\phi_2(t)\right]\} \\ FIM\left(\mathbf{\Psi}\right)_{13} =& \frac{1}{\sigma_1^2}\sum_{t=0}^{P-1} a_1 \sin\left[\phi_1(t)\right]\cos\left[\phi_1(t)\right] \\ & + \frac{1}{\sigma_2^2}\sum_{t=0}^{P-1} a_1 \sin\left[\phi_2(t)\right]\cos\left[\phi_2(t)\right] \\ FIM\left(\mathbf{\Psi}\right)_{14} =& \frac{1}{\sigma_1^2}\sum_{t=0}^{P-1} a_1 t\Delta \sin\left[\phi_1(t)\right]\cos\left[\phi_1(t)\right] \\ & + \frac{1}{\sigma_2^2}\sum_{t=0}^{P-1}\{a_1\left(t\Delta - \tau\right)\sin\left[\phi_2(t)\right] \\ & \times \cos\left[\phi_2(t)\right]\} \end{aligned}$$

$$FIM\left(\mathbf{\Psi}\right)_{15}=\frac{1}{\sigma_1^2}\sum_{t=0}^{P-1}a_1t^2\Delta^2\sin\left[\phi_1(t)\right]\cos\left[\phi_1(t)\right]$$
$$+\frac{1}{\sigma_2^2}\sum_{t=0}^{P-1}\{a_1\left(t\Delta-\tau\right)^2\sin\left[\phi_2(t)\right]$$
$$\times\cos\left[\phi_2(t)\right]\}$$

$$FIM\left(\mathbf{\Psi}\right)_{21}=FIM\left(\mathbf{\Psi}\right)_{12}$$
$$FIM\left(\mathbf{\Psi}\right)_{22}=\frac{1}{\sigma_2^2}\sum_{t=0}^{P-1}\{a_1^2\left(2b_2\left(\tau-t\Delta\right)-b_1\right)^2$$
$$\times\cos^2\left[\phi_2(t)\right]\}$$
$$FIM\left(\mathbf{\Psi}\right)_{23}=\frac{1}{\sigma_2^2}\sum_{t=0}^{P-1}\{a_1^2\left(2b_2\left(\tau-t\Delta\right)-b_1\right)$$
$$\times\cos^2\left[\phi_2(t)\right]\}$$

$$FIM\left(\mathbf{\Psi}\right)_{24}=\frac{1}{\sigma_2^2}\sum_{t=0}^{P-1}\{a_1^2\left(2b_2\left(\tau-t\Delta\right)-b_1\right)$$
$$\times\left(t\Delta-\tau\right)\Delta\cos^2\left[\phi_2(t)\right]\}$$
$$FIM\left(\mathbf{\Psi}\right)_{25}=\frac{1}{\sigma_2^2}\sum_{t=0}^{P-1}\{a_1^2\left(2b_2\left(\tau-t\Delta\right)-b_1\right)$$
$$\times\left(t\Delta-\tau\right)^2\cos^2\left[\phi_2(t)\right]\}$$
$$FIM\left(\mathbf{\Psi}\right)_{31}=FIM\left(\mathbf{\Psi}\right)_{13}$$
$$FIM\left(\mathbf{\Psi}\right)_{32}=FIM\left(\mathbf{\Psi}\right)_{23}$$
$$FIM\left(\mathbf{\Psi}\right)_{33}=\frac{1}{\sigma_1^2}\sum_{t=0}^{P-1}a_1^2\cos^2\left[\phi_1(t)\right]$$
$$+\frac{1}{\sigma_2^2}\sum_{t=0}^{P-1}a_1^2\cos^2\left[\phi_2(t)\right]$$
$$FIM\left(\mathbf{\Psi}\right)_{34}=\frac{1}{\sigma_1^2}\sum_{t=0}^{P-1}a_1^2t\Delta\cos^2\left[\phi_1(t)\right]$$
$$+\frac{1}{\sigma_2^2}\sum_{t=0}^{P-1}a_1^2\left(t\Delta-\tau\right)\cos^2\left[\phi_2(t)\right]$$

$$FIM\left(\mathbf{\Psi}\right)_{35}=\frac{1}{\sigma_1^2}\sum_{t=0}^{P-1}a_1^2t^2\Delta^2\cos^2\left[\phi_1(t)\right] + \frac{1}{\sigma_2^2}\sum_{t=0}^{P-1}a_1^2\left(t\Delta-\tau\right)^2\cos^2\left[\phi_2(t)\right]$$

$$FIM\left(\mathbf{\Psi}\right)_{41}=FIM\left(\mathbf{\Psi}\right)_{14}$$

$$FIM\left(\mathbf{\Psi}\right)_{42}=FIM\left(\mathbf{\Psi}\right)_{24}$$

$$FIM\left(\mathbf{\Psi}\right)_{43}=FIM\left(\mathbf{\Psi}\right)_{34}$$

$$FIM\left(\mathbf{\Psi}\right)_{44}=\frac{1}{\sigma_1^2}\sum_{t=0}^{P-1}a_1^2t^2\Delta^2\cos^2\left[\phi_1(t)\right] + \frac{1}{\sigma_2^2}\sum_{t=0}^{P-1}a_1^2\left(t\Delta-\tau\right)^2\cos^2\left[\phi_2(t)\right]$$

$$FIM\left(\mathbf{\Psi}\right)_{45}=\frac{1}{\sigma_1^2}\sum_{t=0}^{P-1}a_1^2t^3\Delta^3\cos^2\left[\phi_1(t)\right] + \frac{1}{\sigma_2^2}\sum_{t=0}^{P-1}a_1^2\left(t\Delta-\tau\right)^3\cos^2\left[\phi_2(t)\right]$$

$$FIM\left(\mathbf{\Psi}\right)_{51}=FIM\left(\mathbf{\Psi}\right)_{15}$$

$$FIM\left(\mathbf{\Psi}\right)_{52}=FIM\left(\mathbf{\Psi}\right)_{25}$$

$$FIM\left(\mathbf{\Psi}\right)_{53}=FIM\left(\mathbf{\Psi}\right)_{35}$$

$$FIM\left(\mathbf{\Psi}\right)_{54}=FIM\left(\mathbf{\Psi}\right)_{45}$$

$$FIM\left(\mathbf{\Psi}\right)_{55}=\frac{1}{\sigma_1^2}\sum_{t=0}^{P-1}a_1^2t^4\Delta^4\cos^2\left[\phi_1(t)\right] + \frac{1}{\sigma_2^2}\sum_{t=0}^{P-1}a_1^2\left(t\Delta-\tau\right)^4\cos^2\left[\phi_2(t)\right],$$

where $\tau=\tau_{12}$, $b_0=b_{01}$, $b_1=b_{11}$, $b_2=b_{21}$, $\phi_1(t)=b_0+b_1t\Delta+b_2t^2\Delta^2$, and $\phi_2(t)=b_0+b_1\left(t\Delta-\tau\right)+b_2\left(t\Delta-\tau\right)^2$.

5.2 *Application to Polynomial Phase Signals*

The first example consists of three linear frequency modulated sources impinging on a 4-sensor array arriving from directions $\alpha_1 = 10^o$, $\alpha_2 = 20^o$, and $\alpha_3 = 30^o$ with respect to the broadside [33]. Hence, we have $N = 3$, $L_1 = L_2 = L_3 = 2$ and $M = 4$ with:

$$\begin{aligned} a_1 = 1.0,\ \ b_{01} = \tfrac{\pi}{2} \text{ rd},\ \ b_{11} = 0.5\ \tfrac{rd}{s},\ \ b_{21} = \ \ 0.0025\ \tfrac{rd}{s^2}. \\ a_2 = 0.8,\ \ b_{02} = \tfrac{\pi}{4} \text{ rd},\ \ b_{12} = 1.5\ \tfrac{rd}{s},\ \ b_{22} = -0.0020\ \tfrac{rd}{s^2}. \\ a_3 = 0.7,\ \ b_{03} = \tfrac{\pi}{6} \text{ rd},\ \ b_{13} = 0.1\ \tfrac{rd}{s},\ \ b_{23} = \ \ 0.0010\ \tfrac{rd}{s^2}. \end{aligned}$$

We choose the initial diagonal covariance matrix with the following diagonal elements 10^{-2}, 10^{-2}, 10^{-3}, 10^{-8}, 10^{-2}, 10^{-2}, 10^{-2}, 10^{-8}, 10^{-2}, 10^{-2}, 10^{-4}, 10^{-8}. The propagation delays are given as follows:

$\tau_{12} = 0.000174$ second, $\tau_{22} = 0.000342$ second, $\tau_{32} = 0.0005$ second.

$\tau_{13} = 0.000348$ second, $\tau_{23} = 0.000684$ second, $\tau_{33} = 0.0010$ second.

$\tau_{14} = 0.000522$ second, $\tau_{24} = 0.001026$ second, $\tau_{34} = 0.0015$ second.

And where the delays are related to the DOAs according to the relation: $\tau_{nm} = ((m-1)d/v \sin(\alpha_n), n = 1, \ldots, 3, m = 2, \ldots, 4)$.

Figure 5.1 shows the filter error covariance matrix evolution for SNR = 10 dB along with the MSEs/CRLBs comparison in the case of known phase degree (part (a)) and overestimated phase degree (part (b)). In both cases, the algorithm performs well, where the estimator MSE's achieve their corresponding CRLB's for SNR lower than 5 dB, with earlier convergence of the filter in case (a) (concluded from the error covariance matrix trace plot). For case (b), a wider model was considered by taking in expression (3.12) $N = 3$ and $L_1 = L_2 = L_3 = 5$. The filter converges to zero for the parameters $\{b_{ln},\ n = 1, \ldots, 3,\ \ l = 3, \ldots, 5\}$. This can be seen as phase degree determination method when these latter are unknown. We only considered the two high order coefficients $\{b_{ln}, l = 1, \ldots, 2, n = 1, \ldots, 3\}$ to illustrate the algorithm performance since it was noticed, after an extensive number of simulations, that these parameters are estimated prior to the initial phases $\{b_{0n}, n = 1, \ldots, 3\}$, and their

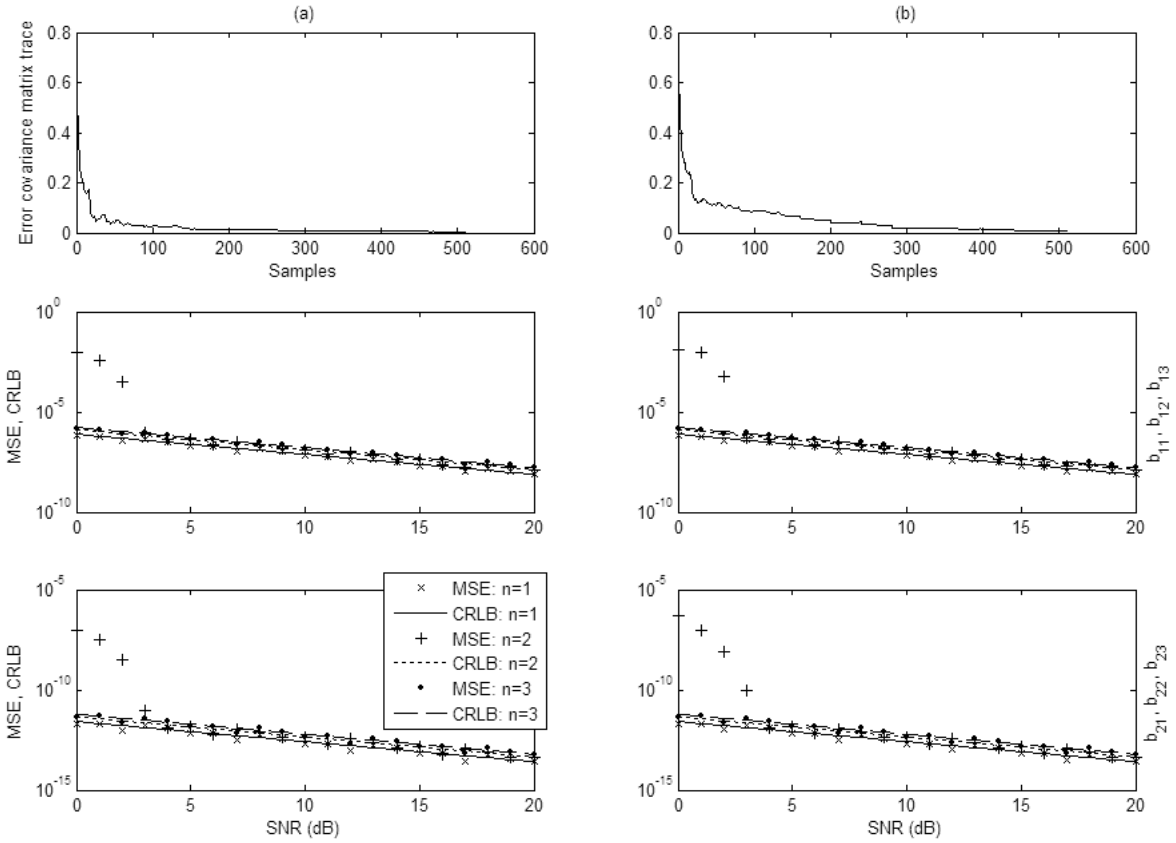

Fig. 5.1. Mean square errors and the corresponding Cramér-Rao lower bounds versus varying signal-to-noise ratio, along with the error covariance matrix trace evolution at SNR = 10 dB. a- case known phase degrees (equalling 3), b- unknown phase degrees (actual values equalling 3 and overestimated to 5). .

good estimation would implicate good estimation of the initial phases.

Figure 5.2 illustrates the evaluation of the algorithm performance in the case where two of the three sources impinge from the same direction. The same simulation conditions as in the first example, part (a), are kept except the angles of arrival, where we now have $\alpha_1 = 10^o$, $\alpha_2 = 10^o$, and $\alpha_3 = 30^o$. Our estimator remains efficient with performances similar to Figure 5.1 (a). The situation of similar angles of arrival translates into similar delays in the state-vector. Reducing the dimension of the

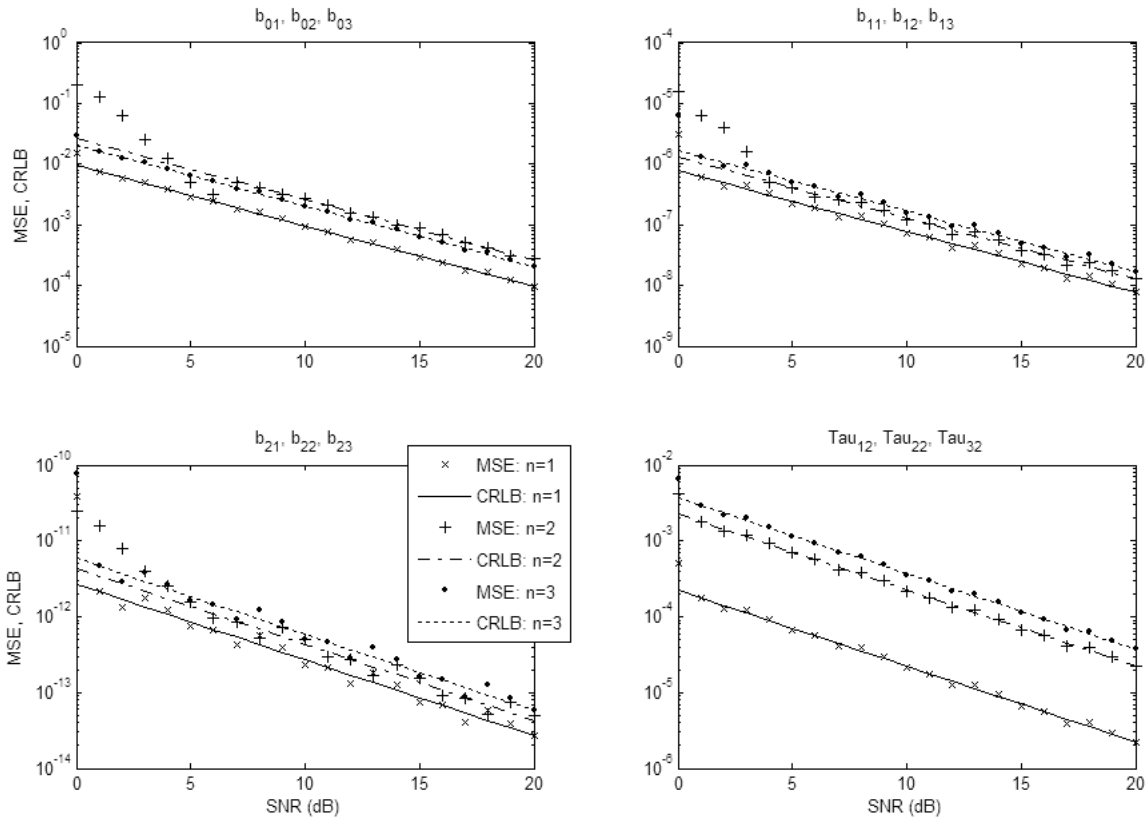

Fig. 5.2. Mean square errors and the corresponding Cramér-Rao lower bounds versus varying signal-to-noise ratio, case where two signals impinge from the same direction.

state-vector is possible in applications where we a priori know that some sources are impinging from the same direction. This is done by omitting the redundant delay variable obtaining a reduced computation cost.

In example 3, the performance of the algorithm is presented for fifth order PPS source models where the same state-vector as in Example 1, (b) is considered. Figure 5.3 illustrates the error covariance matrix trace evolution for SNR = 10 dB. A bad evolution can be noticed for the first 20 samples and a good evolution for the remaining samples, where the filter converges to the actual parameter values. An extensive number of simulations have been performed where we observe cases of filter

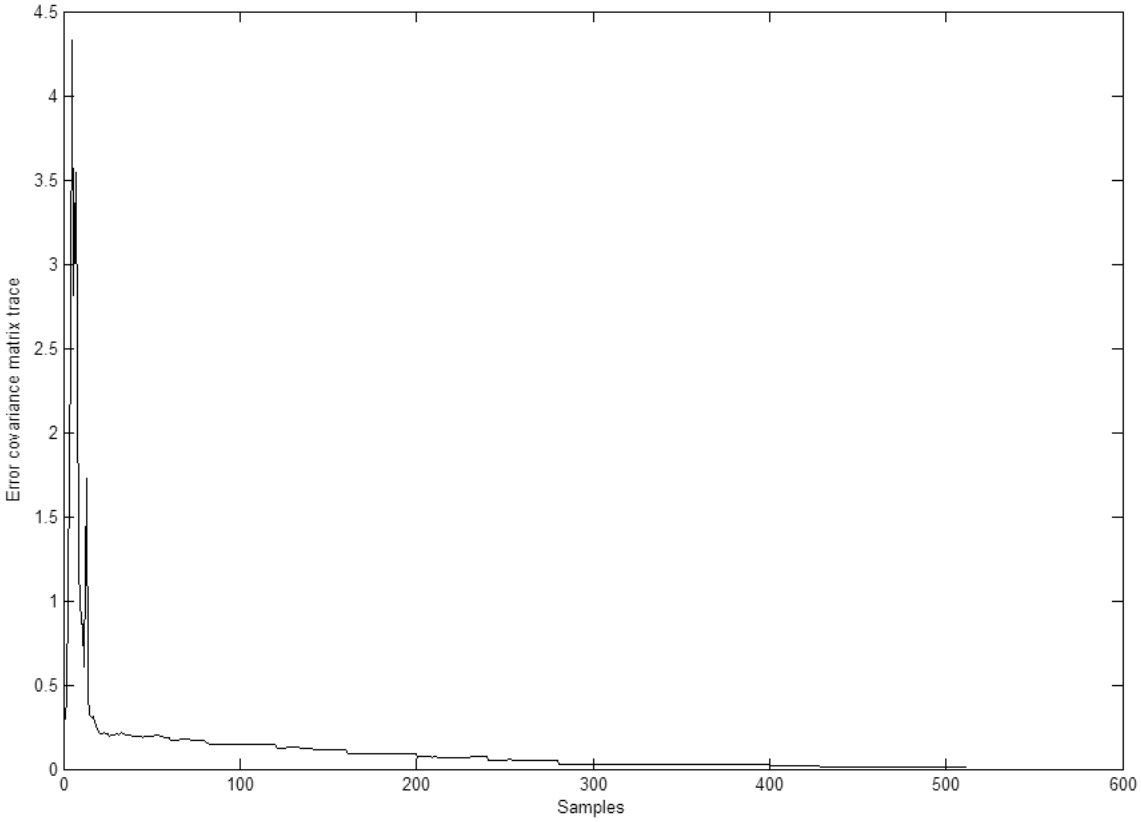

Fig. 5.3. Error covariance matrix trace evolution at SNR = 10 dB, case of PPS's of high phase degree (5th order).

divergence. This is due to the very small values of the higher order phase coefficients producing a badly conditioned error covariance matrix.

In example 4, the approach of [34] has been implemented and compared to our algorithm with considering a wideband chirp signal with the following parameters: $a_0 = 1$, $b_0 = 0$ rd, $b_1 = 0\ \frac{rd}{s}$, and $b_2 = 0.0061\ \frac{rd}{s^2}$.

Figure 5.4 shows that the proposed method outperforms the one of [34] where, for this latter, we have non-decaying MSE's for SNR greater than 4 dB whereas for our estimator, the MSE's become closer to their respective CRLB's for higher SNR values (for the phase parameters).

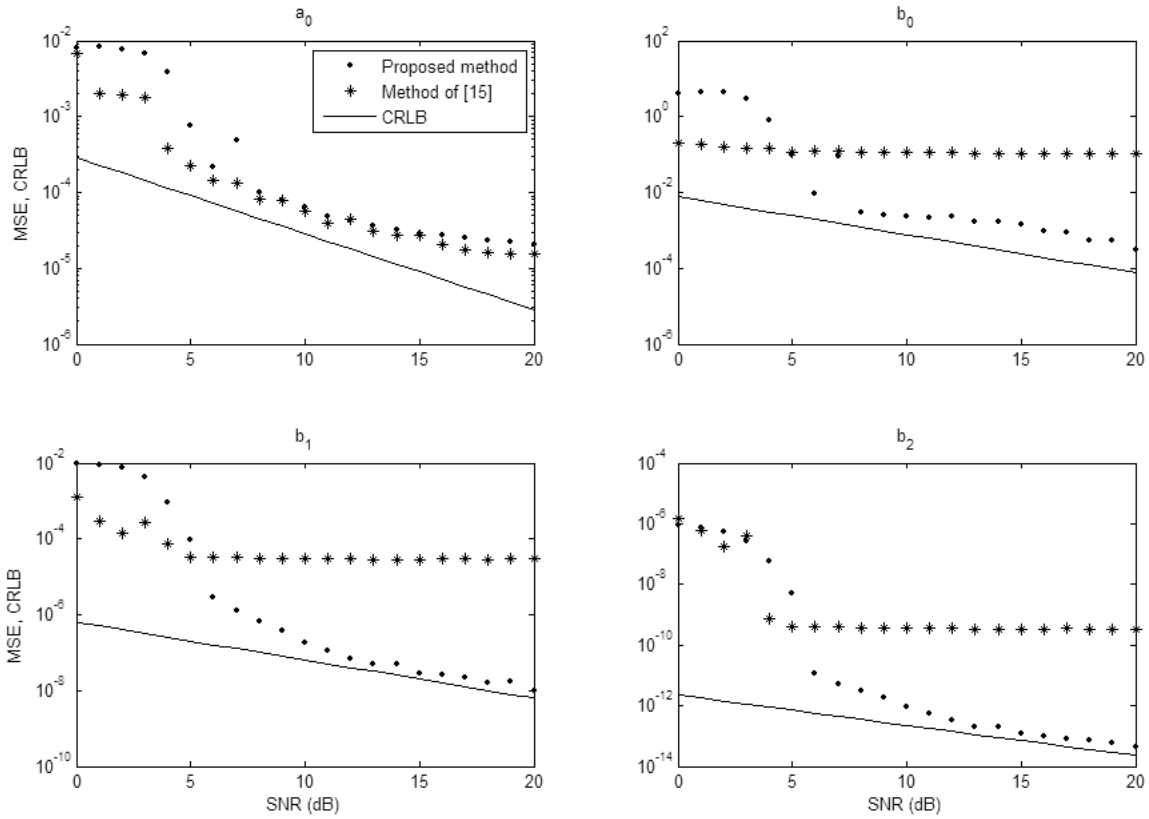

Fig. 5.4. Performance comparison with [34], case wideband chirp signal (a 2-sensor array has been used for our approach).

In example 5 the comparison of our algorithm is extended to the method developed in [19] (Product High-Order Ambiguity Function, PHAF). Example 1 - (a) scenario is taken with the actual PPS's parameter values (narrowband signals)

$$a_1 = 1,\ \ b_{01} = 0 \text{ rd},\ \ b_{11} = 0.25\ \tfrac{rd}{s},\ \ b_{21} = 0.25/512\ \tfrac{rd}{s^2}.$$
$$a_2 = 1,\ \ b_{02} = 0 \text{ rd},\ \ b_{12} = 0.50\ \tfrac{rd}{s},\ \ b_{22} = 0.50/512\ \tfrac{rd}{s^2}.$$
$$a_3 = 1,\ \ b_{03} = 0 \text{ rd},\ \ b_{13} = 0.75\ \tfrac{rd}{s},\ \ b_{23} = 0.75/512\ \tfrac{rd}{s^2}.$$

Figure 5.5 illustrates the simulation results. Our algorithm offers abetter performance where a more efficient estimator is obtained. Performances of both methods have been evaluated considering the higher order coefficients because PHAF performance

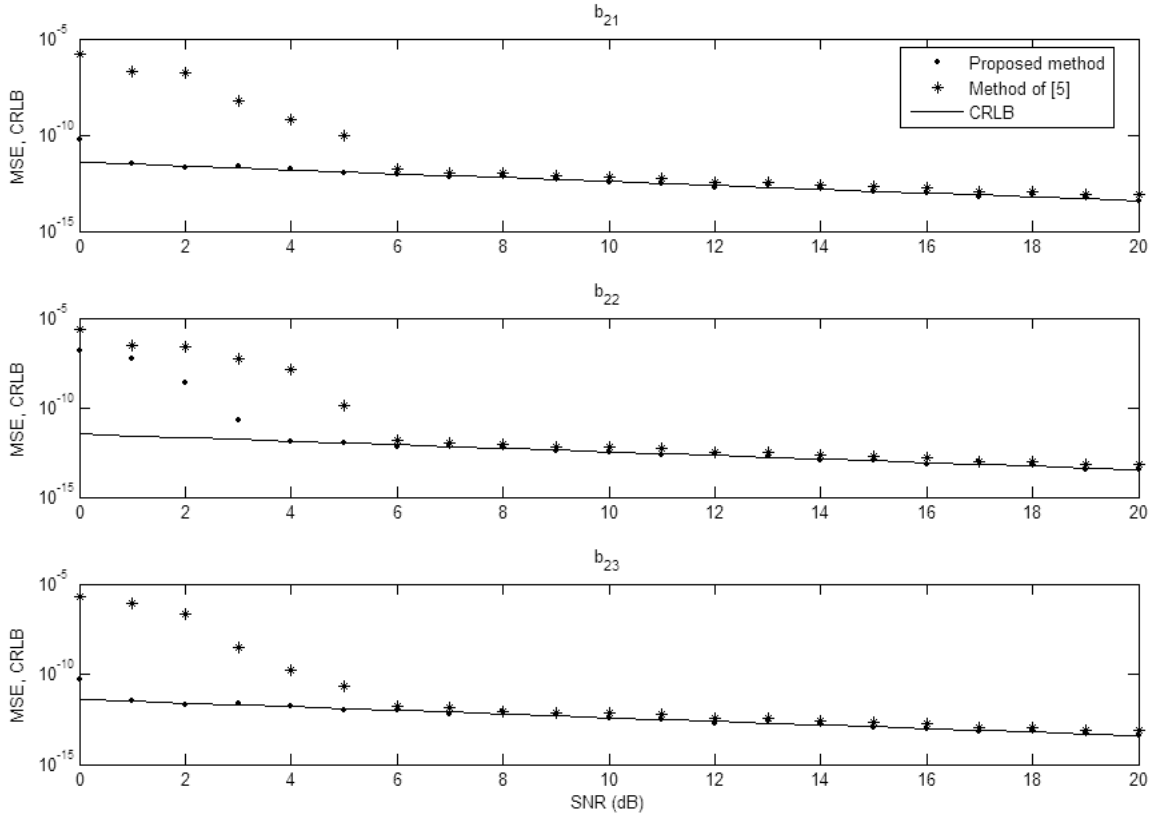

Fig. 5.5. Performance comparison with [19], case 3 narrowband chirp signals (a 4-sensor array has been used for our approach).

is highly dependent on the estimation result of these parameters [19] (the number of lags used for PHAF implementation equals 6). We note that using our approach, it is possible to estimate the DOA of the sources whereas this is impossible using PHAF.

In example 6, the performances of our approach are compared with those of [16] (ML approach) in the case of wideband sources by considering a scenario given in [16] where we have two sources impinging on a 10-sensor array

$$a_1 = 1, \;\; b_{01} = 0 \text{ rd}, \;\; b_{11} = 0.24\pi \; \tfrac{rd}{s}, \;\; b_{21} = -0.0024\pi \; \tfrac{rd}{s^2}.$$
$$a_2 = 1, \;\; b_{02} = 0 \text{ rd}, \;\; b_{12} = 0.30\pi \; \tfrac{rd}{s}, \;\; b_{22} = \;\; 0.0024\pi \; \tfrac{rd}{s^2}.$$

The sampling period is taken equal to 0.01 seconds and the sources impinge from the directions $\alpha_1 = 20^o$ and $\alpha_2 = 25^o$. The simulation results are shown in Figure 5.6.

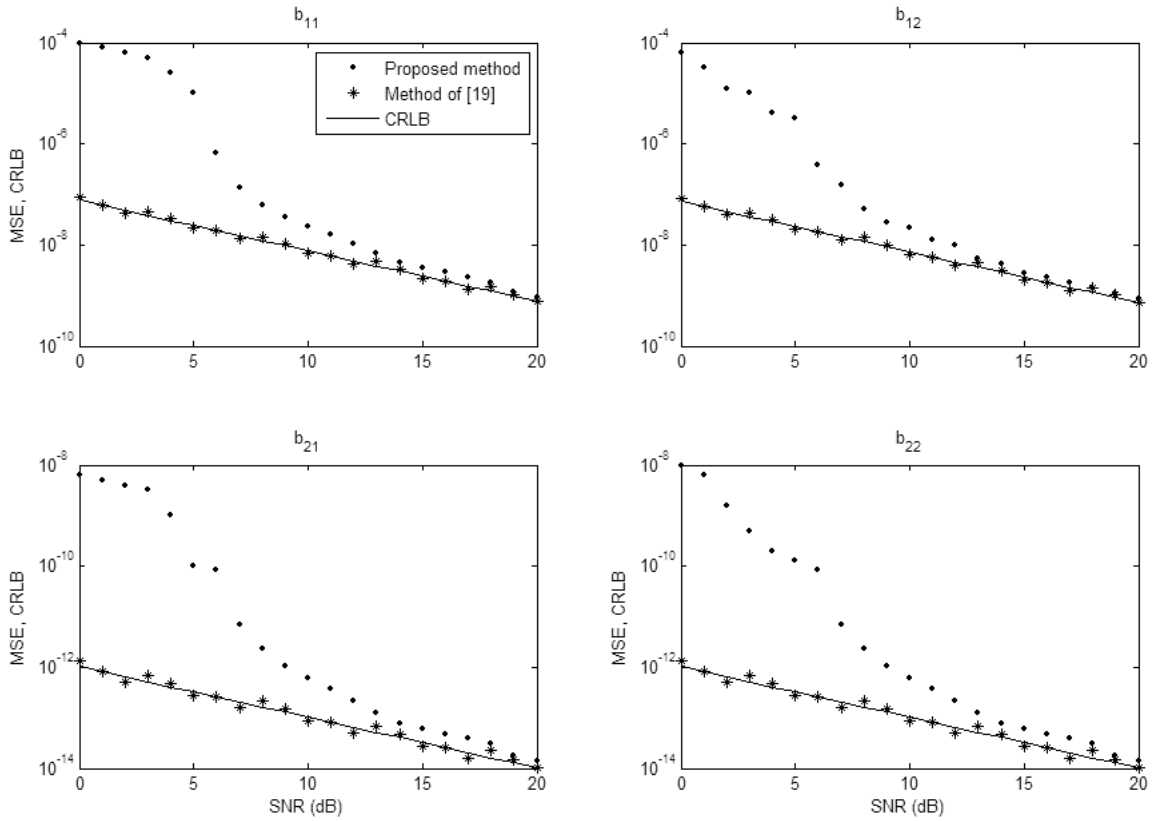

Fig. 5.6. Performance comparison with [16], case two wideband chirp signals impinging on a 10-sensor array.

Our algorithm, although being a suboptimal estimator, offers a good alternative to the ML estimator when seeking less complexity and real-time applications. Indeed, the estimator MSE's become closer to their respective CRLB's for high SNR values.

In the last example, the performances of our approach is evaluated in the case of 3 wideband sources impinging on a 2-sensor array (number of sources greater than the number of sensors)

$$a_1 = 1,\ \ b_{01} = 0 \text{ rd},\ \ b_{11} = 0\pi\ \tfrac{rd}{s},\ \ b_{21} = 0.0061\pi\ \tfrac{rd}{s^2}.$$
$$a_2 = 1,\ \ b_{02} = 0 \text{ rd},\ \ b_{12} = 0.24\pi\ \tfrac{rd}{s},\ \ b_{22} = \ \ -0.0024\pi\tfrac{rd}{s^2}.$$
$$a_1 = 1,\ \ b_{01} = 0 \text{ rd},\ \ b_{11} = 0.30\pi\ \tfrac{rd}{s},\ \ b_{21} = 0.0024\pi\ \tfrac{rd}{s^2}.$$

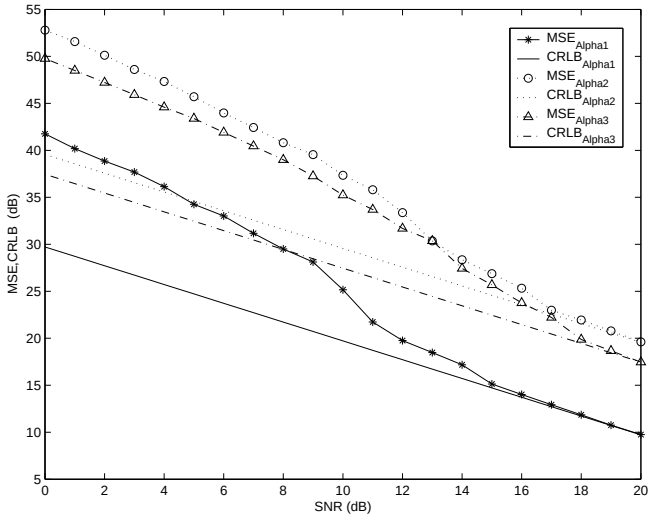

Fig. 5.7. DOA estimation performance, case three wideband chirp signals impinging on a 2-sensor array.

where the sources impinge from the directions $\alpha_1 = 10^o$ and $\alpha_2 = 20^o$, and $\alpha_3 = 30^o$. The simulation results are shown in Figure 5.7. Our algorithm provides good results where the estimator MSE's become closer to their respective CRLB's for high SNR values.

To compare our approach with the one used in [19] and [34] in terms of computational cost (CC), we consider the general case of N PPS's of degrees L_n impinging on a sensor array of M elements. By assuming P observations and I iterations ($I = P$), the following CC is obtained for our algorithm in terms of number of scalar multiplications Mul_{cost} (division) and scalar additions (Add_{cost}) (subtractions):

$$\begin{aligned} Mul\_cost = &\left[\left(1 + N + 2U + 3U^2 + U^3\right) M \right. \\ &\left. + \left(U^2 + 2U^3\right)\right] I - U^3 \\ Add\_cost = &\left[\left(1 + N + U + U^2\right) M - U - U^2 + 2U^3\right] I \\ &+ U^2 + 3U^3. \end{aligned}$$

Where $U = N(L_n + 2)$ and $U = N(L_n + 3)$ when the delays are considered known and unknown, respectively. The CC for the method presented in [34] is as follows

$$Mul\_cost = \left(2 + 4U + 7U^2 + 4U^3 + 2N\right) I + U^2 + U^3$$
$$Add\_cost = \left(2 + U + U^2 + 4U^3 + 2N\right) I - U + U^3.$$

Where $U = N(L_n + 2)$.

For the PHAF algorithm presented in [19], The CC is as follows:

$$Mul\_cost = 2N + 2(2 - L)P + (L + 1)P^2 + (L - 1)P^3$$
$$Add\_cost = -1 - (L + 1)P + (2 + L)P^2.$$

Where L represents the number of lags used in the algorithm.

Let's now consider the following example: three well separated chirp signals ($N = 3$, $l_n = 2$), where 512 observations are available ($P = 512$). Two sensors, at least, are needed for our algorithm to be applicable, so we consider this situation and hence take $M = 2$. The minimum number of lags for the PHAF is considered taking $L = 2$ in the corresponding CC relations. For a fair comparison between our algorithm and the one presented in [34], the situation where the delays are unknown is considered by taking $U = N(L_n + 3) = 15$ in our CC relation (where $U = N(L_n + 2) = 12$ in [34] CC relation).

Finally, although the proposed EKF algorithm might converge earlier than the last observation iteration, we consider the worst case where $I = P$. Figures cited in Table 5.1 are then obtained. It can be noticed from this example that our algorithm needs less number of operations than the one presented in [19] and needs relatively the same number of operations as the one presented in [34] (knowing that the convergence of the filter for our approach happens earlier than in the case of [34]).

Table 5.1
Computational cost comparisons

Method	***Mul_cost***	***Add_cost***
Our approach	7749841	3593326
Method of [34]	4085584	3624628
Method of [19]	135004166	1047039

6. CONCLUSIONS

In our study, we performed a synthesis work of the literature existing methods treating the problem of polynomial phase signal parameters estimation. We have identified the problems and restrictions encountered by these latter: The majority of the proposed approaches are only applicable to the case of monocomponent signals. For the methods extensible to the multicomponent case, a high signal-to-noise ratio is needed to guarantee a good parameter estimation result. In addition, the majority of the existing methods do not directly address the problem of source localisation when identifying the signals, and require the use of dedicated techniques, making the conjoint resolution of the identification and localisation of the signals a complex problem. Moreover, when dealing with wideband signals, the majority of the existing techniques use a pre-processing step and a transformation to the frequency domain, increasing by this the computation cost.

This work presents a new methodology using the combination of the state-space representation and the use of the Kalman filtering technique with the exploitation of the spatial information available through the use of an antenna array. We showed how this combination presents a new outlooks and offers many advantages to problems in the field:

- The approach is proven improving the estimation result compared to the case where no spatial information is exploited using a single sensor.
- The algorithm is applicable to both monocomponent and multicomponent cases and allows the joint estimation of the signals' phase parameters and their angles-of-arrival.

- The particular choice of the state vector allows a direct estimation of the signals' instantaneous frequency, a very important parameter in many applications, and hence decreasing its estimation error.

- The performance of the algorithm remains good in the case when the number of sources is superior to the number of the antenna elements and in situations where the phases' polynomial degree is unknown.

- The approach is applicable in situation requiring real-time processing of the data, this thankfully to the nature of the Kalman filter.

- Finally, and in particular, our approach allows the wideband signal processing to be performed in the time-domain and without any additional processing cost (compared to the narrowband application).

There are a few areas that are worth being explored in the future, such as the implementation of the algorithm on DSPs or FPGAs and the verification of the algorithms with real-life data. Throughout the entire research, only simulated data were used in the development of the algorithm and all results were based on these simulated data. While the performance of this algorithm was consistent with the theoretical test residing in the Cram$\acute{(e)}$r-Rao lower bound, real-life data should be collected and used to verify its practical performance. In addition, the array sensor elements in the entire research were assumed appropriately calibrated and identical. Robustness of the algorithm to these assumptions should be conducted as well. In addition, the implementation of the algorithm on DSPs or FPGAs is also considered

LIST OF REFERENCES

LIST OF REFERENCES

[1] B. Porat, Digital Processing of Random Signals. Theory and Methods, Prentice-Hall, 1994.

[2] D. Johnson, "The application of spectral estimation to bearing estimation problem," Proceedings of the IEEE, pp. 1018-1028, 1982.

[3] H. L. Van Trees, Optimum Array Processing. John Wiley & Sons, New York, 2002.

[4] B. Boashash, Time Frequency Signal Analysis and Processing: A Comprehensive Reference. Oxford, UK, Elsevier, 2003.

[5] W. Rudin, Principles of Mathematical Analysis. 3rd edition, McGraw-Hill, New York, 1976.

[6] A. Ouldali, M. Benidir, " Distinction between polynomial phasesignals with constant amplitude and random amplitude," ICASSP-97, Vol. 5, pp. 3653-3656, Munich, Germany, Apr. 1997.

[7] M. Benidir, A. Ouldali, "Polynomial phase signal analysis based onthe polynomial derivatives decompositions," IEEE Tran. Signal Processing, Vol. 47, pp.1954-1965, Jul. 1999.

[8] Ouldali, M. Benidir, "Statistical analysis of polynomial phasesignals affected by multiplicative and additive noise," Signal Processing, Vol. 78, Issue 1, Oct. 1999.

[9] M. Benidir, A. Ouldali, "Statistical analysis of a time-varying amplitude polynomial phase signal," ISSPA 2001, Vol. 1, pp.323-326, Kuala Lumpur, Malaysia, Aug. 2001.

[10] M. T. Ozgen, "Extension of the Capon's spectral estimator to time-frequency analysis and to the analysis of polynomial-phase signals," Signal Processing, pp. 575-592, Mar. 2003.

[11] M. Djeddi, H. Belkacemi, M. Benidir, and S. Marcos, "A robust MUSIC estimator for polynomial phase signals in alpha-stable noise," Acoustics, Speech, and Signal Processing ICASSP '05, Mar. 2005.

[12] L. Stankovic, V. Popovic, and M. Dakovic, "On the Capons method application in time frequency analysis," Proceedings of the 3rd IEEE International Symposium on Signal Processing and Information Technology, pp. 721-724, 2003.

[13] S. Marcos, A. Marsal, and M. Benidir, "The propagator method for source bearing estimation," Signal Processing, pp. 121-138, 1994.

[14] A. Belouchrani, Traitement d'antenne par Propagateur monocoup à diversité d'espace. MSc Thesis, Institut NationalPolytechnique de Grenoble, France, 1992.

[15] A. Belouchrani and K. Abed Meraim, "Estimation du propagateur au quatrieme ordre," Proc. GRETSI., Juan-les-pins, France, vol. 1, pp.463-466, Sep. 1995.

[16] A. B. Gershman, M. Pesavento, and M. G. Amin, "Estimating parameters of multiple wideband polynomial-phase sources in sensor arrays," IEEE Trans. Signal Process., vol. 49, pp. 2924-2934, 2001.

[17] M. Benidir, A. Ouldali, and M. Sahmoudi, "Performances analysis forthe HAF-estimator for a time-varying amplitude phase-modulated signals," in Proceeding of CA 2002, IASTED International Conference in Control and Applications, Cancun, Mexico, May. 2002.

[18] P. M. Woodward, Probability and Information Theory, with Application to Radar. London, Pergamon Press, 1955.

[19] S. Barbarossa, A. Scaglione, and G. B. Giannakis, "Product high-order ambiguity function for multicomponent polynomial-phase signal modeling," IEEE Trans. Signal Process., vol. 46, pp. 691-708, 1998.

[20] R. G. Brown and P. Y. C. Hwang, Introduction to Random Signals and Applied Kalman Filtering. Third Edition, New York, Wiley, 1997.

[21] K. Buckley and L. Griffiths, "Broadband signal subspace spatial spectrum (BASSALE) Estimation," IEEE Trans. Signal. Process., vol. 36, 953-964, 1988.

[22] S. U. Pillai, Array Signal Processing. Springer-Verlag, New York, 1989.

[23] B. Boashash, "Estimating and interpreting the instantaneous frequency of a signal part 1: fundamentals," Proceedings of the IEEE, vol. 80, 1992.

[24] D. L. Snyder, The state-variable approach to continuous estimation with applications to analog communications theory. M.I.T. Press, Boston, Massachusetts, 1969.

[25] P. J. Parker and B.D.O. Anderson, "Frequency tracking of nonsinusoidal periodic signals in noise," Signal Processing, pp. 127-152, 1990.

[26] P. M. Djuric, S. M. Kay, "Parameter estimation of chirp signals," IEEE. Trans. Acoustic Speech and Signal Process., vol. 38, pp. 2118-2126, 1990.

[27] A. Ouldali, "Estimation of a time-varying amplitude polynomial phase signal using the extended kalman filter," PSSP2002, First Polytechnic Symposium on Signal Processing, Ecole Nationale polytechnique, Algiers, Apr. 2002.

[28] J. M Piasco, M. Guglielmi, and L. Durou, "Identification de chirps par filtrage de Kalman tendu," GRETSI, pp. 29-32, Sep. 1993.

[29] J. M. Piasco, W. El Kaakour, and M. Guglielmi, "Identification parametrique de differents modle d'un signal m.f.l. multicomposantes. GRETSI, pp. 193-196, Sep. 1995.

[30] M. Adjrad, A. Belouchrani, and A. Ouldali, "Estimation of chirp signal parameters using state space modelization by incorporating spatial information," 7th International Symposium on Signal Processing and Its Applications, pp. 531 -534, Jul. 2003.

[31] M. Adjrad, A. Belouchrani, and K. Abed-Meraim, "Parameter estimation of multi-component polynomial-phase signals impinging on a multi-sensor array using extended Kalman filter," in Proc. 3rd IEEE Int. Symp. Signal Processing Inf. Technol. (ISSPIT), Darmstadt, Germany, pp. 471-474, 2003.

[32] P. J. Kootsookos and J. M. Spanjaard, "An extended Kalman filter for demodulation of polynomial phase signals," IEEE Signal Processing Letters, pp. 69-70, 1998.

[33] M. Adjrad and A. Belouchrani, "Estimation of multicomponent polynomial-phase signals impinging on a multisensor array using state-space modelling," IEEE. Trans. Signal. Process., vol. 55, pp. 32-45, 2007

[34] W. El Kaakour, Modélisation et identification des signaux à phase polynomiale. PhD thesis, Université de Nantes, Ecole Centrale de Nantes, Jun. 1998.

[35] F. Hlawatsch and G. F. Boudreaux-Bartels, "Linear and quadratic time frequency signal representations," IEEE Signal Process. Mag., vol. 9, pp. 21-67, 1992.

[36] V. F. Pisarenko, "The retrieval of harmonics from a covariance function," Geophysical Royal Journal of Astronomical Society, Vol 33, pp. 347366, 1973.

[37] R. Schmidt, "Multiple emitter location and signal parameter estimation,". IEEE Trans. Antennas and Propagation., Vol 34, pp. 284280, 1986.

[38] A. Barabell, "Improving the resolution performance of eigenstructure-based direction finding algorithm," In Proceedings Proceedings of the International Conference on Acoustics, Speech, and Signal Processing, pp. 336339, Boston, MA, 1983.

[39] B. D. Rao, and K. Hari, "Performance analysis of root-music," IEEE Trans. Signal Process., Vol. 37, pp. 19391949, 1989.

[40] Y. W. Lee, Statistical Theory of Communication. John Wiley & Sons, New York, 1960.

[41] J. P. Reilly, Nonlinear array processing techniques with applications to correlated multipath. Ph.D. thesis, McMaster University, Hamilton, Ontario, Canada, 1981.

[42] S. Haykin, Adaptive Filter Theory. Prentice Hall, Englewood Cliffs, NJ, 4th edition, 2000.

[43] Q. Wu, and K. M. Wong, "UN-MUSIC and UN-CLE: An application of generalized correlation analysis to the estimation of the direction of arrival of signals in unknown correlated noise," IEEE Trans. Signal Process., Vol. 42, pp. 23312343, 1994.

[44] M. Viberg, B. Ottersten, and T. Kailath, "Detection and estimation in sensor arrays using weighted subspace fitting," IEEE Trans. Signal Process., Vol. 39, pp. 24362449, 1991.

[45] S. Valaee, and P. Kabal, "Wideband array processing using a two-sided correlation transformation," IEEE Trans. Signal Process., Vol. 44, pp. 160172, 1995.

[46] H. Hung, and M. Kaveh, "Focusing matrices for coherent signal-subspace processing," IEEE Trans. Acoustics, Speech, and Signal Processing., Vol. 36, pp. 12721281, 1988.

[47] J. Boehme, "Separated estimation of wave parameters and spectral parameters," In Proceedings of the International Conference on Acoustics, Speech, and Signal Processing, pp. 28192822, Tokyo, Japan, 1986.

[48] J. Boehme, "Location and spectrum estimation by approximate maximum likelihood," In Proceedings SPIE, vol 1, pp. 326337, Orlando, Florida, 1989.

[49] M. A. Doron, and A. J. Weiss, "On focusing matrices for wide-band array processing," IEEE Trans. Signal Process., Vol. 40, pp. 12951302, 1992.

[50] M. A. Doron, A. J. Weiss, and H. Messer, "Maximum-likelihood direction .nding of wide-band sources," IEEE Trans. Signal Process, Vol. 41, pp. 411414, 1993.

[51] S. M. Kay, Fundamentals of Statistical Signal Processing Volume 1: Estimation Theory, Prentice Hall, 1998.

7. APPENDIX 1: DISSEMINATION

- M. Adjrad, A. Belouchrani, "Estimation of Multi-Component Polynomial-Phase Signals Impinging on a Multi-Sensor Array Using State-Space Modeling," IEEE Trans. Signal Processing, Vol 55, pp. 32-45, Jan 2007.
- M. Adjrad, A. Belouchrani, and K. Abed-Meraim, "Parameter Estimation of Multicomponent Polynomial-phase Signals Impinging on a Multi-sensor array Using Extended Kalman Filter", in Proc. of ISSPIT, Darmstadt, Germany, Dec. 2003.
- M. Adjrad, A. Belouchrani, and A. Ouldali, "Estimation of Chirp Signal Parameters Using State Space Modelization by Incorporating Spatial Information," In Proc. of ISSPA, Paris, France, Jul. 2003.
- M. Adjrad, A. Ouldali, and A. Belouchrani, "Chirp Parameters Estimation Using The extended Kalman Filter", In Proc. of CGE'02, Bordj El Bahri, Algeria, Dec. 2002.

8. APPENDIX 2: MAIN PAPER

Estimation of Multi-Component Polynomial-Phase Signals Impinging on a Multi-Sensor Array Using State-Space Modeling

Mounir Adjrad and Adel Belouchrani, *Member, IEEE*

***Abstract*— This contribution addresses the problem of estimating the parameters of multi-component polynomial-phase signals when impinging on a multi-sensor array. An original approach is proposed based on a state-space modelization of the signal and the application of an extended Kalman filter for the state estimation. The use of a multi-sensor array allows the exploitation of a spatial information and leads to the consideration of multiple filters with different observation equations. Computer simulations are used to demonstrate the effectiveness of the proposed algorithm.**

I. INTRODUCTION

POLYNOMIAL-PHASE signals (PPS's) are good model in a variety of applications, e.g., radar systems transmitting chirp signals or in communications systems using continuous-phase modulation where the amplitude is constant and the phase is a continuous function of time. The phase of the signals used in these applications can then be modeled as a finite-order polynomial within a finite-duration interval as is known from Weierstrass theorem where any continuous function on a closed interval can be uniformly approximated by polynomials [13]. In some applications, there is a direct use of a polynomial shaping pulse, in which case the polynomial modeling would be exact. This explains why the parameter estimation of constant-amplitude PPS's embedded in noise has received a considerable attention in the literature [14], [24], [26]. The extension to PPS's with time-varying amplitude was also dealt with in [9], [30], [35]. Recently, there has been a growing interest in estimating the parameters of multiple polynomial-phase sources impinging on a multi-sensor array [4], [17], [27], [29]. Such situation arises, for example, in SAR signal processing or in the propagation of PPS's through multipath channels.

The maximum likelihood (ML) is one of several algorithms that have been proposed to solve the problem at hand. It is known to possess good asymptotic properties. However, its implementation is difficult because it requires the resolution of multivariate nonlinear optimization problem. The problem becomes more difficult when dealing with multi-component signals. Several simpler approaches were proposed for linear FM signals [1]. Another method for estimating the instantaneous phase of sinusoids embedded in noise was proposed in [31], where the estimation was obtained by linear regression of the instantaneous phase calculated directly from the signal after phase unwrapping. The method provides good results for signal-to-noise ratio (SNR) above 15 dB. This approach was then extended in [24] for analyzing PPS's of a generic degree. However, the application of these methods is limited to the case of single-component signals [1] . The high-order ambiguity function (HAF) was specifically introduced to estimate the parameters of PPS's [6], [8], [16], [23]. The HAF-based method is suboptimal with respect to the ML method, but it is much simpler to implement and provides performances quite close to the optimal ones, at least at high SNR. However, since the HAF is a nonlinear method, it suffers from two basic problems: noise-masking effects at low SNR and cross terms in the presence of multicomponent signals. Moreover, if the observed signal is composed of the sum of PPS's having the same highest order phase coefficients, its HAF exhibits spurious peaks generating an ambiguity problem in the HAF-based estimation method. The ambiguity problem was solved by introducing the product-HAF (PHAF) [5]. Spatial time-frequency distribution concept has been developed and employed in [7], [34] for the purpose of localization of spatial sources, where the PPS-like sources have been given great importance.

The majority of methods presented in the literature are limited to processing narrowband data. In many applications (e.g. radar and communications), this is indeed a realistic assumption. However, in other cases (e.g. sonar), the received signal may be broadband. Most algorithms developed to solve problems for wideband signals usually transform the received signals from the time domain to the frequency domain using Fourier transform as a pre-processing step [18], [32]. The motivation of this transformation is that the transformed model in the frequency domain is structurally similar to that for narrowband signals in the time domain. The following burdens are further reasons why most algorithms for wideband signal processing operate in the frequency domain: given that the time delay parameters are seldom scalar multiples of the sampling rate, resolving signals from different delays is very difficult, unless the sampling rate is increased significantly, so that the error between the inter-sensor delay and the closest sampling instant is reduced sufficiently. In other words, if

Manuscript received July 3, 2005; revised February 15, 2006. The associate editor coordinating the review of this manuscript and approving it for publication was Dr. Franz Hlawatsch.

The authors are with the Electrical Engineering Department, Ecole Nationale Polytechnique, B.P 182 EL Harrach, Algiers 16200, Algeria (e-mail: mounir. adjrad@enp.edu.dz; adel.belouchrani@enp.edu.dz)

Digital Object Identifier 10.1109/TSP.2006.882055

[1]The resulting signal from the sum of PPS's is not necessarily a PPS [6].

one develops an algorithm in an attempt to resolve wideband signals in the time domain, oversampling may be required and more sophisticated hardware is also required. Quite few authors have dealt with the wideband situation in the time domain [19], [33] and using spatial time-frequency concept [20].

This paper introduces a new technique based on the Kalman filter (KF) algorithm. The KF is considered as the best minimum mean-squared linear estimator for the problem at hand and has been used in [2], [15], [25]. It offers the possibility of extending the single-component PPS parameter estimation to the Multi-Components (MC) PPS's case [3] where the approach proposed in [2] is generalized to the MC PPS's case of any order impinging on a multi-sensor array. The method presents a number of other attractive features. It is very adequate for real-time applications because of the recursive nature of the resulting algorithm and the modest use of memory (due to the nature of the KF itself). Moreover, in contrast to the majority of the literature, it allows the consideration of a real-valued (RV) modelization hence the applicability of the algorithm to situations where the source signals are wideband without need to transform the received signals from the time domain to the frequency domain. This last point will be developed further in the next section.

The paper is organized as follows. In Section II, The problem of MC PPS's parameter estimation is stated and a summary of the KF technique is presented along with the chosen state-space modelization. The proposed algorithm is presented in Section III. Numerical simulations illustrating the usefulness of the proposed technique and comparisons with the methods proposed in [5], [15], [19] are given in Section IV.

II. Problem Formulation

A. Data Model

The general model considered in the majority of the literature is as follows

$$s(t) = \sum_{n=1}^{N} a_n \exp\left[j\phi_n(t)\right], \tag{1}$$

with $\phi_n(t) = \sum_{l=0}^{L_n} b_{ln}(t\Delta)^l$ for $t = 0, \ldots, P-1$, where P, N, and L_n represent the sample size, the number of components, and the component phase degree, respectively. The amplitude a_n is a real constant and the instantaneous phase $\phi_n(t)$ of each component is a polynomial. Δ represents the sampling interval.

In many practical applications, the original sources are RV, while most of the previously mentioned methods assume the data consists of a double number of complex-valued (CV) PPS's. To do so, knowing that generally the transmitted signal parameters are unknown, we apply the Hilbert transform (HT) on the RV data. Modeling the signals by an exponential assumes that the HT exactly generates the quadrature component of the RV PPS. This assumption is always verified for narrowband signals, where the PPS's amplitude and phase spectrums are separated [10], [11]. This is the *absolute* definition of a narrowband PPS. In the majority of the literature, the narrowband situation is defined *relatively* to the sensor array where a signal is considered narrowband if its complex envelope satisfies the condition $B_s\tau_{max} \ll 1$ with B_s representing the maximum bandwidth of the signal complex envelope and τ_{max} equaling the maximum travel time between any two elements in the array. This latter is considered as a consequence of the narrowband assumption on the source signals rather than a definition. This analysis becomes more clear when dealing with time-varying amplitude PPS's. The conclusion for this analysis is as follows: *the more closely a signal approaches a narrowband condition, the better the Hilbert- transformed signal approximates the quadrature signal, and the more likely the Hilbert-based analytic signal is to provide an accurate model of a real system with a particular Instantaneous Frequency (IF); also the better in general will be the estimate of the instantaneous frequency* [10]. This justifies the choice of modelization (2) presented hereafter instead of (1). In addition, taking a RV modelization allows considering half of the number of the data needed in the CV case.

Considering the following signal modelization

$$s(t) = \sum_{n=1}^{N} a_n \sin\left[\phi_n(t)\right], \tag{2}$$

We propose to exploit the spatial information provided by a Uniform linear array (ULA) of M sensors. Hence, the vector array outputs $\{y_m, m = 1, \ldots, M\}$ obey the following model

$$y_1(t) = \sum_{n=1}^{N} a_n \sin\left[\phi_n(t)\right] + v_1(t), \tag{3}$$

$$y_m(t) = \sum_{n=1}^{N} a_n \sin\left[\phi_n\left(t - \frac{\tau_{nm}}{\Delta}\right)\right] + v_m(t), \quad m = 2, \ldots, M, \tag{4}$$

where $\{v_m, m = 1, \ldots, M\}$ are independent, real valued, additive white Gaussian noises (AWGN) with zero means and variances $\{\sigma_m^2, m = 1, \ldots, M\}$. $\{\tau_{nm}, n = 1, \ldots, N, m = 2, \ldots, M\}$ are real valued parameters representing the propagation time delays of the n^{th} source waveform impinging at the m^{th} array sensor with respect to signal received at the first sensor [2].

B. Kalman Filter Theory

The KF addresses the general problem of trying to estimate the state $x \in \Re^n$ of a discrete-time controlled process that is governed by a linear stochastic difference equation [12]. It estimates the process by using a form of feedback control: the filter estimates the process state at some time and then obtains feedback in the form of $noisy$ measurements. As such, the equations for the KF fall into two groups: time update equations and measurement update equations. The time update equations are responsible for projecting forward (in time) the current state and error covariance estimates to obtain the a priori estimates for the next time step. The measurement update equations are responsible for the feedback - *i.e.* for incorporating a new measurement into the a priori estimate

[2]These delays are not necessarily multiples of the sampling period.

to obtain an improved a posteriori estimate. The time update equation can also be thought of as predictor equations, while the measurement update equations can be thought of as corrector equations. Indeed the final estimation algorithm resembles that of a predictor-corrector algorithm for solving numerical problems.

Some of the most successful applications of Kalman filtering have been in situations with nonlinear dynamics and/or nonlinear measurement relationships which is the case of PPS's parameter estimations problem according to (1). Two basic ways of linearizing the problem exist: one is to linearize about some nominal trajectory in state-space that does not depend on the measurement data. The resulting filter is usually referred to as a linearized KF. The other method is to linearize about a trajectory that is continually updated with the state estimates resulting from the measurements. When this is done, the filter is called an extended KF (EKF). The former assumes that an approximate trajectory may be determined by some means. This assumption is less likely to be true in the majority of radar, sonar and communications applications. This last point explains the use of the EKF version of the KF.

C. State-Space Modelization

The state-space modelization consists of putting the state and measurement equations according to the state-vector choice. In practice, from (4), two cases can arise: situations where the delays are known and applications where these parameters are unknown. We then give the state-space representation for both cases.

1) Known Delays: The chosen state-model has the following state-vector

$$\begin{aligned}\mathbf{X}(t) &= [a_1 \;\; \phi_1(t) \;\; \phi_1^{(1)}(t) \ldots \phi_1^{(L_1)}(t) \ldots\ldots \\ &\quad a_N \;\; \phi_N(t) \;\; \phi_N^{(1)}(t) \ldots \phi_N^{(L_N)}(t)]^T, \end{aligned} \tag{5}$$

where $(.)^T$ and $(.)^{(l)}$ stand for the matrix transpose operator and the l^{th} derivative operator with respect to t, respectively (the component phase degrees $\{L_n\}$ are assumed known [3]). The dimension of $\mathbf{X}(t)$ is given by [4]: $d_N = \sum_{n=1}^{N}(L_n+2)$. The following state-model is in order

$$\begin{cases} \mathbf{X}(t+1) = \mathbb{F}\mathbf{X}(t) \\ y_m(t) = g_m[\mathbf{X}(t)] + v_m(t), \;\; m = 1, \ldots, M \end{cases}, \tag{6}$$

where $\mathbb{F}$ and g are given by

$$\mathbb{F} = \begin{bmatrix} \mathbb{F}_1 & 0 & \cdots & 0 \\ 0 & \mathbb{F}_2 & \ddots & \vdots \\ \vdots & \ddots & \ddots & 0 \\ 0 & \cdots & 0 & \mathbb{F}_N \end{bmatrix}, \tag{7}$$

with

$$\mathbb{F}_n = \begin{bmatrix} 1 & 0 & 0 & \cdots & 0 \\ 0 & 1 & \frac{\Delta}{1!} & \cdots & \frac{\Delta^{L_n}}{L_n!} \\ \vdots & \ddots & \ddots & \ddots & \vdots \\ \vdots & \ddots & \ddots & 1 & \frac{\Delta}{1!} \\ 0 & \cdots & \cdots & 0 & 1 \end{bmatrix}, \quad n = 1, \ldots, N, \tag{8}$$

and

$$\begin{aligned} g_1[\mathbf{X}(t)] &= x_1(t)\sin[x_2(t)] + x_{1+d_1}(t)\sin[x_{2+d_1}(t)] + \cdots \\ &\quad + x_{1+d_{N-1}}(t)\sin\left[x_{2+d_{N-1}}(t)\right], \end{aligned} \tag{9}$$

$$\begin{aligned} g_m[\mathbf{X}(t)] &= x_1(t)\sin\left[\sum_{l=0}^{L_1}\frac{(-\tau_{1m})^l}{l!}x_{l+2}(t)\right] \\ &\quad + x_{1+d_1}(t)\sin\left[\sum_{l=0}^{L_2}\frac{(-\tau_{2m})^l}{l!}x_{l+2+d_1}(t)\right] + \cdots \\ &\quad + x_{1+d_{N-1}}(t)\sin\left[\sum_{l=0}^{L_N}\frac{(-\tau_{Nm})^l}{l!}x_{l+2+d_{N-1}}(t)\right], \\ &\quad m = 2, \ldots, M, \end{aligned} \tag{10}$$

where $\{x_k(t), k = 1, \ldots, d_N\}$ are the entries of $\mathbf{X}(t)$.

By defining the parameter vector as

$$\boldsymbol{\Theta} = [a_1 \;\; b_{01} \;\; b_{11} \;\; \ldots \;\; b_{L_1 1} \;\; \ldots\ldots \;\; a_N \;\; b_{0N} \;\; b_{1N} \;\; \ldots \;\; b_{L_N N}]^T, \tag{11}$$

one obtains

$$\hat{\boldsymbol{\Theta}}(t) = \mathbb{A}\mathbb{F}^{-t}\hat{\mathbf{X}}(t), \tag{12}$$

where $\hat{\boldsymbol{\Theta}}$, $\hat{\mathbf{X}}$ are the estimates of $\boldsymbol{\Theta}$ and $\mathbf{X}$, respectively, $\mathbb{F}$ is as defined in (7) and $\mathbb{A}$ is given by

$$\mathbb{A} = \begin{bmatrix} \mathbb{A}_1 & 0 & \cdots & 0 \\ 0 & \mathbb{A}_2 & \ddots & \vdots \\ \vdots & \ddots & \ddots & 0 \\ 0 & \cdots & 0 & \mathbb{A}_N \end{bmatrix}, \tag{13}$$

where

$$\mathbb{A}_n = \begin{bmatrix} 1 & 0 & \cdots & \cdots & 0 \\ 0 & 1 & \ddots & \ddots & \vdots \\ \vdots & \ddots & \frac{1}{1!} & \ddots & \vdots \\ \vdots & \ddots & \ddots & \ddots & 0 \\ 0 & \cdots & \cdots & 0 & \frac{1}{L_n!} \end{bmatrix}, \quad n = 1, \ldots, N. \tag{14}$$

2) Unknown Delays: In this situation, the delays need to be included by augmenting the state-vector given by (5) where the n^{th} signal component will be represented in the state-vector by (L_n+3) elements and the dimension of $\mathbf{X}(t)$ becomes equal to $d_N = \sum_{n=1}^{N}(L_n+3)$. The state-vector expression is given by

$$\begin{aligned}\mathbf{X}(t) &= [a_1 \;\; \tau_{12} \;\; \phi_1(t) \;\; \phi_1^{(1)}(t) \ldots \phi_1^{(L_1)}(t) \ldots\ldots \\ &\quad a_N \;\; \tau_{N2} \;\; \phi_N(t) \;\; \phi_N^{(1)}(t) \ldots \phi_N^{(L_N)}(t)]^T \end{aligned} \tag{15}$$

[3] This assumption can be relaxed as will be seen in the Simulation Section.

[4] The n^{th} signal component is represented in the state-vector by (L_n+2) elements.

We note that only the set $\{\tau_{n2},\ n=1,\ldots,N\}$ has been included. The reason is because for an ULA, the remaining delays are found using the relation $\tau_{nm+1}=m\tau_{n2},\ m=2,\ldots,M$.

The same state-model and state transition matrix $\mathbb{F}$ given by (6) and (7), respectively, are considered with new expressions for $\mathbb{F}_n$ and g

$$\mathbb{F}_n=\begin{bmatrix} 1 & 0 & 0 & \cdots & \cdots & 0 \\ 0 & 1 & 0 & \cdots & \cdots & 0 \\ 0 & 0 & 1 & \frac{\Delta}{1!} & \cdots & \frac{\Delta^{L_n}}{L_n!} \\ \vdots & \vdots & \ddots & \ddots & \ddots & \vdots \\ \vdots & \vdots & \ddots & \ddots & 1 & \frac{\Delta}{1!} \\ 0 & \cdots & \cdots & \cdots & 0 & 1 \end{bmatrix},\quad n=1,\ldots,N, \tag{16}$$

$$\begin{aligned} g_1\left[\mathbf{X}(t)\right]&=x_1(t)\sin\left[x_3(t)\right]+x_{1+d_1}(t)\sin\left[x_{3+d_1}(t)\right]+\cdots \\ &\quad+x_{1+d_{N-1}}(t)\sin\left[x_{3+d_{N-1}}(t)\right], \end{aligned} \tag{17}$$

$$\begin{aligned} g_m\left[\mathbf{X}(t)\right]&=x_1(t)\sin\left[\sum_{l=0}^{L_1}\frac{(-(m-1)x_2)^l}{l!}x_{l+3}(t)\right] \\ &+x_{1+d_1}(t)\sin\left[\sum_{l=0}^{L_2}\frac{\left(-(m-1)x_{2+d_1}\right)^l}{l!}x_{l+3+d_1}(t)\right]+\cdots \\ &+x_{1+d_{N-1}}(t)\sin\left[\sum_{l=0}^{L_N}\frac{\left(-(m-1)x_{2+d_{N-1}}\right)^l}{l!}x_{l+3+d_{N-1}}(t)\right], \\ &\quad m=2,\ldots,M, \end{aligned} \tag{18}$$

The parameter vector given by (11) is augmented by the inclusion of the nuisance parameters as follows

$$\begin{aligned} \mathbf{\Theta}\ &=\ [a_1\ \tau_{12}\ b_{01}\ b_{11}\ \ldots\ b_{L_11}\ \ldots\ldots\ a_N\ \tau_{N2}\ b_{0N}\ b_{1N} \\ &\quad \ldots\ b_{L_NN}]^T, \end{aligned} \tag{19}$$

The same relation as (12) relates the parameter vector to the estimated state-vector with $\mathbb{F}$ and $\mathbb{A}$ defined in (7) and (13) ($\mathbb{F}_n$ is given by (16)). $\mathbb{A}_n$ expression is as follows

$$\mathbb{A}_n=\begin{bmatrix} 1 & 0 & \cdots & \cdots & \cdots & 0 \\ 0 & 1 & \ddots & \ddots & \ddots & \vdots \\ 0 & 0 & 1 & \ddots & \ddots & \vdots \\ \vdots & \ddots & \ddots & \frac{1}{1!} & \ddots & \vdots \\ \vdots & \ddots & \ddots & \ddots & \ddots & 0 \\ 0 & \cdots & \cdots & \cdots & 0 & \frac{1}{L_n!} \end{bmatrix},\quad n=1,\ldots,N. \tag{20}$$

The main motivations behind the chosen structure of the state-vector are: the obtention of a minimum number of nonlinear equation and direct estimation of the instantaneous frequency (IF), a very important parameter as stressed in [10], [21]. Indeed, from (6), we obtain a state-space modelization with a linear state equation and nonlinear observation equations. Furthermore, from (5) and (15), it is possible to directly estimate the IF $\{\phi_n^{(1)}(t),\ \ n=1,\ldots,N\}$ of each component, and hence minimizing the estimation error that would have resulted from indirect estimation. In the next Section, we present the EKF-based algorithm.

III. THE PROPOSED EXTENDED KALMAN FILTER

A. Estimation Algorithm

The EKF technique consists of linearizing, to the first order, models (3) and (4) and applying an optimal state estimation filter. The filter equations are given for both cases of known and unknown delay paramters.

1) Known Delays: The update equations are given as follows

$$\begin{cases} \hat{\mathbf{X}}^-(t)=\mathbb{F}\hat{\mathbf{X}}_M(t) \\ \mathbb{P}^-(t)=\mathbb{F}\mathbb{P}_M(t)\mathbb{F}^T \end{cases}, \tag{21}$$

where $\hat{\mathbf{X}}^-(t)$ and $\mathbb{P}^-(t)$ are the predicted state-vector and covariance error matrix at the time instant $\mathbf{t}$, respectively.

The estimation equations are

$$\begin{cases} \mathbf{K}_1(t)=\mathbb{P}^-(t)\mathbf{G}_1^T(t)\left[\mathbf{G}_1(t)\mathbb{P}^-(t)\mathbf{G}_1^T(t)+\sigma_1^2\right]^{-1} \\ \hat{y}_1(t)\ =\hat{x}_1^-(t)\sin\left[\hat{x}_2^-(t)\right]+\hat{x}_{1+d_1}^-(t)\sin\left[\hat{x}_{2+d_1}^-(t)\right] \\ \qquad +\cdots+\hat{x}_{1+d_{N-1}}^-(t)\sin\left[\hat{x}_{2+d_{N-1}}^-(t)\right] \\ \hat{\mathbf{X}}_1(t)=\hat{\mathbf{X}}^-(t)+\mathbf{K}_1(t)\left[y_1(t)-\hat{y}_1(t)\right] \\ \mathbb{P}_1(t)\ =\left[\mathbb{I}-\mathbf{K}_1(t)\mathbf{G}_1(t)\right]\mathbb{P}^-(t) \end{cases}, \tag{22}$$

$$\begin{cases} \mathbf{K}_2(t)=\mathbb{P}_1(t)\mathbf{G}_2^T(t)\left[\mathbf{G}_2(t)\mathbb{P}_1(t)\mathbf{G}_2^T(t)+\sigma_2^2\right]^{-1} \\ \hat{y}_2(t)\ =\hat{x}_1^{\mathbf{1}}(t)\sin\left[\hat{x}_2^{\mathbf{1}}(t)\right]+\hat{x}_{1+d_1}^{\mathbf{1}}(t)\sin\left[\hat{x}_{2+d_1}^{\mathbf{1}}(t)\right] \\ \qquad +\cdots+\hat{x}_{1+d_{N-1}}^{\mathbf{1}}(t)\sin\left[\hat{x}_{2+d_{N-1}}^{\mathbf{1}}(t)\right] \\ \hat{\mathbf{X}}_2(t)=\hat{\mathbf{X}}_1(t)+\mathbf{K}_2(t)\left[y_2(t)-\hat{y}_2(t)\right] \\ \mathbb{P}_2(t)\ =\left[\mathbb{I}-\mathbf{K}_2(t)\mathbf{G}_2(t)\right]\mathbb{P}_1(t) \\ \vdots \\ \mathbf{K}_M(t)=\mathbb{P}_{M-1}(t)\mathbf{G}_M^T(t)\left[\mathbf{G}_M(t)\mathbb{P}_{M-1}(t)\mathbf{G}_M^T(t)+\sigma_M^2\right]^{-1} \\ \hat{y}_M(t)\ =\hat{x}_1^{\mathbf{M-1}}(t)\sin\left[\hat{x}_2^{\mathbf{M-1}}(t)\right]+\hat{x}_{1+d_1}^{\mathbf{M-1}}(t)\sin\left[\hat{x}_{2+d_1}^{\mathbf{M-1}}(t)\right] \\ \qquad +\cdots+\hat{x}_{1+d_{N-1}}^{\mathbf{M-1}}(t)\sin\left[\hat{x}_{2+d_{N-1}}^{\mathbf{M-1}}(t)\right] \\ \hat{\mathbf{X}}_M(t)=\hat{\mathbf{X}}_{M-1}(t)+\mathbf{K}_M(t)\left[y_M(t)-\hat{y}_M(t)\right] \\ \mathbb{P}_M(t)\ =\left[\mathbb{I}-\mathbf{K}_M(t)\mathbf{G}_M(t)\right]\mathbb{P}_{M-1}(t) \end{cases}, \tag{23}$$

where $\{\hat{\mathbf{X}}_m(t), m=1,\ldots,M, t=0,\ldots,P-1\}$ are the estimated state-vectors, $\{\hat{x}_k^-, k=1,\ldots,2+d_{N-1}\}$ and $\{\hat{x}_k^{\mathbf{m}}, k=1,\ldots,2+d_{N-1}, \mathbf{m}=1,\ldots,M-1\}$ are the entries of $\hat{\mathbf{X}}^-$ and $\{\hat{\mathbf{X}}_m, m=1,\ldots,M-1\}$, respectively. $\{\mathbb{P}_m(t), m=1,\ldots,M\}$ are the covariance error matrices, $\{\mathbf{K}_m,\ m=1,\ldots,M\}$ are the Kalman filter gain vectors and $\mathbb{I}$ is the $(d_N\times d_N)$ identity matrix.

The filter is initialized by $\hat{\mathbf{X}}_0^-$ and $\mathbb{P}_0^-$. The final estimate $\hat{\mathbf{X}}$ of $\mathbf{X}$ equals $\hat{\mathbf{X}}_M(P-1)$. The vectors $\{\mathbf{G}_m, m=1,\ldots,M\}$ are found by linearizing, at the first order, (9) and (10) around the predicted state-vector and the estimated state-vector, respectively. Hence, the following relations

$$\mathbf{G}_1(t)=\left(\frac{\partial g_1[\mathbf{X}(t)]}{\partial\mathbf{X}(t)}\right)_{\mathbf{X}(t)=\hat{\mathbf{X}}^-(t)}, \tag{24}$$

$$\mathbf{G}_m(t) = \left(\frac{\partial g_m[\mathbf{X}(t)]}{\partial \mathbf{X}(t)} \right)_{\mathbf{X}(t)=\hat{\mathbf{X}}_{m-1}(t)}, \quad m = 2, \ldots, M, \tag{25}$$

where ∂ stands for the partial derivation operator. We then find

$$\mathbf{G}_1(t) = \left[\mathbf{G}_{1,1}(t) \quad \ldots \quad \mathbf{G}_{1,N}(t) \right], \tag{26}$$

$$\mathbf{G}_m(t) = \left[\mathbf{G}_{m,1,\tau_{1m}}(t) \quad \ldots \quad \mathbf{G}_{m,N,\tau_{Nm}}(t) \right], \ m = 2, \ldots, M, \tag{27}$$

where

$$\mathbf{G}_{1,1}(t) = \left[\sin\left[\hat{x}_2^-(t)\right] \quad \hat{x}_1^-(t)\cos\left[\hat{x}_2^-(t)\right] \quad 0 \ldots 0 \right], \tag{28}$$

$$\mathbf{G}_{1,n}(t) = [\sin\left[\hat{x}_{2+d_{n-1}}^-(t)\right] \quad \hat{x}_{1+d_{n-1}}^-(t)\cos\left[\hat{x}_{2+d_{n-1}}^-(t)\right] \quad 0 \ldots 0], \quad n = 2, \ldots, N, \tag{29}$$

$$\mathbf{G}_{m,1,\tau_{1m}}^T(t) = \begin{bmatrix} \sin\left[\alpha_{1\tau_{1m}}\left(\hat{\mathbf{X}}_{m-1}(t)\right)\right] \\ \hat{x}_1^{\mathbf{m-1}}(t)\cos\left[\alpha_{1\tau_{1m}}\left(\hat{\mathbf{X}}_{m-1}(t)\right)\right] \\ \frac{-\tau_{1m}}{1!}\hat{x}_1^{\mathbf{m-1}}(t)\cos\left[\alpha_{1\tau_{1m}}\left(\hat{\mathbf{X}}_{m-1}(t)\right)\right] \\ \vdots \\ \frac{(-\tau_{1m})^{L_1}}{L_1!}\hat{x}_1^{\mathbf{m-1}}(t)\cos\left[\alpha_{1\tau_{1m}}\left(\hat{\mathbf{X}}_{m-1}(t)\right)\right] \end{bmatrix}$$
$$m = 2, \ldots, M, \tag{30}$$

$$\mathbf{G}_{m,n,\tau_{nm}}^T(t) = \begin{bmatrix} \sin\left[\alpha_{n\tau_{nm}}\left(\hat{\mathbf{X}}_{m-1}(t)\right)\right] \\ \hat{x}_{1+d_{n-1}}^{\mathbf{m-1}}(t)\cos\left[\alpha_{n\tau_{nm}}\left(\hat{\mathbf{X}}_{m-1}(t)\right)\right] \\ \frac{-\tau_{nm}}{1!}\hat{x}_{1+d_{n-1}}^{\mathbf{m-1}}(t)\cos\left[\alpha_{n\tau_{nm}}\left(\hat{\mathbf{X}}_{m-1}(t)\right)\right] \\ \vdots \\ \frac{(-\tau_{nm})^{L_n}}{L_n!}\hat{x}_{1+d_{n-1}}^{\mathbf{m-1}}(t)\cos\left[\alpha_{n\tau_{nm}}\left(\hat{\mathbf{X}}_{m-1}(t)\right)\right] \end{bmatrix}$$
$$n = 2, \ldots, N, \quad m = 2, \ldots, M, \tag{31}$$

where $\{\alpha_{n\tau_{nm}}, n = 1, \ldots, N, m = 2, \ldots, M\}$ are given by

$$\alpha_{1\tau_{1m}}\left(\hat{\mathbf{X}}_{m-1}(t)\right) = \sum_{l=0}^{L_1} \frac{(-\tau_{1m})^l}{l!}\hat{x}_{l+2}^{\mathbf{m-1}}(t), \tag{32}$$

$$\alpha_{n\tau_{nm}}\left(\hat{\mathbf{X}}_{m-1}(t)\right) = \sum_{l=0}^{L_n} \frac{(-\tau_{nm})^l}{l!}\hat{x}_{l+2+d_{n-1}}^{\mathbf{m-1}}(t), \quad n = 2, \ldots, N. \tag{33}$$

2) Unknown Delays: As performed in the previous section, the state-vector will be augmented. The update equation follows (21) where the same definitions hold as in the previous subsection. The remaining equations are given hereafter

$$\begin{cases} \mathbf{K}_1(t) = \mathbb{P}^-(t)\mathbf{G}_1^T(t)\left[\mathbf{G}_1(t)\mathbb{P}^-(t)\mathbf{G}_1^T(t) + \sigma_1^2\right]^{-1} \\ \hat{y}_1(t) = \hat{x}_1^-(t)\sin\left[\hat{x}_3^-(t)\right] + \hat{x}_{1+d_1}^-(t)\sin\left[\hat{x}_{3+d_1}^-(t)\right] \\ \qquad + \cdots + \hat{x}_{1+d_{N-1}}^-(t)\sin\left[\hat{x}_{3+d_{N-1}}^-(t)\right] \\ \hat{\mathbf{X}}_1(t) = \hat{\mathbf{X}}^-(t) + \mathbf{K}_1(t)\left[y_1(t) - \hat{y}_1(t)\right] \\ \mathbb{P}_1(t) = \left[\mathbb{I} - \mathbf{K}_1(t)\mathbf{G}_1(t)\right]\mathbb{P}^-(t) \end{cases}, \tag{34}$$

$$\begin{cases} \mathbf{K}_2(t) = \mathbb{P}_1(t)\mathbf{G}_2^T(t)\left[\mathbf{G}_2(t)\mathbb{P}_1(t)\mathbf{G}_2^T(t) + \sigma_2^2\right]^{-1} \\ \hat{y}_2(t) = \hat{x}_1^{\mathbf{1}}(t)\sin\left[\hat{x}_3^{\mathbf{1}}(t)\right] + \hat{x}_{1+d_1}^{\mathbf{1}}(t)\sin\left[\hat{x}_{3+d_1}^{\mathbf{1}}(t)\right] \\ \qquad + \cdots + \hat{x}_{1+d_{N-1}}^{\mathbf{1}}(t)\sin\left[\hat{x}_{3+d_{N-1}}^{\mathbf{1}}(t)\right] \\ \hat{\mathbf{X}}_2(t) = \hat{\mathbf{X}}_1(t) + \mathbf{K}_2(t)\left[y_2(t) - \hat{y}_2(t)\right] \\ \mathbb{P}_2(t) = \left[\mathbb{I} - \mathbf{K}_2(t)\mathbf{G}_2(t)\right]\mathbb{P}_1(t) \\ \vdots \\ \mathbf{K}_M(t) = \mathbb{P}_{M-1}(t)\mathbf{G}_M^T(t)\left[\mathbf{G}_M(t)\mathbb{P}_{M-1}(t)\mathbf{G}_M^T(t) + \sigma_M^2\right]^{-1} \\ \hat{y}_M(t) = \hat{x}_1^{\mathbf{M-1}}(t)\sin\left[\hat{x}_3^{\mathbf{M-1}}(t)\right] + \hat{x}_{1+d_1}^{\mathbf{M-1}}(t)\sin\left[\hat{x}_{3+d_1}^{\mathbf{M-1}}(t)\right] \\ \qquad + \cdots + \hat{x}_{1+d_{N-1}}^{\mathbf{M-1}}(t)\sin\left[\hat{x}_{3+d_{N-1}}^{\mathbf{M-1}}(t)\right] \\ \hat{\mathbf{X}}_M(t) = \hat{\mathbf{X}}_{M-1}(t) + \mathbf{K}_M(t)\left[y_M(t) - \hat{y}_M(t)\right] \\ \mathbb{P}_M(t) = \left[\mathbb{I} - \mathbf{K}_M(t)\mathbf{G}_M(t)\right]\mathbb{P}_{M-1}(t) \end{cases}, \tag{35}$$

with G_1 given by (26) and

$$\mathbf{G}_m(t) = \left[\mathbf{G}_{m,1}(t) \quad \ldots \quad \mathbf{G}_{m,N}(t) \right], \quad m = 2, \ldots, M, \tag{36}$$

where

$$\mathbf{G}_{1,1}(t) = \left[\sin\left[\hat{x}_3^-(t)\right] \ 0 \ \hat{x}_1^-(t)\cos\left[\hat{x}_3^-(t)\right] \quad 0 \ldots 0 \right], \tag{37}$$

$$\mathbf{G}_{1,n}(t) = [\sin\left[\hat{x}_{3+d_{n-1}}^-(t)\right] \ 0 \ \hat{x}_{1+d_{n-1}}^-(t)\cos\left[\hat{x}_{3+d_{n-1}}^-(t)\right] \quad 0 \ldots 0], \quad n = 2, \ldots, N, \tag{38}$$

$$\mathbf{G}_{m,1}^T(t) = \begin{bmatrix} \sin\left[\alpha_1\left(\hat{\mathbf{X}}_{m-1}(t)\right)\right] \\ \hat{x}_1^{\mathbf{m-1}}(t)\sum_{l=1}^{L_1}\frac{(-(m-1))^l\left(\hat{x}_2^{\mathbf{m-1}}\right)^{l-1}}{(l-1)!}\hat{x}_{l+3}^{\mathbf{m-1}}(t) \\ \qquad \times \cos\left[\alpha_1\left(\hat{\mathbf{X}}_{m-1}(t)\right)\right] \\ \hat{x}_1^{\mathbf{m-1}}(t)\cos\left[\alpha_1\left(\hat{\mathbf{X}}_{m-1}(t)\right)\right] \\ \frac{-(m-1)\hat{x}_2^{\mathbf{m-1}}}{1!}\hat{x}_1^{\mathbf{m-1}}(t)\cos\left[\alpha_1\left(\hat{\mathbf{X}}_{m-1}(t)\right)\right] \\ \vdots \\ \frac{\left(-(m-1)\hat{x}_2^{\mathbf{m-1}}\right)^{L_1}}{L_1!}\hat{x}_1^{\mathbf{m-1}}(t)\cos\left[\alpha_1\left(\hat{\mathbf{X}}_{m-1}(t)\right)\right] \end{bmatrix}$$
$$m = 2, \ldots, M, \tag{39}$$

$$\mathbf{G}_{m,n}^{T}(t) =$$

$$\begin{bmatrix} \sin\left[\alpha_n\left(\hat{\mathbf{X}}_{m-1}(t)\right)\right] \\ \hat{x}^{\mathbf{m-1}}_{1+d_{n-1}}(t)\sum_{l=1}^{L_1}\frac{(-(m-1))^l\left(\hat{x}^{\mathbf{m-1}}_{l+2+d_{n-1}}\right)^{l-1}}{(l-1)!}\hat{x}^{\mathbf{m-1}}_{l+3+d_{n-1}}(t) \\ \qquad\times\cos\left[\alpha_n\left(\hat{\mathbf{X}}_{m-1}(t)\right)\right] \\ \hat{x}^{\mathbf{m-1}}_{1+d_{n-1}}(t)\cos\left[\alpha_n\left(\hat{\mathbf{X}}_{m-1}(t)\right)\right] \\ \frac{-(m-1)\hat{x}^{\mathbf{m-1}}_{2+d_{n-1}}}{1!}\hat{x}^{\mathbf{m-1}}_{1+d_{n-1}}(t)\cos\left[\alpha_n\left(\hat{\mathbf{X}}_{m-1}(t)\right)\right] \\ \vdots \\ \frac{\left(-(m-1)\hat{x}^{\mathbf{m-1}}_{2+d_{n-1}}\right)^{L_n}}{L_n!}\hat{x}^{\mathbf{m-1}}_{1+d_{n-1}}(t) \\ \qquad\times\cos\left[\alpha_{n\tau_{nm}}\left(\hat{\mathbf{X}}_{m-1}(t)\right)\right] \end{bmatrix}$$

$$n = 2,\ldots,N, \quad m = 2,\ldots,M, \tag{40}$$

where $\{\alpha_n, n = 1,\ldots,N, m = 2,\ldots,M\}$ are given by

$$\alpha_1\left(\hat{\mathbf{X}}_{m-1}(t)\right) = \sum_{l=0}^{L_1}\frac{\left(-(m-1)\hat{x}_2^{\mathbf{m-1}}\right)^l}{l!}\hat{x}^{\mathbf{m-1}}_{l+3}(t), \tag{41}$$

$$\alpha_n\left(\hat{\mathbf{X}}_{m-1}(t)\right) = \sum_{l=0}^{L_n}\frac{\left(-(m-1)\hat{x}^{\mathbf{m-1}}_{l+2+d_{n-1}}\right)^l}{l!}\hat{x}^{\mathbf{m-1}}_{l+3+d_{n-1}}(t), \quad n = 2,\ldots,N. \tag{42}$$

We note the dependence of $\mathbf{G}$ upon the delay parameters, which shows the importance of correct estimation of these latter when they are unknown.

B. Discussion

The proposed algorithm is illustrated in Figure. 1. It is based on the application of the EKF M times: The first EKF is applied on the non-delayed signal by computing the predicted values of the state-vector and the covariance matrix of the prediction error. This is followed by the computation of the Kalman filter gain, the estimated values of the state-vector and of the estimation error covariance matrix after introduction of the first sensor observation. The result is used as prediction for the second EKF applied on the signal delayed by τ_{n2}. The Kalman gain is then computed as well as the state-vector estimate with the corresponding estimation error covariance matrix after introducing the second sensor measurement. This procedure is repeated until the application of the M^{th} EKF, where the estimation result of the $(m-1)^{th}$ EKF is used as prediction for the m^{th} EKF applied on the delayed signal by τ_{nm}. The final estimates of the M^{th} EKF constitute the estimator outputs and in the same time are used by the first EKF as prediction equations to project ahead and close the algorithm loop.

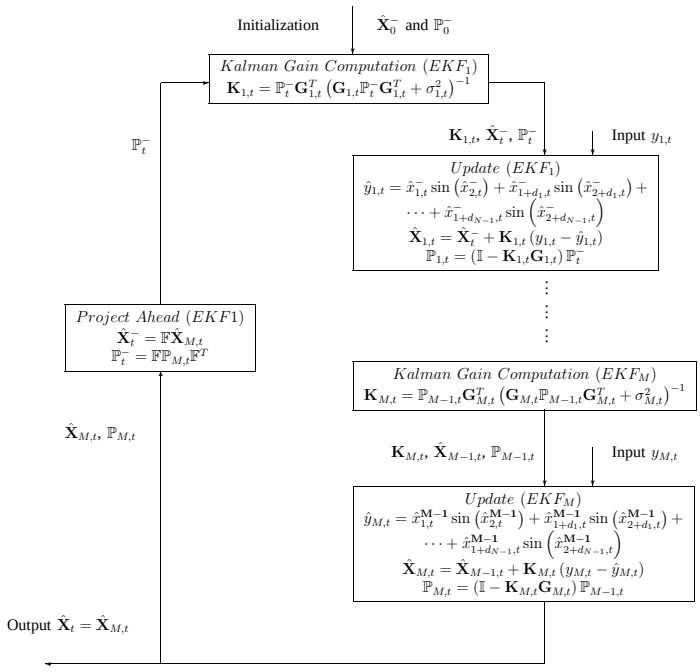

Fig. 1. Flow chart of the proposed extended Kalman filter-based algorithm.

The algorithm can diverge if the reference about which the linearization takes place is poor. The most common situation of this type occurs at the initial starting point of the recursive process. Frequently, the *a priori* information about the true state of the system is poor. This causes a large error in $\hat{\mathbf{X}}_0^-$ and forces $\mathbb{P}_0^-$ to be large. Thus two problems can arise in getting the extended filter started [12]:

1) A very large $\mathbb{P}_0^-$ combined with low-noise measurements at the first step will cause the $\mathbb{P}$ matrix to "jump" from a very large value to a small value in one step. In practice this is permissible. However, this can lead to numerical problems due to roundoff. A non-positive definite $\mathbb{P}$ matrix at any point in the recursive process usually leads to divergence.
2) If the error in $\hat{\mathbf{X}}_0^-$ is large, the first-order approximation used in the linearization will be poor, and divergence may occur, even with perfect arithmetic.

With respect to problem 1, we should be especially careful to use all the usual numerical precautions to preserve the symmetry and positive definiteness of the $\mathbb{P}$ matrix on the first step. In some cases, simply using the symmetric form of the $\mathbb{P}$-update equation is sufficient to ward off the divergence. This form is as follows:

$\mathbb{P}_{M,t} = (\mathbb{I} - \mathbf{K}_{M,t}\mathbf{G}_{M,t})\mathbb{P}_{M-1,t}(\mathbb{I} - \mathbf{K}_{M,t}\mathbf{G}_{M,t})^T + \mathbf{K}_{M,t}\sigma_{M,t}^2\mathbf{K}_{M,t}^T$.

Another way of mitigating the numerical problem is to let $\mathbb{P}_0^-$ be considerably smaller than would normally be dictated by the true a priori uncertainty in $\hat{\mathbf{X}}_0^-$. This will cause suboptimal operation for the first few steps, but this is better than divergence! A similar result can be accomplished by letting $\sigma_{M,t}^2$ be abnormally large for the first few steps. There is no one single cure for all numerical problems. Each case

must be considered on its own merits.

Problem 2 is more subtle than problem 1. Even with perfect arithmetic, poor linearization can cause a poor $\hat{\mathbf{X}}_0^-$ to be updated into an even poorer *a posteriori* estimate, which in turn gets projected on ahead, and so forth. One remedy to the poor-linearization problem, that works quite well when the information contained in the initial measurement is sufficient to determine the initial state-vector algebraically, is to use the initial measurement to solve for the state-vector, just as if there were no measurement error. It is hoped this will yield a better estimate of the state-vector than the original coarse $\hat{\mathbf{X}}_0^-$.

It must be noted that none of the solutions just mentioned play any role in the basic filtering process. Their sole purpose is simply to provide a good reference for linearization, so that the EKF can do its job of suboptimal estimation [5].

In [15], one finds an approach using an EKF applied for a single-component chirp signal case. The analytical signal of the chirp was considered, leading to complex valued measurement equations. An EKF was applied twice for the parameter estimations. A first EKF was applied on the real part of the signal model. A second EKF was applied using the imaginary part of the signal model by taking the first filter estimations as prediction results. Our algorithm originality consists of bypassing the prediction equations of the m^{th} EKF's, for $m = 2, \ldots, M$, and substituting them by the outputs of the $(m-1)^{th}$ EKF's, hence, leading to an anticipation in the process. The same approach is applied for the prediction equations of the first EKF where the output of the M^{th} EKF is used speeding up the convergence process.

In comparison with the method used in [15], where the linearization was made around the predicted state-vector, we note that our linearization point is the preceding EKF estimated state-vector, which represents a better linearization point, compared to the predicted state-vector, since it is closer to the solution (When the filter converges). Furthermore, [15] second observation equation does not carry any new information compared to the first observation equation (Since these equations represent the analytical signal components). In contrast, in our approach we can find a new information represented by the time delays. Finally, [15] assumes the chirp analytical signal representation, hence constraining the algorithm applicability to the narrowband case only, whereas our algorithm can be applied in the case of narrowband and wideband signals (See Section IV, Example 5).

C. Computational Cost

To compare our approach with the one used in [5] and [15] in terms of computational cost (*CC*), let's consider the general case of N PPS's of degrees L_n impinging on a sensor array of M elements. By assuming P observations and I iterations $(I \leq P)$, the following *CC* is obtained for our algorithm in terms of number of scalar multiplications *Mul_cost* (division) and scalar additions *Add_cost* (subtractions):

$$\begin{aligned} Mul\_cost &= \left[\left(1+N+2U+3U^2+U^3\right)M \right. \\ &\quad \left. + \left(U^2+2U^3\right)\right]I - U^3 \\ Add\_cost &= \left[\left(1+N+U+U^2\right)M - U - U^2 + 2U^3\right]I \\ &\quad + U^2 + 3U^3. \end{aligned}$$

Where $U = N(L_n+2)$ and $U = N(L_n+3)$ when the delays are considered known and unknown, respectively. The *CC* for the method presented in [15] is as follows

$$\begin{aligned} Mul\_cost &= \left(2+4U+7U^2+4U^3+2N\right)I + U^2 + U^3 \\ Add\_cost &= \left(2+U+U^2+4U^3+2N\right)I - U + U^3. \end{aligned}$$

Where $U = N(L_n+2)$.

For the PHAF algorithm presented in [5], The *CC* is as follows:

$$\begin{aligned} Mul\_cost &= 2N + 2(2-L)P + (L+1)P^2 + (L-1)P^3 \\ Add\_cost &= -1 - (L+1)P + (2+L)P^2. \end{aligned}$$

Where L represents the number of lags used in the algorithm.

Let's now consider the following example: three well separated chirp signals $(N = 3,\ L_n = 2)$, where 512 observations are available $(P = 512)$. Two sensors, at least, are needed for our algorithm to be applicable, so we consider this situation and hence take $M = 2$. The minimum number of lags for the PHAF is considered taking $L = 2$ in the corresponding *CC* relations. For a fair comparison between our algorithm and the one presented in [15], the situation where the delays are unknown is considered by taking $U = N(L_n+3) = 15$ in our *CC* relation (where $U = N(L_n+2) = 12$ in [15] *CC* relation). Finally, although the proposed EKF algorithm might converge earlier than the last observation iteration, we consider the worst case where $I = P$. Figures cited in Table. 1 are then obtained. It can be noticed from this example that our algorithm needs less number of operations than the one presented in [5] and needs relatively the same number of operations as the one presented in [15] (knowing that the convergence of the filter for our approach happens earlier than in the case of [15]).

TABLE I
COMPUTATIONAL COST COMPARISONS

Method	*Mul_cost*	*Add_cost*
Our approach	7749841	3593326
Method of [15]	4085584	3624628
Method of [5]	135004166	1047039

IV. NUMERICAL RESULTS

In all our simulation examples, we assume a ULA with omnidirectional sensors. The sonar case is considered with the sound propagation speed $v = 1500\ m/s$ and the inter-element spacing $d = 1.5\ m$. The signal is generated according to (2) with a sampling period and a sample size of 1 second and 512 samples, respectively. The parameter initializations are at 20 % of the actual values (see footnote 5). The signal-to-noise ratio is defined by $SNR\,(dB) = 10\log_{10}\left[\sum_{n=1}^{N}\left(a_n^2\right)/(2\sigma^2)\right]$ and

[5]In our simulations, we assumed the parameter initializations at 20 % of their actual values, following [25].

ranges from 0 dB to 20 dB, where the additive noises are zero-mean white Gaussian with variances $\{\sigma_i^2,\ i=1,\ldots,N\}$. The performances are measured by comparing the mean square errors (MSE's), obtained through 100 Monte-Carlo trials, with their corresponding Cramér-Rao lower bounds (CRLB's, see appendix for the bound derivations). The delays are assumed unknown in all our simulation examples. Hence, the state-vector form given in (15) is considered. These nuisance parameters were initialized at 20 % of their actual values.

The first example consists of three linear frequency modulated sources impinging on a 4-sensor array arriving from directions $\alpha_1 = 10^o$, $\alpha_2 = 20^o$, and $\alpha_3 = 30^o$ with respect to the broadside [3]. Hence, we have $N=3$, $L_1 = L_2 = L_3 = 2$ and $M=4$ with:

$$\begin{array}{llll} a_1 = 1.0, & b_{01} = \frac{\pi}{2} \text{ rd}, & b_{11} = 0.5\ \frac{rd}{s}, & b_{21} = \ \ 0.0025\ \frac{rd}{s^2}. \\ a_2 = 0.8, & b_{02} = \frac{\pi}{4} \text{ rd}, & b_{12} = 1.5\ \frac{rd}{s}, & b_{22} = -0.0020\ \frac{rd}{s^2}. \\ a_3 = 0.7, & b_{03} = \frac{\pi}{6} \text{ rd}, & b_{13} = 0.1\ \frac{rd}{s}, & b_{23} = \ \ 0.0010\ \frac{rd}{s^2}. \end{array}$$

We choose the initial diagonal covariance matrix with the following diagonal elements 10^{-2}, 10^{-2}, 10^{-3}, 10^{-8}, 10^{-2}, 10^{-2}, 10^{-2}, 10^{-8}, 10^{-2}, 10^{-2}, 10^{-4}, 10^{-8}. The propagation delays are given as follows [6]:
$\tau_{12} = 0.000174$ second, $\tau_{22} = 0.000342$ second, $\tau_{32} = 0.0005$ second.
$\tau_{13} = 0.000348$ second, $\tau_{23} = 0.000684$ second, $\tau_{33} = 0.0010$ second.
$\tau_{14} = 0.000522$ second, $\tau_{24} = 0.001026$ second, $\tau_{34} = 0.0015$ second.

Figure. 2 shows the filter error covariance matrix evolution for SNR = 10 dB along with the MSE's/CRLB's comparison in the case of known phase degree (part (a)) and overestimated phase degree (part (b)). In both cases, the algorithm performs well, where the estimator MSE's achieve their corresponding CRLB's for SNR lower than 5 dB, with earlier convergence of the filter in case (a) (concluded from the error covariance matrix trace plot). For case (b), a wider model was considered by taking in (15) $N=3$ and $L_1 = L_2 = L_3 = 5$. The filter converges to zero for the parameters $\{b_{ln},\ n=1,\ldots,3,\ \ l=3,\ldots,5\}$. This can be seen as phase degrees determination method when these latter are unknown. We only considered the two high order coefficients $\{b_{ln}, l=1,\ldots,2, n=1,\ldots,3\}$ to illustrate the algorithm performance since it was noticed, after an extensive number of simulations, that these parameters are estimated prior to the initial phases $\{b_{0n}, n=1,\ldots,3\}$, and their good estimation would implicate good estimation of the initial phases.

Figure. 3 illustrates the evaluation of the algorithm performance in the case where two of the three sources impinge from the same direction. The same simulation conditions as in the first example, part (a), are kept except the angles of arrival, where we have now $\alpha_1 = 10^o$, $\alpha_2 = 10^o$, and $\alpha_3 = 30^o$. Our estimator remains efficient with performances similar to Figure. 1 - (a). The situation of similar angles of arrival translates into similar delays in the state-vector. Reducing the dimension of the state-vector is possible in applications where we *a priori* know that some sources are impinging from the same direction. This is done by omitting the redundant delay variable obtaining a reduced computation cost.

[6]The delays are related to the direction-of-arrival (DOA) according to the relation $\tau_{nm} = \frac{(m-1)d}{v}\sin(\alpha_n)$, $n=1,\ldots,3$, $m=2,\ldots,4$.

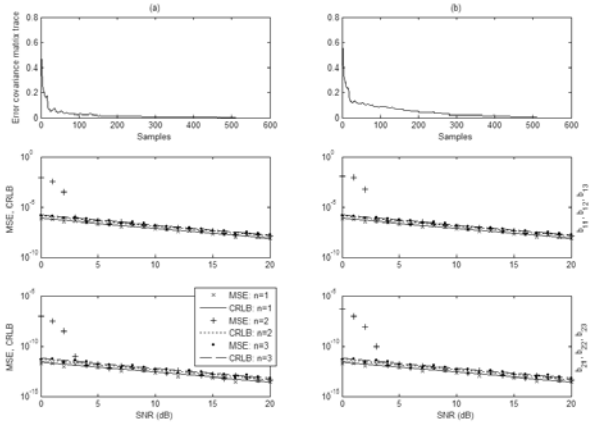

Fig. 2. Example. 1: Mean square errors and the corresponding Cramér-Rao lower bounds versus varying signal-to-noise ratio, along with the error covariance matrix trace evolution at SNR = 10 dB. a- case known phase degrees (equaling 3), b- unknown phase degrees (actual values equaling 3 and overestimated to 5).

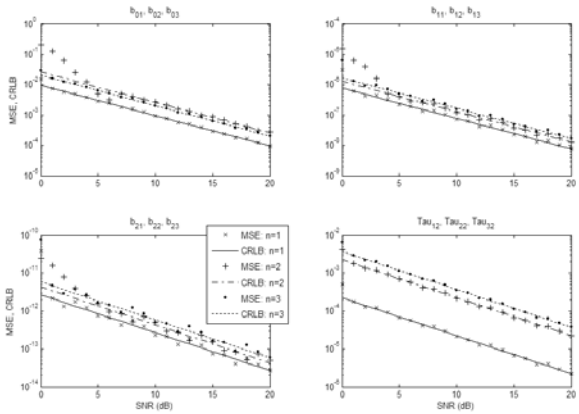

Fig. 3. Example. 2: Mean square errors and the corresponding Cramér-Rao lower bounds versus varying signal-to-noise ratio, case where two signals impinge from the same direction.

In examples 3, The performance of the algorithm is presented for fifth order PPS source models where the same state-vector as in Example. 1, (b) is considered. Figure. 4 illustrates the error covariance matrix trace evolution for SNR = 10. A bad evolution can be noticed for the first 20 samples and a good evolution for the remaining samples, where the filter converges to the actual parameter values. An extensive number of simulations have been performed where we cases of filter divergence. This is due to the very small values of the higher order phase coefficients producing a badly conditioned error covariance matrix.

In example 4, the approach of [15] has been implemented and compared to our algorithm with considering a wideband chirp signal with the following parameters: $a_0 = 1,\ \ b_0 = 0$ rd, $\ b_1 = 0\ \frac{rd}{s}$, and $b_2 = 0.0061\ \frac{rd}{s^2}$.

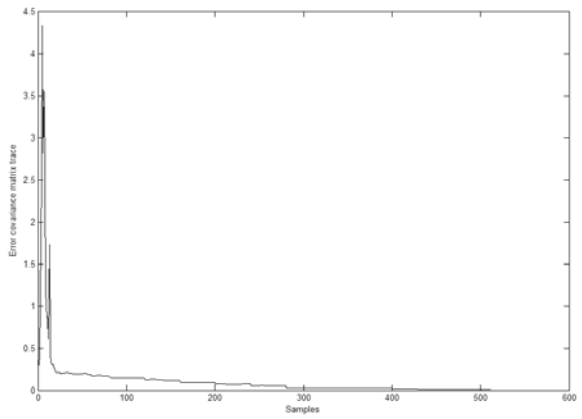

Fig. 4. Example. 3: Error covariance matrix trace evolution at SNR = 10 dB, case of PPS's of high phase degree (5^{th} order).

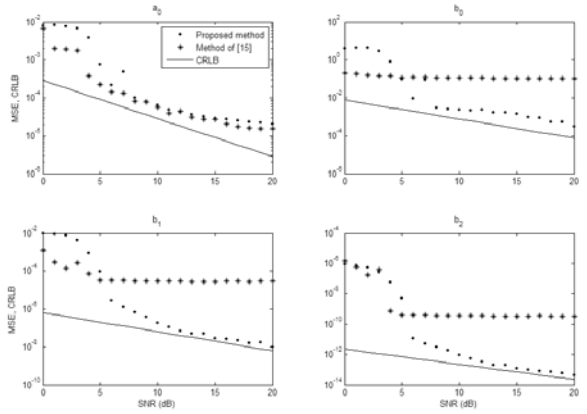

Fig. 5. Example. 4: Performance comparison with [15], case wideband chirp signal (a 2-sensor array has been used for our approach).

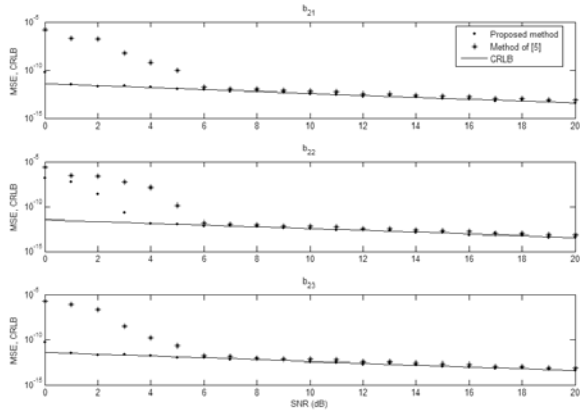

Fig. 6. Example. 5: Performance comparison with [5], case 3 narrowband chirp signals (a 4-sensor array has been used for our approach).

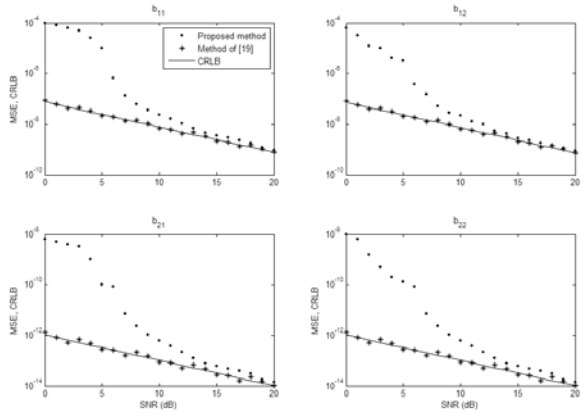

Fig. 7. Example. 6: Performance comparison with [19], case two wideband chirp signals impinging on a 10-sensor array.

Figure. 5 shows that the proposed method outperforms the one of [15] where, for this latter, we have non-decaying MSE's for SNR greater than 4 dB whereas for our estimator, the MSE's become closer to their respective CRLB's for higher SNR values (for the phase parameters).

In example 5 the comparison of our algorithm is extended to the method developed in [5] (Product High-Order Ambiguity Function, PHAF). Example 1 - (a) scenario is assumed with the actual PPS's parameter values (narrowband signals)

$$\begin{array}{llll} a_1 = 1, & b_{01} = 0 \text{ rd}, & b_{11} = 0.25\ \frac{rd}{s}, & b_{21} = 0.25/512\ \frac{rd}{s^2}. \\ a_2 = 1, & b_{02} = 0 \text{ rd}, & b_{12} = 0.50\ \frac{rd}{s}, & b_{22} = 0.50/512\ \frac{rd}{s^2}. \\ a_3 = 1, & b_{03} = 0 \text{ rd}, & b_{13} = 0.75\ \frac{rd}{s}, & b_{23} = 0.75/512\ \frac{rd}{s^2}. \end{array}$$

Figure. 6 illustrates the simulation results. Our algorithm offers a better performance where a more efficient estimator is obtained. Performances of both methods have been evaluated considering the higher order coefficients because PHAF performance is highly dependent on the estimation result of these parameters [5] (the number of lags used for PHAF implementation equals 6). We note that using our approach, it is possible to estimate the DOA of the sources (see footnote 6) whereas this is impossible using PHAF.

In the last example, the performances of our approach are compared with those of [19] (Maximum Likelihood approach, ML) in the case of wideband sources by considering a scenario given in [20] where we have two sources impinging on a 10-sensor array

$$\begin{array}{llll} a_1 = 1, & b_{01} = 0 \text{ rd}, & b_{11} = 0.24\pi\ \frac{rd}{s}, & b_{21} = -0.0024\pi\ \frac{rd}{s^2}. \\ a_2 = 1, & b_{02} = 0 \text{ rd}, & b_{12} = 0.30\pi\ \frac{rd}{s}, & b_{22} = \ \ 0.0024\pi\ \frac{rd}{s^2}. \end{array}$$

The sampling period is taken equal to 0.01 seconds and the sources impinge from the directions $\alpha_1 = 20^o$ and $\alpha_2 = 25^o$. The simulation results are shown in Figure. 7. Our algorithm, although being a suboptimal estimator, offers a good alternative to the ML estimator when seeking less complexity and real-time applications. Indeed, the estimator MSE's become closer to their respective CRLB's for high SNR values.

Finally, the algorithm has been tested for other scenarios like cases where there are more sources than sensors and we found that the algorithm performs well.

V. CONCLUSION

Extended Kalman Filter-based approach was applied to derive a new algorithm for parameter estimations of MC PPS's impinging on a multi-sensor array. The combination of this scheme with the exploitation of a spatial information given by a multi-sensor array was shown to provide a high convergence rate and statistical features close to the CRLB's. The new method was compared with competitive algorithms to evaluate its performance. It was demonstrated through simulations that the proposed method performs well in both cases of wideband and narrowband signals.

VI. APPENDIX

In this section, we derive the Fisher information matrix ($\mathbb{FIM}$) for our model.

A. Parameters of M Signals in AWGN

We suppose M deterministic signals $\{s_m(t,\mathbf{\Psi}), m = 1,\ldots,M\}$ with unknown parameter vector $\mathbf{\Psi}$ observed in zero mean independent AWGNs $\{v_m(t), m = 1,\ldots,M\}$ of variances $\{\sigma_m^2, m = 1,\ldots,M\}$, respectively. For $t = 0,\ldots,P-1$,

$$\begin{cases} y_1(t,\mathbf{\Psi}) &= s_1(t,\mathbf{\Psi}) + v_1(t) \\ \vdots & \\ y_M(t,\mathbf{\Psi}) = s_M(t,\mathbf{\Psi}) + v_M(t) \end{cases}. \tag{43}$$

The $\mathbb{FIM}$ elements $\{FIM(\mathbf{\Psi})_{i,j}\}$, as defined in [22], are given by

$$FIM(\mathbf{\Psi})_{i,j} = -E\left(\frac{\partial^2 ln\ p\{y_1(t,\mathbf{\Psi}),\ldots,y_M(t,\mathbf{\Psi})\}}{\partial\psi_i\partial\psi_j}\right), \tag{44}$$

where ψ_i, ψ_j are the entries of the vector $\mathbf{\Psi}$ and p stands for the probability density. Having $\{y_m, m = 1,\ldots,M\}$ mutually independent,

$$p\{y_1(t,\mathbf{\Psi}),\ldots,y_M(t,\mathbf{\Psi})\} = p\{y_1(t,\mathbf{\Psi})\}\times p\{y_2(t,\mathbf{\Psi})\}\times\cdots\times p\{y_M(t,\mathbf{\Psi})\}, \tag{45}$$

and

$$\frac{\partial^2 ln\ p\{y_1(t,\mathbf{\Psi}),\ldots,y_M(t,\mathbf{\Psi})\}}{\partial\psi_i\partial\psi_j} = \frac{1}{\sigma_1^2}\sum_{t=0}^{P-1}\left[(y_1(t,\mathbf{\Psi}) - s_1(t,\mathbf{\Psi}))\frac{\partial^2 s_1(t,\mathbf{\Psi})}{\partial\psi_i\partial\psi_j}\right] - \frac{1}{\sigma_1^2}\sum_{t=0}^{P-1}\frac{\partial s_1(t,\mathbf{\Psi})}{\partial\psi_i}\frac{\partial s_1(t,\mathbf{\Psi})}{\partial\psi_j} + \cdots + \frac{1}{\sigma_M^2}\sum_{t=0}^{P-1}\left[(y_M(t,\mathbf{\Psi}) - s_M(t,\mathbf{\Psi}))\frac{\partial^2 s_M(t,\mathbf{\Psi})}{\partial\psi_i\partial\psi_j}\right] - \frac{1}{\sigma_M^2}\sum_{t=0}^{P-1}\frac{\partial s_M(t,\mathbf{\Psi})}{\partial\psi_i}\frac{\partial s_M(t,\mathbf{\Psi})}{\partial\psi_j}. \tag{46}$$

We then obtain

$$FIM(\mathbf{\Psi})_{i,j} = \frac{1}{\sigma_1^2}\sum_{t=0}^{P-1}\left(\frac{\partial s_1(t,\mathbf{\Psi})}{\partial\psi_i}\frac{\partial s_1(t,\mathbf{\Psi})}{\partial\psi_j}\right) + \cdots + \frac{1}{\sigma_M^2}\sum_{t=0}^{P-1}\left(\frac{\partial s_M(t,\mathbf{\Psi})}{\partial\psi_i}\frac{\partial s_M(t,\mathbf{\Psi})}{\partial\psi_j}\right). \tag{47}$$

The $\mathbb{CRLB}$ expression is then given by

$$\mathbb{CRLB}(\mathbf{\Psi}) = \mathbb{FIM}(\mathbf{\Psi})^{-1}. \tag{48}$$

B. Application to Model (3)-(4)

According to (3) and (4),

$$\begin{cases} s_1(t,\mathbf{\Psi}) = \sum_{n=1}^{N} a_n \sin[\phi_n(t)] \\ s_2(t,\mathbf{\Psi}) = \sum_{n=1}^{N} a_n \sin\left[\phi_n\left(t - \frac{\tau_{n2}}{\Delta}\right)\right] \\ \vdots \\ s_M(t,\mathbf{\Psi}) = \sum_{n=1}^{N} a_n \sin\left[\phi_n\left(t - \frac{\tau_{nM}}{\Delta}\right)\right] \\ \mathbf{\Psi} = [a_1\ \tau_{12}\ b_{01}\ b_{11}\ \ldots\ b_{L_1 1}\ \ldots\ldots\ a_N\ \tau_{N2}\ b_{0N}\ b_{1N} \\ \qquad \ldots\ b_{L_N N}]^T = [\psi_1\ \psi_2\ \ldots\ \psi_{d_N}]^T \end{cases}. \tag{49}$$

$\mathbf{\Psi}$ results is equivalent(19).

We give the $\mathbb{FIM}$ entry expressions for the single-component chirp signal impinging on two-sensor array by using (47) and (49) (the $\mathbb{FIM}$ element expressions for the general case of MC PPS's impinging on a multi-sensor array are too heavy to be presented)

$$\begin{aligned}
FIM(\mathbf{\Psi})_{11} &= \frac{1}{\sigma_1^2}\sum_{t=0}^{P-1}\sin^2[\phi_1(t)] + \frac{1}{\sigma_2^2}\sum_{t=0}^{P-1}\sin^2[\phi_2(t)] \\
FIM(\mathbf{\Psi})_{12} &= \frac{1}{\sigma_2^2}\sum_{t=0}^{P-1}\{a_1(2b_2(\tau - t\Delta) - b_1) \times \sin[\phi_2(t)]\cos[\phi_2(t)]\} \\
FIM(\mathbf{\Psi})_{13} &= \frac{1}{\sigma_1^2}\sum_{t=0}^{P-1}a_1\sin[\phi_1(t)]\cos[\phi_1(t)] + \frac{1}{\sigma_2^2}\sum_{t=0}^{P-1}a_1\sin[\phi_2(t)]\cos[\phi_2(t)] \\
FIM(\mathbf{\Psi})_{14} &= \frac{1}{\sigma_1^2}\sum_{t=0}^{P-1}a_1 t\Delta\sin[\phi_1(t)]\cos[\phi_1(t)] + \frac{1}{\sigma_2^2}\sum_{t=0}^{P-1}\{a_1(t\Delta - \tau)\sin[\phi_2(t)] \times \cos[\phi_2(t)]\} \\
FIM(\mathbf{\Psi})_{15} &= \frac{1}{\sigma_1^2}\sum_{t=0}^{P-1}a_1 t^2\Delta^2\sin[\phi_1(t)]\cos[\phi_1(t)] + \frac{1}{\sigma_2^2}\sum_{t=0}^{P-1}\{a_1(t\Delta - \tau)^2\sin[\phi_2(t)] \times \cos[\phi_2(t)]\}
\end{aligned}$$

$$
\begin{aligned}
FIM(\mathbf{\Psi})_{21} &= FIM(\mathbf{\Psi})_{12} \\
FIM(\mathbf{\Psi})_{22} &= \frac{1}{\sigma_2^2}\sum_{t=0}^{P-1}\{a_1^2\left(2b_2\left(\tau-t\Delta\right)-b_1\right)^2 \\
&\qquad \times\cos^2\left[\phi_2(t)\right]\} \\
FIM(\mathbf{\Psi})_{23} &= \frac{1}{\sigma_2^2}\sum_{t=0}^{P-1}\{a_1^2\left(2b_2\left(\tau-t\Delta\right)-b_1\right) \\
&\qquad \times\cos^2\left[\phi_2(t)\right]\} \\
FIM(\mathbf{\Psi})_{24} &= \frac{1}{\sigma_2^2}\sum_{t=0}^{P-1}\{a_1^2\left(2b_2\left(\tau-t\Delta\right)-b_1\right) \\
&\qquad \times\left(t\Delta-\tau\right)\Delta\cos^2\left[\phi_2(t)\right]\} \\
FIM(\mathbf{\Psi})_{25} &= \frac{1}{\sigma_2^2}\sum_{t=0}^{P-1}\{a_1^2\left(2b_2\left(\tau-t\Delta\right)-b_1\right) \\
&\qquad \times\left(t\Delta-\tau\right)^2\cos^2\left[\phi_2(t)\right]\} \\
FIM(\mathbf{\Psi})_{31} &= FIM(\mathbf{\Psi})_{13} \\
FIM(\mathbf{\Psi})_{32} &= FIM(\mathbf{\Psi})_{23} \\
FIM(\mathbf{\Psi})_{33} &= \frac{1}{\sigma_1^2}\sum_{t=0}^{P-1}a_1^2\cos^2\left[\phi_1(t)\right] \\
&\quad +\frac{1}{\sigma_2^2}\sum_{t=0}^{P-1}a_1^2\cos^2\left[\phi_2(t)\right] \\
FIM(\mathbf{\Psi})_{34} &= \frac{1}{\sigma_1^2}\sum_{t=0}^{P-1}a_1^2t\Delta\cos^2\left[\phi_1(t)\right] \\
&\quad +\frac{1}{\sigma_2^2}\sum_{t=0}^{P-1}a_1^2\left(t\Delta-\tau\right)\cos^2\left[\phi_2(t)\right] \\
FIM(\mathbf{\Psi})_{35} &= \frac{1}{\sigma_1^2}\sum_{t=0}^{P-1}a_1^2t^2\Delta^2\cos^2\left[\phi_1(t)\right] \\
&\quad +\frac{1}{\sigma_2^2}\sum_{t=0}^{P-1}a_1^2\left(t\Delta-\tau\right)^2\cos^2\left[\phi_2(t)\right] \\
FIM(\mathbf{\Psi})_{41} &= FIM(\mathbf{\Psi})_{14} \\
FIM(\mathbf{\Psi})_{42} &= FIM(\mathbf{\Psi})_{24} \\
FIM(\mathbf{\Psi})_{43} &= FIM(\mathbf{\Psi})_{34} \\
FIM(\mathbf{\Psi})_{44} &= \frac{1}{\sigma_1^2}\sum_{t=0}^{P-1}a_1^2t^2\Delta^2\cos^2\left[\phi_1(t)\right] \\
&\quad +\frac{1}{\sigma_2^2}\sum_{t=0}^{P-1}a_1^2\left(t\Delta-\tau\right)^2\cos^2\left[\phi_2(t)\right] \\
FIM(\mathbf{\Psi})_{45} &= \frac{1}{\sigma_1^2}\sum_{t=0}^{P-1}a_1^2t^3\Delta^3\cos^2\left[\phi_1(t)\right] \\
&\quad +\frac{1}{\sigma_2^2}\sum_{t=0}^{P-1}a_1^2\left(t\Delta-\tau\right)^3\cos^2\left[\phi_2(t)\right] \\
FIM(\mathbf{\Psi})_{51} &= FIM(\mathbf{\Psi})_{15} \\
FIM(\mathbf{\Psi})_{52} &= FIM(\mathbf{\Psi})_{25} \\
FIM(\mathbf{\Psi})_{53} &= FIM(\mathbf{\Psi})_{35} \\
FIM(\mathbf{\Psi})_{54} &= FIM(\mathbf{\Psi})_{45} \\
FIM(\mathbf{\Psi})_{55} &= \frac{1}{\sigma_1^2}\sum_{t=0}^{P-1}a_1^2t^4\Delta^4\cos^2\left[\phi_1(t)\right] \\
&\quad +\frac{1}{\sigma_2^2}\sum_{t=0}^{P-1}a_1^2\left(t\Delta-\tau\right)^4\cos^2\left[\phi_2(t)\right],
\end{aligned}
$$

where $\tau=\tau_{12}$, $b_0=b_{01}$, $b_1=b_{11}$, $b_2=b_{21}$, $\phi_1(t)=b_0+b_1t\Delta+b_2t^2\Delta^2$, and $\phi_2(t)=b_0+b_1\left(t\Delta-\tau\right)+b_2\left(t\Delta-\tau\right)^2$.

REFERENCES

[1] T. J. Abatzoglou, "Fast maximum likelihood joint estimation of frequency and frequency rate," *IEEE Trans. Aerospace Electron. Syst.*, vol. AES-22, pp. 708-715, Nov. 1986.

[2] M. Adjrad, A. Belouchrani, and A. Ouldali, "Estimation of chirp signal parameters using state-space modelization by incorporating spatial information," in Proc. of the 7th International Symposium on Signal Processing and its Applications (ISSPA), vol. II, pp. 531–534, Paris, France, 1-4 July. 2003.

[3] M. Adjrad, A. Belouchrani, and K. Abed-Meraim, "Parameter estimation of multi-component polynomial-phase signals impinging on a multi-sensor array using extended Kalman filter," in Proc. of the 3rd IEEE International Symposium on Signal Processing and Information Technology (ISSPIT), pp. 471–474, Darmstadt, Germany, 14-17 Dec. 2003.

[4] S. Barbarossa, "Analysis of multicomponent LFM signals by a combined Wigner-Hough transform," *IEEE Trans. Signal Processing*, vol. 43, pp. 1511-1515, Jun. 1995.

[5] S. Barbarossa, A. Scaglione, and G. B. Giannakis, "Product high-order ambiguity function for multicomponent polynomial-phase signal modeling," *IEEE Trans. Signal Processing*, vol. 46, pp. 691-708, Mar. 1998.

[6] S. Barbarossa and V. Petrone, "Analysis of polynomial-phase signals by an integrated generalized ambiguity function," *IEEE Trans. Signal Processing*, vol. 44, pp. 316-327, Feb. 1997.

[7] A. Belouchrani and M. G. Amin, "Time-frequency MUSIC," *IEEE Signal Processing Lett.*, vol. 6, pp. 109-110, 1999.

[8] M. Benidir and A. Ouldali, "Polynomial-phase signal analysis based on the polynomial derivatives decompositions," *IEEE Trans. Signal Processing*, vol. 47, pp. 1954-1965, July 1999.

[9] O. Besson, N. Ghogho, and A. Swami, "Parameter estimation for random amplitude chirp signals," *IEEE Trans. Signal Processing*, vol. 47, pp. 3208-3219, Dec. 1999.

[10] B. Boashash, "Estimating and interpreting the instantaneous frequency of a signal Part 1: Fundamentals," *Proceeding of the IEEE*, vol. 80, Apr. 1992.

[11] B. Boashash, *Time-Frequency Signal Analysis and Processing: A comprehensive reference*. Elsevier, Oxford, UK, 2003 (ISBN: 0-08-044335-4).

[12] R. G. Brown and P. Y. C. Hwang, *Introduction to Random Signals and Applied Kalman Filtering*. John Wiley and Sons., Third Edition, 1997.

[13] P. J. Davis, *Interpolation and Approximation.* Blaisdell Publishing Co., Waltham, Massachusetts, 1963. (Reprinted with corrections by Dover Publications Inc., New York, 1975. Preface to Dover edition includes updated bibliography.)

[14] P. M. Djuric and M. Kay, "Parameter estimation of chirp signals," *IEEE Trans. Acoust., Speech, Signal Process.*, vol. 38, pp. 2118-2126, Dec. 1990.

[15] W. El Kaakour, M. Guglielmi, J.M. Piasco and E. Le Carpentier, "Two identification methods of chirp parameters using state-space models," *DSP' 97, 13 th International Conference on Digital Signal Processing*, pages 903-906, Santorin, Greece, 2-4 July 1997, Greece.

[16] B. Friedlander, "Parametric signal analysis using the polynomial-phase transform," In *Proc. IEEE Workshop Higher-order statistics*, Stanford Sierra Camp June 1993.

[17] B. Friedlander and J. M. Francos, "Estimation of amplitude and phase parameters of multicomponent signals," *IEEE Trans. Signal Processing*, vol. 43, pp. 917-926, Apr. 1995.

[18] B. Friedlander and A. J. Weiss, "Direction finding for wide-band signals using an interpolated array," *IEEE Trans. Signal Processing*, vol. 41, pp. 1618-1634, Apr. 1993.

[19] A. B. Gershman, M. Pesavento and M. G. Amin, "Estimating parameters of multiple wideband polynomial-phase sources in sensor arrays," *IEEE Trans. Signal Processing*, vol. 49, pp. 2924-2934, Dec. 2001.
[20] A. B. Gershman and M. G. Amin, "Wideband direction-of-arrival estimation of multiple chirp signals using spatial time-frequency distributions," *IEEE Signal Processing Lett.*, vol. 7, pp. 152-155, Jun. 2000.
[21] F. Hlawatsch, G. F. Boudreaux-Bartels, "Linear and quadratic time-frequency signal representations," *IEEE Signal Processing Magazine*, Vol. 9, pp. 21-67, Apr. 1992.
[22] S. M. Kay, *Fundamentals of Statistical Signal Processing Volume 1: Estimation Theory*. Prentice Hall, 1998.
[23] S. Peleg and B. Friedlander, "The discrete polynomial phase transform," *IEEE Trans. Signal Processing*, vol. 43, pp. 1901-1914, Aug. 1995.
[24] S. Peleg and B. Porat, "Estimation and classification of signals with polynomial phase," *IEEE Trans. Information Theory*, vol. 37, pp. 422-430, Mar. 1991.
[25] J. M. Piasco, M. Guglielmi and L. Durou, "Identification de chirps par filtrage de Kalman étendu," *Quatorzieme colloque GRETSI*, pages 29-32, Juan les Pins, September 1993.
[26] B. Porat, *Digital Processing of Random Signals, Theory and Methods*. Englewood Cliffs, NJ: Prentice-Hall, 1994.
[27] B. Porat and B. Friedlande, "Accuracy analysis of estimation algorithms for parameters of multiple polynomial-phase signals," in *Proc. IEEE Int. Conf. Acoustics, Speech , and Signal Proc.* (Detroit, MI, May 9-12, 1995), pp. 1800-1803.
[28] J. G. Proakis, *Digital Communications*. New York: Mc Graw-Hill, 1995.
[29] R. Aouada, A. Belouchrani, K. Abed-Meraim, "Multipath parameter estimation of linear chirp signals using sensor arrays," *In Proceedings of the IEEE-SAM'04*, Barcelona, Spain, July 2004.
[30] S. Shamsunder, G. B. Giannakis, and B. Friedlander, "Estimating random-amplitude polynomial phase signals: A cyclostationary approach," *IEEE Trans. Signal Processing*, vol. 43, pp. 492-505, Feb. 1995.
[31] S. Tretter, "Estimating the frequency of a noisy sinusoid by linear regression," *IEEE Trans. Inform. Theory*, vol. IT-31, pp. 832-835, Nov. 1985.
[32] H. Wang and M. Kaveh, "Coherent signal-subspace processing for the detection and estimation of angles of arrival of multiple wide-band sources," *IEEE Trans. Acoust., Speech, Signal Processing*, vol. ASSP-33, pp. 823-831, Aug. 1985.
[33] G. Wang and X.-G. Xia, "Iterative algorithm for direction of arrival estimation with wideband chirp signals," in *Proc. Inst. Elect. Eng., Radar, Sonar, Navig.*, vol. 147, pp. 233-238, Oct. 2000.
[34] Y. Zhang, W. Mu, and M. G. Amin, "Time-Frequency maximum likelihood methods for direction finding," Journal of the Franklin Institute, Vol. 337, pp.483-497, Jul. 2000.
[35] G. Zhou, G. B. Giannakis, and A. Swami, "On polynomial phase signals with time-varying amplitudes," *IEEE Trans. Signal Processing*, vol. 44, pp. 848-861, Apr. 1996.

Mounir Adjrad received the State Engineering degree in electronics in 1999 and the M.Sc. degree in signal processing and communication in 2002, both from the Ecole Nationale Polytechnique (ENP), Algiers, Algeria. He was a Research Officer with the Centre National des Techniques Spatiales (CNTS), Oran, Algeria, from 2002 to 2004. He is currently with the Surrey Space Centre, University of Surrey, Guildford, UK, as a Research Assistant. His research interests are in the areas of statistical signal processing including array processing, performance analysis, adaptive algorithms, and applied signal processing to GPS applications.

Adel Belouchrani was born in 1967. He received the State Engineering degree in 1991 from the Ecole Nationale Polytechnique (ENP), Algiers, Algeria, the M.Sc. degree in signal processing from the Institut National Polytechnique de Grenoble (INPG), France, in 1992, and the Ph.D. degree in signal and image processing from Télécom Paris (ENST), France, in 1995. He was a Visiting Scholar at the Electrical Engineering and Computer Sciences Department, University of California, Berkeley, from 1995 to 1996. He was with the Department of Electrical and Computer Engineering, Villanova University, Villanova, PA, as a Research Associate from 1996 to 1997. He also served as a Consultant to Comcast, Inc., Philadelphia, PA, during the same period. From August 1997 to October 1997, he was with Alcatel ETCA, Belgium. From May to June 2001, he was a visiting scholar at the Department of Cognitive Science of University of California at San Diego, USA. From August to September 2001, he was a visiting researcher at Brain Signal Processing Laboratory, Riken, Japan. From December 2003 to January 2004, he was an invited professor at Telekom Malaysia RnD, Kuala Lumpur, Malaysia. He is currently and since 1998 with the Electrical Engineering Department of ENP as Associate Professor. His research interests are in signal processing for communications and include blind system identification, array signal processing, time frequency analysis, time frequency array signal processing.